



Universiteit
Leiden
The Netherlands

Systemic and cerebral hemodynamics in response to cardiovascular challenges : the heart-brain connection

Verbree, J.

Citation

Verbree, J. (2018, June 12). *Systemic and cerebral hemodynamics in response to cardiovascular challenges : the heart-brain connection*. Retrieved from <https://hdl.handle.net/1887/63082>

Version: Not Applicable (or Unknown)

License: [Licence agreement concerning inclusion of doctoral thesis in the Institutional Repository of the University of Leiden](#)

Downloaded from: <https://hdl.handle.net/1887/63082>

Note: To cite this publication please use the final published version (if applicable).

Cover Page



Universiteit Leiden



The following handle holds various files of this Leiden University dissertation:

<http://hdl.handle.net/1887/63082>

Author: Verbree, J.

Title: Systemic and cerebral hemodynamics in response to cardiovascular challenges : the heart-brain connection

Issue Date: 2018-06-12

Systemic and cerebral
hemodynamics in response to
cardiovascular challenges –
the heart-brain connection

Jasper Verbree



Cover Design by: Jasper Verbree

Layout: Legatron Electronic Publishing, Rotterdam, The Netherlands

Printed and layout: Ipskamp printing, Enschede, The Netherlands

ISBN/EAN: 978-94-028-1053-0

PhD thesis, Leiden University, The Netherlands

Jasper Verbree, 2018

No parts of this book may be reproduced or transmitted in any form or by any means without permission of the copyright owner. Copyright of the published chapters is held by the publisher of the journal in which the work appeared. All rights reserved.

The work presented in this thesis was carried out at the C.J. Gorter Center, department of Radiology at the Leiden University Medical Center, Leiden, The Netherlands and the Laboratory for Clinical Cardiovascular Physiology, Academic Medical Center, Amsterdam, The Netherlands.

This research was supported by the Rembrandt Institute of Cardiovascular Science (Project awarded in 2011).

Systemic and cerebral hemodynamics in response to cardiovascular challenges – the heart-brain connection

Proefschrift

ter verkrijging van

de graad van Doctor aan de Universiteit Leiden,

op gezag van Rector Magnificus prof.mr. C.J.J.M. Stolker,

volgens besluit van het College voor Promoties

te verdedigen op dinsdag 12 juni 2018

klokke 16:15 uur

door

Jasper Verbree

geboren te Zevenhuizen (zh)

in 1986

Promotors

Prof. dr. M.A. van Buchem

Prof. dr. J.J. Van Lieshout (University of Nottingham)

Co-promotor

Dr. ir. M.J.P. van Osch

Committee

Prof. dr. G.J. Blauw

Dr. J.A. Claassen (Radboud University Nijmegen)

Dr. E.A.H. Warnert (Erasmus University Rotterdam)

Prof. A.G. Webb

Table of Contents

CHAPTER 1	Introduction	1
CHAPTER 2	Physiological principles	7
CHAPTER 3	Methods	13
CHAPTER 4	Assessment of middle cerebral artery diameter during hypocapnia and hypercapnia in humans using ultra high-field MRI	27
CHAPTER 5	Using high field magnetic resonance imaging to estimate distensibility of the middle cerebral artery	42
CHAPTER 6	Middle cerebral artery diameter changes during rhythmic handgrip exercise in humans	49
CHAPTER 7	Transcranial Doppler determined middle cerebral artery blood flow velocity does not match MRI global or regional cerebral tissue perfusion during handgrip exercise	63
CHAPTER 8	Influence of the cardiac cycle on pCASL: cardiac triggering of the end-of-labeling	81
CHAPTER 9	Summary	101
CHAPTER 10	General discussion	105
	Samenvatting	113
	List of publications	115
	Dankwoord	117
	Curriculum Vitae	119

CHAPTER

1

Introduction

The Rembrandt project *“Go with the flow: the heart-brain connection over the life-span”*

The studies described in this thesis were part of a larger project funded by the Rembrandt Institute for Cardiovascular Sciences aimed at studying the influence of cardiac functioning on cerebral blood flow. This project was executed within two different centers: the Laboratory for Clinical Cardiovascular Physiology of the Academic Medical Center (AMC; affiliated with the University of Amsterdam) and the C.J. Gorter Center for High-Field MRI, Department of Radiology of the Leiden University Medical Center (LUMC). The research described in this thesis was executed as an integral part of this joined project and the interested reader is also referred to other publications from this project as stated in the list of publications (see: author curriculum vitae).

INTRODUCTION

The brain is a highly metabolically active organ and although it accounts for a small fraction of total body weight (2%), it consumes in the resting condition about 20% of total body oxygen and 25% of total body glucose [1]. Interestingly, the brain by itself has hardly no capillary recruitment and lacks almost any form of energy storage. This requires sufficient and uninterrupted supply of blood to the brain and, to this end, it receives ~15% of the cardiac output (amount of blood being pumped by the heart in one minute) [2]. Acute interruption of the cerebral blood flow (CBF) and with that oxygen delivery to brain tissue, even for a few seconds, has deleterious effects and results in loss of consciousness [3]. On the other hand, an increase in CBF to well above normal values may elicit (brain tissue) hyperperfusion with formation of edema leading to migraine-like headaches, seizures and intracerebral hemorrhage [4]. Therefore, safeguarding the brain from respectively, hypo- and hyperperfusion is of major importance.

The regulation of CBF is complex and comprises of multiple interlinked physiological mechanisms including the cerebral autoregulation, chemoregulation, neurogenic regulation and neurovascular coupling [5,6]. These mechanisms are largely unique to the cerebral vasculature and act directly on the cerebral vascular resistance. The highly effective and seemingly independent CBF regulation at the level of the brain itself is often treated as a separate entity [6]. The perfusion of the brain is, however, also reliant on a sufficient supply of blood from the heart: acute interruption of CBF due to cardiac arrest [7] or by occlusion of a large cerebral artery [8] results in loss of consciousness within seconds. Thus, in addition to an effective set of cerebrovascular control mechanisms, the function of the heart and the condition of the large brain-feeding arteries are important in securing the blood supply to the brain. In other words, CBF is also dependent on factors beyond the brain [9]. The idea of considering the cardiovascular system as an integral component of CBF control has laid the foundation of the work presented in this thesis and will be discussed into more detail in the following paragraphs.

HEART-BRAIN CONNECTION

The circulation of blood starts with the heart pumping blood through the arteries to the tissue under consideration, in this case the brain. To guarantee a sufficient CBF, all elements of the circulation need to function properly (and) in concert. Evidence has emerged that cardiac dysfunction, impaired vessel patency or a critical reduction in central blood volume each may result in insufficient blood supply to the brain [10]. This affects CBF independently from cerebrovascular control whereas in turn, insufficient brain perfusion may eventually be followed by a decline in cognitive performance [11].

This followed, among others, from observations in patients with chronic heart failure in whom a lower CBF [12-14] was associated with a larger prevalence of cognitive dysfunction [15,16]. In

a longitudinal analysis, the Framingham Heart Study revealed a similar association between a low cardiac output and an increased risk of incident dementia and Alzheimer's disease [17]. In addition, about half of the patients in whom the patency of the large vessels to the brain is affected (for instance in carotid artery occlusive disease), have signs and symptoms of mild cognitive impairment [18,19]. Reinstitution of cardiac function by a heart transplantation, a left ventricular assist device or cardiac resynchronization therapy, improved or restored CBF with beneficial effects on cognitive performance [20-25], but the cognitive improvements after extracranial shunts remain an open issue [26]. These findings suggest that optimizing blood supply to the brain by improving cardiovascular function may become a new preventive or therapeutic target for cognitive disorders. Also, a decrease in central blood volume too large to secure cardiac output may affect CBF, for example during standing-up. Changing body position from the supine to the upright posture leads to a gravity induced shift in blood from the upper body towards the legs affecting the return of blood towards the right heart (venous return) [27]. The postural reduction in the amount of blood that is directly available to the heart (central blood volume) results in a decline in cardiac output with a drop in CBF and CBF velocity. As yet, the current monodisciplinary approach from both clinicians and researchers leave the complete heart-brain connection as an unexplored territory. A synergy of different expertise fields may provide more insight into the interesting and clinically increasingly important relationships between the heart and the brain.

AIM

From current knowledge on heart-brain interactions, we hypothesize that CBF control involves cardiovascular function in addition to the principal regulators of cerebral vessel resistance. Disentangling the contributions of systemic versus local brain blood flow regulation is challenging and requires expertise from multiple disciplines. At the start of this research project we had the good fortune to start a multidisciplinary collaboration and work closely with a MRI perfusion expert, a neuroradiologist, a pathologist, and an internist-physiologist sharing our special interest in the heart-brain connection. The primary aim of the project "Go with the flow: the heart-brain connection over the life-span" is to delineate the human heart-brain connection by integrating physiological concepts into the MR-environment and assess CBF and its regulation mechanisms at the macrovascular level (using Transcranial Doppler ultrasonography; TCD) and tissue level (using arterial spin labeling MR imaging; ASL-MRI). This brought together expertise on the characterization of the systemic and cerebrovascular response to physiological challenges in health and disease as well as on brain perfusion at the tissue level using high resolution MRI. This thesis will mainly focus on the validation and comparison of the two main modalities of this project: TCD and ASL-MRI.

OUTLINE OF THIS THESIS

Chapter 1 introduces and outlines the thesis.

Chapter 2 provides a brief overview of the physiological principles involved in systemic and cerebral blood flow control.

Chapter 3 describes the methods of continuous and non-invasive monitoring of systemic, cerebral and pulmonary parameters, followed by a description of the challenges that were used to assess autonomic cardio- and cerebrovascular control.

Chapters 4-6 addresses the validity of cerebral blood flow velocity measurements with transcranial Doppler ultrasonography (see methods section 2.1.2) under a variety of circumstances. It has thus far been assumed that the diameter of the large intracranial arteries remains unaffected by changes in PaCO₂ and brain perfusion pressure. Based on this assumption, changes in CBFv are considered directly proportional to changes in CBF. However, inconsistent findings in literature do not exclude the possibility of diameter changes in large intracranial arteries under the conditions of the studies presented in this thesis. Validity of this assumption is therefore relevant for the interpretation of data on flow velocity obtained by transcranial Doppler ultrasonography. In **chapter 4** we investigated the effects of CO₂ on the diameter of a large cerebral artery using high resolution MRI at 7 Tesla and in **chapter 5** the distensibility of this artery driven by systolic-diastolic pressure differences. In **chapter 6** the effects of sympathetic activity by dynamic handgrip exercise on the diameter of a large cerebral artery using high resolution MRI at 7 Tesla.

Chapter 7 directly compares the CBF tissue response (ASL-MRI) with the CBFv (TCD) response in the middle cerebral artery to sympathetic activation by handgrip exercise in the same subject population to assess whether velocity changes in a large cerebral artery reflect perfusion changes in brain tissue.

Chapter 8 investigates the influence of cardiac pulsations on pseudo-Continuous ASL (pCASL) signal stability.

Chapter 9 summarizes the findings of this thesis and the findings followed by a general discussion in **chapter 10**.

CHAPTER

2

Physiological principles

REGULATION OF SYSTEMIC BLOOD FLOW

In the Rembrandt project, we performed challenges that influenced the systemic blood flow. To provide context for the discussion, the next sections describe the basic concepts of systemic hemodynamics, cardiac output and cardiovascular control.

SYSTEMIC HEMODYNAMICS

Hemodynamics are defined as the physical factors and physiological mechanisms that govern blood flow. Flow through a vessel follows the laws of mass-equality and inertia, but is simplified in steady-state by using the hemodynamic analog of Ohm's law (generally used to describe electrical current). When applied to the cardiovascular system the blood flow is driven by the pressure difference between two points along the vessel together with the vascular resistance (flow = pressure difference / vascular resistance). Under steady state conditions arterial pressure is considered as the driving force behind flow and organ perfusion and is therefore tightly regulated [28].

The first non-invasive arterial blood pressure device was already invented in 1881 by Von Basch [29]. Notwithstanding that the concept of measuring blood flow was already published in 1870 [30], the measurement of cardiac output, either invasively or non-invasively was not possible before the mid of the 20th century. Determination of blood flow, and in particular the flow leaving the heart, is considered vital when managing critically ill patients (for instance those with severe cardiac or pulmonary disease and/or multi-organ failure). Nowadays, several non-invasive techniques (based on rebreathing Fick, Doppler, impedance and finger plethysmography) are available to provide real-time and continuous estimates of cardiac output and stroke volume [31]. Also MRI quantifies cardiac output in a non-invasive way [32]. In this thesis, we primarily focus on blood flow, as the mechanism responsible for the transport of oxygen and nutrients, with blood pressure as the driving power behind flow.

CARDIAC OUTPUT

The amount of blood leaving the heart in one minute is designated as the cardiac output (CO) and equal to left ventricular stroke volume (the amount of blood ejected with each cardiac cycle) times heart rate. Stroke volume is dependent upon preload, contractility and afterload. Cardiac preload is defined as the amount of blood directly available to the left ventricle and relates to thoracic fluid content rather than to central vascular pressures [33]. Therefore, cardiac preload is often –also in this thesis– being referred to as ‘central blood volume’. Contractility refers to the intrinsic muscle strength of the (left) ventricle independent of its loading condition, and afterload refers to the force that opposes ejection of blood out of the ventricle (largely influenced by the

aortic impedance, arterial blood pressure and peripheral vascular resistance). Activities of daily living such as standing-up and physical exercise but also pathophysiological conditions including heart failure and dehydration modify CO by changing one or more of these (extra)cardiac factors [34].

CARDIOVASCULAR CONTROL

To ensure a continuous and appropriate supply of oxygenated blood to the tissues, the cardiovascular system is subject to precise cardiovascular control mechanisms. Although the cardiovascular system is under control of both neural and humoral components of the autonomic nervous system, in this thesis the focus will be on the neuro-cardiovascular system with the arterial baroreflex as its best-known example. The arterial baroreflex is the fastest control mechanism of blood pressure and generally acts within seconds [35]. The reflex arc consists of peripheral (stretch) receptors embedded in the aortic arch and carotid arteries, afferent pathways (toward the central nervous system), pathways within the central nervous system itself, efferent nerves and finally the effector organs (e.g. cardiac conductive tissue, cardiac muscle and vascular wall muscle fibers) [36], see Figure 2.1). Hence, a fall in arterial pressure leads to reflex adjustments by parasympathetic inhibition and sympathetic activation, with an increase in heart rate, in cardiac contractility, and in vascular resistance and venous return [37]. Conversely, an increase in arterial pressure results in opposite reflex changes. This provides a real-time feedback control on the arterial blood pressure, involving the heart as well as the peripheral vasculature.

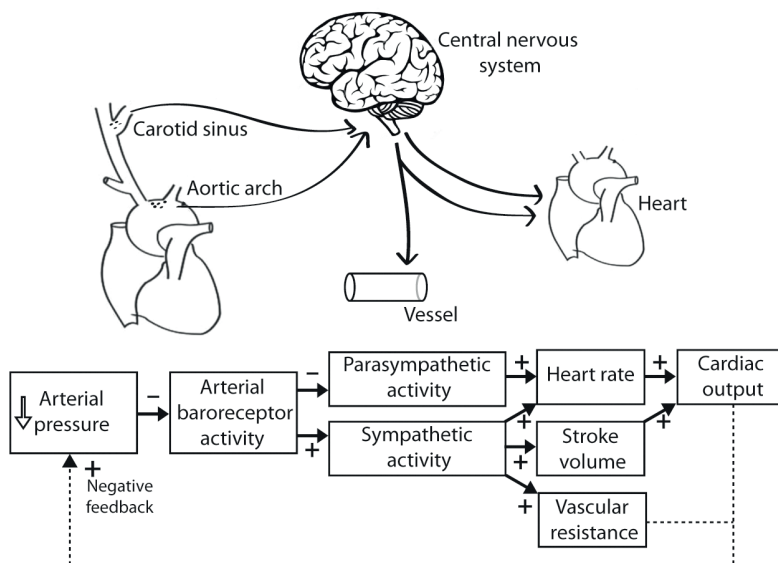


Figure 2.1 | Schematic drawing of the afferent and efferent pathways of the baroreceptor reflex arc (modified from Wehrwein and Joyner 2013) and a block diagram of baroreflex mediated adjustments to a fall in arterial pressure.

REGULATION OF CEREBRAL BLOOD FLOW

The regulation of CBF is considered to be independent of the systemic hemodynamics and the cerebral control mechanisms maintains CBF more or less constant by adjusting the cerebrovascular resistance. Therefore, these regulatory mechanisms provide the “background” to which systemic changes in blood flow effect their influence. The mechanisms involved in CBF regulation, i.e. cerebral autoregulation (i.e. mechanoregulation), chemoregulation, neurogenic regulation, and neurovascular coupling, mechanisms will be discussed in the next few paragraphs.

CEREBRAL AUTOREGULATION

In the late fifties of the last century, Lassen proposed the ‘classic’ concept of cerebral autoregulation (CA) which relates CBF to the cerebral perfusion pressure (CPP) [2]. The CPP is the difference between mean arterial blood pressure (MAP) at the base of the brain (i.e. the circle of Willis) and intracranial pressure, encompassing cerebral spinal fluid pressure and the central venous pressure [38]. The traditional CA curve suggests a constant CBF for a wide range of perfusion pressures via adaptations in the cerebrovascular resistance (Figure 2.2) [39]. Beyond the so-called pressure limits of regulation (e.g. lower and upper limit), autoregulation is lost and CBF changes proportionally to (the change in) MAP. It has been suggested that the lower limit is not a fixed value and that it may shift towards a higher MAP in hypertensive subjects [38] and vice versa to a lower MAP in patients with orthostatic hypotension related to sympathetic failure [38,40-44]. When the cerebral perfusion pressure falls below the lower limit of autoregulation, CBF decreases and cerebral ischemia ensues.

Within the normal physiological range, CA increases or decreases cerebrovascular tone in response to changes in CPP using a stretch sensing mechanism of the vascular smooth muscle cells (‘the Bayliss myogenic response’ [46]). Stretching of these cells is considered to induce the signals that provoke vasoconstriction while reduced transmural pressure leads to vasodilation. Although the stretch response is attributed to be an innate property of vascular smooth muscle cells [47], the exact underlying signaling pathways are incompletely defined.

To adapt to the brain’s metabolic demand on CBF in daily life, both fast and slower acting components of the CA are required. In the laboratory, static (hours to days) and dynamic (seconds to minutes) components of CA can be distinguished in either the time- or frequency domain. The dynamic component is assumed to reflect mainly the capacity to counteract the alterations in CBF in response to fast changes in blood pressure. This component operates within seconds, and represents the response delay of the cerebral vasoregulatory system [48].

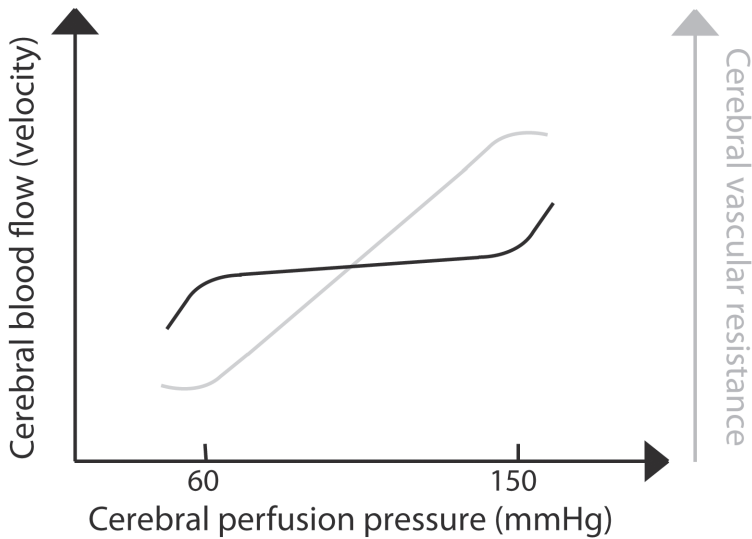


Figure 2.2 | The classical cerebral autoregulation curve describing the pressure-flow relationship for the brain. The CBF(v) is controlled to be more or less constant (the so-called autoregulatory plateau) via changes in the cerebrovascular resistance. Below and above the limits of autoregulation (<60 and >150 mmHg), the brain becomes 'pressure-passive' as represented by the linear portion of the curve. Modified from Lucas et al. 2010 [45].

CHEMOREGULATION

The brain vasculature is extremely sensitive to changes in carbon dioxide partial pressure (PaCO_2), designated as the cerebrovascular carbon dioxide responsiveness, and in a similar vein to and oxygen (PaO_2) [49-53]. Lowering vs. elevating the PaCO_2 (e.g. hypo- and hypercapnia) causes, respectively, vasoconstriction and vasodilatation of the arteries, leading to alterations in CBF. Conceptually, chemoregulation operates independently from the CA, but they may have common pathways and mechanisms [6,54-58]. The mechanism of chemoregulation is complex has not been fully clarified. For long it has been thought that the PaCO_2 -driven changes in pH modify CBF by direct relaxation and contraction of the smooth muscle [59-61]. There is, however, also data suggesting that PaCO_2 affects CBF both in combination with altered pH and with unaltered pH [56] (see for review [61]).

The sensitivity of CBF to changes in carbon dioxide (CO_2) is generally expressed as the percentage change per mmHg in PaCO_2 , and is often quantified non-invasively by relating changes in CBF(v) to alterations in end-tidal CO_2 [56]. In the normocapnic range, CBFv measured in the middle cerebral artery changes approximately 3.5% per mmHg change in end-tidal CO_2 [58,62-64].

NEUROGENIC REGULATION

Sympathetic nerves originating from the cervical ganglion abundantly innervate the cerebral arteries, but the role of the innervations in CBF control is still under debate [42,65,66]. It is assumed that under normal physiological conditions the influence of the central nervous system on CBF and its regulation is minor [66]. Increased sympathetic activation during exercise, however, is likely to enhance cerebral vascular tone thus counteracting imminent cerebral hyperperfusion as a consequence of an excessive increase in BP beyond the cerebral autoregulatory range [67-70]. Both sympathetic and cholinergic mechanisms are considered important for restricting the exercise-induced increase in cerebral perfusion on CBF without affecting the cerebral metabolic rate for oxygen (CMRO₂) [71,67].

NEUROVASCULAR COUPLING

Neuronal activation increases cerebral metabolic demand, i.e. the supply of oxygen and nutrients is rapidly adjusted by locally increasing the CBF, as the brain lacks extensive storage for energetic compounds [6,5,72-74]. This interplay of supply and demand implies a connection between neurons and the local vasculature, to which the term neurovascular coupling was coined. This process is probably mediated through the astrocytic end-feet that surround the arterioles [75-78]. In response to neuronal activation, elicited for example by a sensory stimulus, the CBF shows an overshoot with the supply transiently exceeding the demand, resulting in a local increase in oxygenation level. Imaging methods sensitive to either oxygen concentration such as BOLD fMRI or to CBF such as SPECT, PET and ASL, apply this principle in order to identify functional regions in the brain in relation to specific stimuli (e.g. fMRI). Although neurovascular coupling is often portrayed as being independent, interaction with the other regulatory mechanisms is likely, for example the local production of CO₂. The main distinguishing property of neurovascular coupling is the localized nature of this response.

CHAPTER 3

Methods

PARAMETERS

Investigation of the cardio- and cerebrovascular response to physiological stress requires (simultaneous) monitoring of systemic, cerebral and respiratory parameters. This chapter provides an overview of the parameters that were measured in the studies described in this thesis.

SYSTEMIC

Blood pressure

Continuous arterial blood pressure (BP) can be measured non-invasively by finger plethysmography (Nexfin, Edwards Lifesciences BMEYE, Amsterdam, the Netherlands) using a volume-clamp technique [79]. The cuff is placed around the midphalanx of the non-dominant hand and held at heart level. An optical plethysmograph in the finger cuff measured arterial volume continuously. The pressure in the cuff around the finger is adjusted in near real-time (~100 Hz) to keep the arterial volume clamped, allowing continuous tracking of the blood pressure. A height reference system is placed around a finger next to the cuff and at heart level to account for the hydrostatic pressure difference. To estimate changes in BP accurately over time, an automatic built-in calibration system (Physiocal) tracks the unloaded diameter of the finger artery to keep the arterial unloaded volume constant [80]. The arterial pressure measured at the finger is fundamentally different from brachial pressure both in absolute terms (hydrostatic difference) and wave shape, such that necessary corrections are applied in the Nexfin system to transform finger pressure into brachial pressure [81].

In case finger plethysmography is not available (for instance in the MR-environment), BP measurements were taken every 2–4 min using an inflatable arm-cuff (Magnitude, In-Vivo, Orlando, FL) while HR is continuously monitored by means of an MR-compatible finger pulse-oximetry unit.

Heart rate, stroke volume and cardiac output

A pulse contour method (Nexfin CO-trek, Edwards Lifesciences BMEYE, Amsterdam, the Netherlands) – adapted for age, sex, height and weight [82] – can provide left ventricular stroke volume (SV) and cardiac output (CO; SV multiplied by instantaneous HR). This method has been thoroughly validated against invasive thermodilution measurements [82,83]. In our work, Nexfin derived CO was validated by means of inert gas rebreathing (Innocor, Innovision A/S, Odense, Denmark) [84,85]. The rebreathing method relies on two inert gasses that are inhaled in tracer quantities through a bag. The blood-soluble N_2O diffuses into the lung capillaries and the blood insoluble NF_6 remains in the alveoli and air. The rate at which the soluble gas disappears from the bag is assumed to be equal to the CO of the left ventricle [86].

BRAIN

In this thesis, we assessed using two non-invasive modalities the CBF response to a variety of physiological challenges. The first modality, transcranial Doppler ultrasonography (TCD), provides high temporal resolution assessments of CBF velocity (CBFv) in large brain-feeding arteries. This method is a relatively simple and low-cost bedside technique and is assumed to provide accurate quantification of the mean CBF over a large area of the brain, that is, the flow territory perfused by the insonated artery. The second modality, MRI, provides techniques such as arterial spin labeling (ASL) and blood-oxygen-level dependent (BOLD) imaging which enable the measurement of whole brain CBF and oxygenation changes at the microvascular level. MRI is a complex, costly and time-consuming procedure that offers a non-invasive measure of brain perfusion and oxygenation at a high spatial resolution. A combination of TCD and MRI-based quantifications of CBF has the potential to complement each other in obtaining a more complete understanding of brain perfusion at both the macro- and microvascular level. In the following paragraphs we will discuss both modalities into more detail.

Middle cerebral artery blood flow velocity

Measuring CBFv in the basal cerebral arteries by TCD was introduced in the early eighties of the twentieth century by Aaslid and coworkers [87] and has found wide acceptance in both clinical and research settings. The ultrasound probe emits a high-pitched sound wave through the intact skull, which is then reflected from erythrocytes moving through ultrasound beam. The CBFv is recorded from the Doppler shift spectrum of the reflected sound waves [88]. Mean CBFv reports the velocity associated with the maximal frequency of the Doppler shift (“the envelope”), rather than the cross-sectional average velocity that defines the blood flow through the artery [89]. The average velocity can be obtained from the intensity-weighted mean flow velocity or the total signal power, but is sensitive to small changes in insonation angle of the artery [89]. Therefore, the maximum velocity is preferred as reported entity.

A TCD system (DWL Multidop X4, Sipplingen, Germany) with a pulsed ultrasound frequency of 2 MHz can be used to satisfactorily penetrate the skull. As the bone of the temporal region is thin and therefore the best promising area for ultrasound insonation [87]. CBFv measurements were localized in the proximal segments of the left or right middle cerebral artery (MCA). The ultrasound probe is placed on the temporal region of the skull just above the zygomatic arch (Figure 3.1). At an insonation depth between 45 and 60 mm, the signal is optimized. Subsequently, the probe is secured in position by a head-band.

The relation between calculated vs. actual CBFv depends on angle of insonation [90]. When the angle increases from 0° to 30°, its cosine will decrease from 1 to 0.86 resulting in a maximum error up to 15% [88]. By immobilizing the probe by a head-band, we minimized the influence of a potential change in angle as might occur during the experiments. An important issue of TCD whether blood flow velocity accurately reflects the actual underlying blood flow. Changes

in blood flow velocity reflect those in blood flow when the cross-sectional area of the insonated vessel remains constant (blood flow = blood flow velocity x cross-sectional area).

Vessel diameter does not change significantly during moderate variations in mean BP or CO₂ tension according to direct observations made during craniotomy [91]. Also orthostatic stress, as stimulated by lower body negative pressure (LBNP), does not induce detectable changes in the diameter of the MCA as observed with 3 Tesla MRI [92]. These findings suggest that the MCA diameter does not change and that changes in TCD-determined CBFv will track those in CBF. In three studies presented in **chapters 4-6**, we examined these assumptions under influence of carbon dioxide and sympathetic stimulation using high-resolution MRI at 7 Tesla.

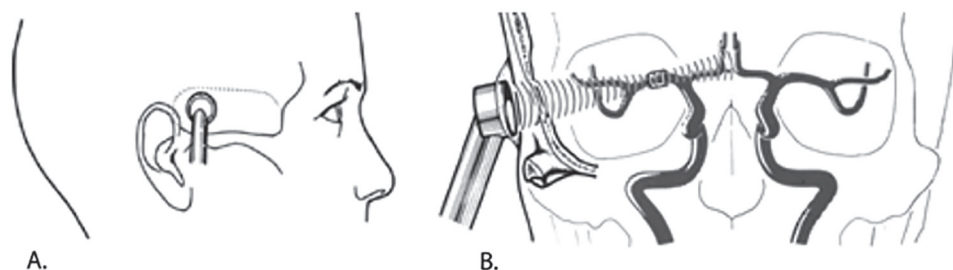


Figure 3.1 | The ultrasound probe is placed on the temporal region of the skull (dotted line indicates the ‘temporal window’) just above the zygomatic arch **A**). A frontal view of the ultrasound probe directed toward the MCA **B**). The cylindrical sample volume is indicated by a circle over the MCA, i.e. observation region; the distance from the middle of the cylinder to the probe corresponds to the depth setting. Reproduced from J Neurosurg [87].

Whole brain blood flow

Since the proposal of ASL two decades ago [93], the non-invasive quantification of regional CBF with MRI has progressively developed into a well-accepted and clinically suitable technique. ASL MRI is based on the detection of a tracer that is delivered to and cleared from the tissue by blood flow [94], and usually expressed in ml/min/100g tissue [95,96]. With ASL, an endogenous tracer is created by inverting the proton spins of blood, mainly located in water molecules (H₂O). Magnetic labeling of arterial blood water spins is done by a long series of radiofrequency pulses (in pseudo-continuous ALS) that are applied in a plane perpendicular to the neck. Subsequently, labeled protons in the arterial blood water act as (almost) freely diffusible tracers. From the labeling location the labeled protons migrate within 1–2 seconds via the arterial vessels and capillaries into the brain tissue where the label accumulates, thereby altering the local tissue magnetization. The change in tissue magnetization is measured by acquiring multiple image slices covering the whole brain and a comparison to an identical control scan in which the inflowing blood was

not labeled. A 3-dimensional perfusion map can be obtained by subtracting the labeled image volume from the control image volume (no label) (Figure 3.2).

The ASL-signal, i.e. the difference in signal intensity between label and control images, is small (~1%). To obtain a sufficient signal-to-noise ratio (SNR), many repetitions of the control and label pairs are acquired during 3–5 minutes. The ASL technique applied here is pseudo-continuous ASL, as the recommended standard for use in a clinical setting [96] and which has been recently compared with $^{15}\text{H}_2\text{O}$ positron emission tomography (PET) CBF measurements [97]. Background suppression RF pulses were used to enhance the SNR of the CBF signal. In addition, the imaging module was extended with an extra echo block to obtain the BOLD fMRI signal with minimal additional scan time [98]. The BOLD signal is mainly sensitive to the concentration of deoxy-hemoglobin, and also depends on blood flow, blood volume and tissue properties, such as diffusion. This makes this method less specific than ASL. Changes in ASL or BOLD determined regional are often used as proxy for neuronal activation [99]. **Chapter 7** describes a comparative study of the determination of the CBF changes upon small muscle group exercise as measured by either ASL MRI or TCD.

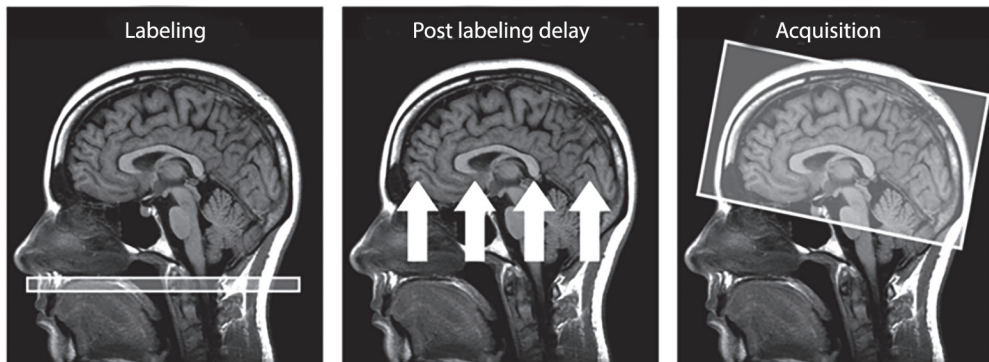


Figure 3.2 | Principle of arterial spin labeling. Arterial blood flowing to the brain is magnetically labeled in the neck by applying radiofrequency pulses. The labeled protons (i.e. water in arterial blood) flow to the brain tissue, where the labeled water protons mix and accumulate in the extravascular space and tissue. To allow the protons to reach the brain tissue, a delay time is applied (i.e. post labeling delay, PLD) after which the images are acquired, often with full brain coverage. The static brain tissue is subtracted by acquiring a separate set of control images. The control images are obtained without labeling the arterial blood. A full brain quantified ASL measurement requires multiple measurements of label and control images, and takes 3–5 minutes.

RESPIRATION

Brain perfusion is highly sensitive to changes in PaCO_2 (see section on Chemoregulation). To enable a correct interpretation of the CBF and CBFv responses, it is highly recommended to also monitor (changes in) PaCO_2 . The partial pressure of CO_2 in exhaled air (designated as end-tidal

CO_2 ; PetCO_2) is generally used as a non-invasive proxy for PaCO_2 and therefore measured in the studies described in this thesis.

Partial end-tidal carbon dioxide pressure

PetCO_2 is continuously monitored, via a nasal cannula, by a sampling infrared capnograph (Tonocap, Datex-Ohmeda, Madison, USA or Datex Normocap 200, Helsinki, Finland). This technique is based upon the absorption of infrared radiation by CO_2 , with the amount of absorbed radiation having a nearly exponential relation to the CO_2 concentration. Detecting a change in infrared radiation levels, using photo-detectors, allows for the calculation of the CO_2 concentration in the gas sample.

Physiological challenges

The present thesis discusses various physiological methods (including orthostatic stress tests, small muscle group exercise and inhalation of a gas mixture containing CO_2) that were applied to address autonomic cardio- and cerebrovascular control. This section summarizes these methods with respect to their known physiological mechanism and the way in which they were performed.

Orthostatic stress tests

Passive head-up tilt (HUT), lower body negative pressure (LBNP) and orthostasis (standing up) all lead to a gradual translocation of blood from the intra-thoracic region into the lower parts of the body. As a result, CO decreases and a series of cardiovascular regulating mechanisms and reflexes come into action to maintain arterial blood pressure and cerebral perfusion.

Passive head-up tilt

Passive HUT is performed with the subject lying supine and safely strapped on a tilt table (custom built by AMC Medical Technological Development / Dr. Kaiser Medizintechnik, Bad Hersfeld, Germany) and then either mechanically or manually tilted to a semi-supine (30°), semi-upright (45°) and/or almost completely upright (70°) position. Tilting back from 70° HUT to the supine position leads to central blood volume repletion and mimics a fluid challenge.

The bulk blood volume translocates between upper and lower body because the hydrostatic indifference point for intravascular pressure (i.e. point in the vascular tree at which pressure remains constant independent of body position) is located at the level of the diaphragm [100]. Moreover, blood volume measurements by electrical impedance suggest that the indifference point for volume as is even lower, positioned between the navel and iliac crest [101,100]. As a consequence, in upright position, roughly 70% of the blood volume is located below the level [100] of the heart. The translocated blood is mainly being contained in the (compliant) veins and venules and, therefore, does not contribute to the effective arterial blood volume [100,102]. This shift in blood volume distribution is estimated to be 300–800 ml of which 50% takes place within the first few seconds [34,103,104]. The central blood volume is challenged further by an estimated

10% or ~500 ml reduction after 5 min and 15% or ~750 ml reduction after another 5 minutes in the HUT position [105].

Lower body negative pressure

During LBNP, sub-atmospheric pressure is applied to the lower limbs in a supine subject such that blood redistributes from the upper parts of the body into the compliant compartment of the lower extremities. In preparation for LBNP, the lower body of the subject is positioned inside an LBNP box (Dr. Kaiser Medizintechnik, Bad Hersfeld, Germany / Dept. Instrumental Development, LUMC) and sealed at the level of the iliac crest [106]. An advantage of this technique compared to passive HUT, is its utilization within the static and horizontal setup of the MRI-scanner.

Standing up

The presumed mechanism behind the gravitational translocation of blood from the intra-thoracic region to the veins in the legs during passive HUT is similar to that when humans stand up from the supine position. However, the active change in posture during standing-up produces a hemodynamic response that is different from what happens with passive tilt during the first 30 s of upright posture [107].

Small muscle group exercise

Rhythmic handgrip exercise is a form of small muscle group exercise that increases HR and CO, with modest changes in blood pressure [108]. An advantage of rhythmic handgripping is that it can be performed in the supine position while ensuring minimal (head) motion, which makes it a suitable exercise method during MRI monitoring. Moreover, a mild to moderate handgrip exercise level can be maintained for a longer period of time to achieve the steady state needed for acquisition of ASL-measurements, which typically take about 3–5 minutes. To standardize the workload between individuals, the subjects were first instructed to squeeze a handgrip dynamometer (fOrb Gripforce, Current Designs Inc., Philadelphia PA, USA) to the maximum extent possible for 2–3 s without tensing the entire body. The so-measured maximum force was taken as 100%. The exercise experiments consisted of 0.5 Hz intermittent handgrip contractions performed for the first minute at 80% of the maximum force followed by 4 minutes at 60%. The decreasing force protocol was used to achieve a steady-state in minutes 3 to 5.

Inhalation of a gas mixture containing CO₂

In order to quantify the cerebral vasomotor reactivity, a wide range of PetCO₂ was established by, respectively, inhaling a gas mixture containing 5% CO₂ and 95% O₂ (carbogen) through a mouthpiece for 2 minutes, followed by 2 minutes of breathing room air and hyperventilating for approximately 2 minutes.

REFERENCE LIST

1. Scheinberg P, Stead EA (1949) The cerebral blood flow in male subjects as measured by the nitrous oxide technique. Normal values for blood flow, oxygen utilization, glucose utilization and peripheral resistance, with observations on the effect of tilting and anxiety. *J Clin Invest* 28:1163-1171
2. Lassen NA (1959) Cerebral blood flow and oxygen consumption in man. *Physiological Review* 39:183-238
3. Heiss WD, Rosner G (1983) Functional recovery of cortical neurons as related to degree and duration of ischemia. *AnnNeurol* 14 (3):294-301
4. Bernstein M, Fleming JF, Deck JH (1984) Cerebral hyperperfusion after carotid endarterectomy: a cause of cerebral hemorrhage. *Neurosurgery* 15 (1):50-56
5. Peterson EC, Wang Z, Britz G (2011) Regulation of cerebral blood flow. *IntJVascMed* 2011:823525
6. Willie CK, Tzeng YC, Fisher JA, Ainslie PN (2014) Integrative regulation of human brain blood flow. *J Physiol* 592 (Pt 5):841-859. doi:10.1113/jphysiol.2013.268953
7. Moskowitz MA, Lo EH, Iadecola C (2010) The science of stroke: mechanisms in search of treatments. *Neuron* 67 (2):181-198. doi:10.1016/j.neuron.2010.07.002
8. Bishop CC, Powell S, Insall M, Rutt D, Browse NL (1986) Effect of internal carotid artery occlusion on middle cerebral artery blood flow at rest and in response to hypercapnia. *Lancet* 1:710-712
9. van Buchem MA, Biessels GJ, Brunner la Rocca HP, de Craen AJ, van der Flier WM, Ikram MA, Kappelle LJ, Koudstaal PJ, Mooijaart SP, Niessen W, van Oostenbrugge R, de Roos A, van Rossum AC, Daemen MJ (2014) The heart-brain connection: a multidisciplinary approach targeting a missing link in the pathophysiology of vascular cognitive impairment. *Journal of Alzheimer's disease : JAD* 42 (0):S443-451. doi:10.3233/JAD-141542
10. Rickards CA (2015) Cerebral Blood-Flow Regulation During Hemorrhage. *Compr Physiol* 5 (4):1585-1621. doi:10.1002/cphy.c140058
11. Gorelick PB, Scuteri A, Black SE, Decarli C, Greenberg SM, Iadecola C, Launer LJ, Laurent S, Lopez OL, Nyenhuis D, Petersen RC, Schneider JA, Tzourio C, Arnett DK, Bennett DA, Chui HC, Higashida RT, Lindquist R, Nilsson PM, Roman GC, Sellke FW, Seshadri S (2011) Vascular contributions to cognitive impairment and dementia: a statement for healthcare professionals from the american heart association/american stroke association. *Stroke* 42 (9):2672-2713
12. Scheinberg P (1950) Cerebral circulation in heart failure. *Am J Med* 8:148-152
13. Vogels RL, Oosterman JM, Laman DM, Gouw AA, Schroeder-Tanka JM, Scheltens P, van der Flier WM, Weinstein HC (2008) Transcranial Doppler blood flow assessment in patients with mild heart failure: correlates with neuroimaging and cognitive performance. *Congestive heart failure* 14 (2):61-65
14. Loncar G, Bozic B, Lepic T, Dimkovic S, Prodanovic N, Radojicic Z, Cvorovic V, Markovic N, Brajovic M, Despotovic N, Putnikovic B, Popovic-Brkic V (2011) Relationship of reduced cerebral blood flow and heart failure severity in elderly males. *Aging Male* 14 (1):59-65
15. Choi BR, Kim JS, Yang YJ, Park KM, Lee CW, Kim YH, Hong MK, Song JK, Park SW, Park SJ, Kim JJ (2006) Factors associated with decreased cerebral blood flow in congestive heart failure secondary to idiopathic dilated cardiomyopathy. *AmJCardiol* 97 (9):1365-1369
16. Vogels RL, Scheltens P, Schroeder-Tanka JM, Weinstein HC (2007) Cognitive impairment in heart failure: a systematic review of the literature. *Eur J Heart Fail* 9 (5):440-449. doi:10.1016/j.ejheart.2006.11.001
17. Jefferson AL, Beiser AS, Himali JJ, Seshadri S, O'Donnell CJ, Manning WJ, Wolf PA, Au R, Benjamin EJ (2015) Low cardiac index is associated with incident dementia and Alzheimer disease: the Framingham Heart Study. *Circulation* 131 (15):1333-1339. doi:10.1161/circulationaha.114.012438
18. Bakker FC, Klijn CJ, van der Grond J, Kappelle LJ, Jennekens-Schinkel A (2004) Cognition and quality of life in patients with carotid artery occlusion: a follow-up study. *Neurology* 62 (12):2230-2235
19. Bakker FC, Klijn CJ, Jennekens-Schinkel A, van der Tweel I, Tulleken CA, Kappelle LJ (2003) Cognitive impairment in patients with carotid artery occlusion and ipsilateral transient ischemic attacks. *Journal of neurology* 250 (11):1340-1347. doi:10.1007/s00415-003-0222-1
20. Roman DD, Kubo SH, Ormaza S, Francis GS, Bank AJ, Shumway SJ (1997) Memory improvement following cardiac transplantation. *JClinExpNeuropsychol* 19 (5):692-697

21. Bornstein RA, Starling RC, Myerowitz PD, Haas GJ (1995) Neuropsychological function in patients with end-stage heart failure before and after cardiac transplantation. *Acta NeurolScand* 91 (4):260-265
22. Gruhn N, Larsen FS, Boesgaard S, Knudsen GM, Mortensen SA, Thomsen G, Aldershvile J (2001) Cerebral blood flow in patients with chronic heart failure before and after heart transplantation. *Stroke* 32 (11):2530-2533. doi:DOI 10.1161/hs1101.098360
23. Brassard P, Jensen AS, Nordsborg N, Gustafsson F, Moller JE, Hassager C, Boesgaard S, Hansen PB, Olsen PS, Sander K, Secher NH, Madsen PL (2011) Central and peripheral blood flow during exercise with a continuous-flow left ventricular assist device: constant versus increasing pump speed: a pilot study. *CircHeart Fail* 4 (5):554-560
24. Bhat G, Yost G, Mahoney E (2015) Cognitive function and left ventricular assist device implantation. *The Journal of heart and lung transplantation : the official publication of the International Society for Heart Transplantation* 34 (11):1398-1405. doi:10.1016/j.healun.2015.05.015
25. Ozdemir O, Soylu M, Durmaz T, Tosun O (2013) Early haemodynamic changes in cerebral blood flow after cardiac resynchronisation therapy. *Heart, lung & circulation* 22 (4):260-264. doi:10.1016/j.hlc.2012.10.009
26. Marshall RS, Festa JR, Cheung YK, Pavol MA, Derdeyn CP, Clarke WR, Videen TO, Grubb RL, Slane K, Powers WJ, Lazar RM (2014) Randomized Evaluation of Carotid Occlusion and Neurocognition (RECON) trial: main results. *Neurology* 82 (9):744-751. doi:10.1212/wnl.0000000000000167
27. Rowell LB (1986) *Human circulation: regulation during physical stress*. Oxford University Press, USA, Oxford
28. Guyenet PG (2006) The sympathetic control of blood pressure. *Nature reviews Neuroscience* 7 (5):335-346. doi:10.1038/nrn1902
29. Booth J (1977) A short history of blood pressure measurement. *Proceedings of the Royal Society of Medicine* 70 (11):793-799
30. Fick A (1870) Ueber die Messung des Blutquantums in den Herzventrikeln. In: *Verhandlungen der Physikalisch-medicinischen Gesellschaft in Wurzburg*. Physikalisch-medicinische Gesellschaft in Wurzburg, pp XVI-XVII
31. Truijen J, van Lieshout JJ, Wesselink WA, Westerhof BE (2012) Noninvasive continuous hemodynamic monitoring. *J Clin Monit Comput* 26 (4):267-278. doi:10.1007/s10877-012-9375-8
32. Lin HY, Freed D, Lee TW, Arora RC, Ali A, Almoustadi W, Xiang B, Wang F, Large S, King SB, Tomanek B, Tian G (2011) Quantitative assessment of cardiac output and left ventricular function by noninvasive phase-contrast and cine MRI: validation study with invasive pressure-volume loop analysis in a swine model. *Journal of magnetic resonance imaging : JMRI* 34 (1):203-210. doi:10.1002/jmri.22587
33. van Lieshout JJ, Harms MP, Pott F, Jenstrup M, Secher NH (2005) Stroke volume of the heart and thoracic fluid content during head-up and head-down tilt in humans. *Acta Anaesthesiol Scand* 49 (9):1287-1292. doi:10.1111/j.1399-6576.2005.00841.x
34. Truijen J, Bundgaard-Nielsen M, van Lieshout JJ (2010) A definition of normovolaemia and consequences for cardiovascular control during orthostatic and environmental stress. *Eur J Appl Physiol* 109 (2):141-157. doi:10.1007/s00421-009-1346-5
35. Guyton AC, Cowley AW, Norman AR, Coleman TG, Samar RE (1980) The arterial baroreceptor reflex, a pressure buffering system. In: Guyton AC (ed) *Circulatory physiology III. Arterial pressure and hypertension*. Saunders, W.B., Philadelphia, pp 248-265
36. Shepherd JT, Vanhoutte PM (1979) *The Human Cardiovascular System. Facts and concepts*. Raven Press, New York
37. Lanfranchi PA, Somers VK (2002) Arterial baroreflex function and cardiovascular variability: interactions and implications. *American Journal of Physiology - Regulatory, Integrative and Comparative Physiology* 283 (4):R815-R826
38. Van Lieshout JJ, Wieling W, Karemaker JM, Secher NH (2003) Syncope, cerebral perfusion, and oxygenation. *J Appl Physiol* 94 (3):833-848. doi:10.1152/jappphysiol.00260.2002
39. Fisher JP, Ogoh S, Young CN, Raven PB, Fadel PJ (2008) Regulation of middle cerebral artery blood velocity during dynamic exercise in humans: influence of aging. *J Appl Physiol* 105 (1):266-273
40. Thomas DJ, Bannister R (1980) Preservation of autoregulation of cerebral blood flow in autonomic failure. *Journal of Neurological Science* 44:205-212

41. Lipsitz LA, Gagnon M, Vyas M, Iloputaife I, Kiely DK, Sorond FA, Serrador JM, Cheng DM, Babikian V, Cupples LA (2005) Antihypertensive therapy increases cerebral blood flow and carotid distensibility in hypertensive elderly subjects. *Hypertension* 45 (2):216-221
42. Van Lieshout JJ, Secher NH (2008) Point: Counterpoint: Sympathetic activity does/does not influence cerebral blood flow. *Journal of Applied Physiology* 105 (4):1364-1366. doi:10.1152/jappphysiol.90597.2008
43. Daffertshofer M, Diehl RR, Ziems GU, Hennerici M (1991) Orthostatic changes of cerebral blood flow velocity in patients with autonomic dysfunction. *Journal of the Neurological Sciences* 104 (1):32-38
44. Zhang R, Witkowski S, Fu Q, Claassen JA, Levine BD (2007) Cerebral hemodynamics after short- and long-term reduction in blood pressure in mild and moderate hypertension. *Hypertension* 49 (5):1149-1155
45. Lucas SJ, Tzeng YC, Galvin SD, Thomas KN, Ogoh S, Ainslie PN (2010) Influence of changes in blood pressure on cerebral perfusion and oxygenation. *Hypertension* 55 (3):698-705
46. Bayliss WM (1902) On the local reaction of the arterial wall to changes of internal pressure. *J Physiol (Lond)* 28:220-231
47. Davis MJ, Hill MA (1999) Signaling mechanisms underlying the vascular myogenic response. *Physiol Rev* 79 (2):387-423
48. Panerai RB, Dawson SL, Potter JF (1999) Linear and nonlinear analysis of human dynamic cerebral autoregulation. *Am J Physiol* 277 (3 Pt 2):H1089-1099
49. Lennox WG, Gibbs EL (1932) Blood flow in brain and leg of man, and changes induced by alteration of blood gases. *Journal of Clinical Investigation* 11:1155-1177
50. Poulin MJ, Liang PJ, Robbins PA (1996) Dynamics of the cerebral blood flow response to step changes in end-tidal PCO₂ and PO₂ in humans. *Journal of Applied Physiology* 81 (3):1084-1095
51. Kety SS, Schmidt CF (1948) The effects of altered arterial tensions of carbon dioxide and oxygen on cerebral blood flow and cerebral oxygen consumption of normal young men. *J Clin Invest* 27:484-492
52. Tominaga S, Strandgaard S, Uemura K, Ito K, Kutsuzawa T (1976) Cerebrovascular CO₂ reactivity in normotensive and hypertensive man. *Stroke* 7 (5):507-510
53. Poulin MJ, Liang PJ, Robbins PA (1998) Fast and slow components of cerebral blood flow response to step decreases in end-tidal PCO₂ in humans. *Journal of Applied Physiology* 85 (2):388-397
54. Immink RV, Secher NH, van Lieshout JJ (2006) Cerebral autoregulation and CO₂ responsiveness of the brain. *Am J Physiol Heart Circ Physiol*, vol 291. doi:10.1152/ajpheart.00390.2006
55. Claassen JA, Levine BD, Zhang R (2009) Cerebral vasomotor reactivity before and after blood pressure reduction in hypertensive patients. *AmJHypertens* 22 (4):384-391
56. Immink RV, Pott FC, Secher NH, van Lieshout JJ (2014) Hyperventilation, cerebral perfusion, and syncope. *J Appl Physiol* 116 (7):844-851. doi:10.1152/jappphysiol.00637.2013
57. Fierstra J, Sobczyk O, Battisti-Charbonney A, Mandell DM, Poublanc J, Crawley AP, Mikulis DJ, Duffin J, Fisher JA (2013) Measuring cerebrovascular reactivity: What stimulus to use? *JPhysiol*. doi:jphysiol.2013.259150 [pii];10.1113/jphysiol.2013.259150 [doi]
58. Peebles K, Celi L, McGrattan K, Murrell C, Thomas K, Ainslie PN (2007) Human cerebrovascular and ventilatory CO₂ reactivity to end-tidal, arterial and internal jugular vein PCO₂. *J Physiol* 584 (Pt 1):347-357. doi:10.1113/jphysiol.2007.137075
59. Kontos HA, Wei EP, Raper AJ, Patterson JL, Jr. (1977) Local mechanism of CO₂ action of cat pial arterioles. *Stroke* 8 (2):226-229
60. Lassen NA (1968) Brain extracellular pH: the main factor controlling cerebral blood flow. *ScandJ ClinLab Invest* 22 (4):247-251
61. Yoon S, Zuccarello M, Rapoport RM (2012) pCO₂ and pH regulation of cerebral blood flow. *Front Physiol* 3:365. doi:10.3389/fphys.2012.00365
62. Kastrop A, Thomas C, Hartmann C, Schabet M (1997) Sex dependency of cerebrovascular CO₂ reactivity in normal subjects. *Stroke* 28 (12):2353-2356
63. Willie CK, Macleod DB, Shaw AD, Smith KJ, Tzeng YC, Eves ND, Ikeda K, Graham J, Lewis NC, Day TA, Ainslie PN (2012) Regional brain blood flow in man during acute changes in arterial blood gases. *J Physiol* 590 (Pt 14):3261-3275. doi:10.1113/jphysiol.2012.228551

64. Hoiland RL, Ainslie PN, Wildfong KW, Smith KJ, Bain AR, Willie CK, Foster G, Monteleone B, Day TA (2015) Indomethacin-induced impairment of regional cerebrovascular reactivity: implications for respiratory control. *J Physiol* 593 (5):1291-1306. doi:10.1113/jphysiol.2014.284521
65. Strandgaard S, Sigurdsson ST (2008) Point:Counterpoint: Sympathetic activity does/does not influence cerebral blood flow. Counterpoint: Sympathetic nerve activity does not influence cerebral blood flow. *J Appl Physiol* 105 (4):1366-1367
66. ter Laan M, van Dijk JM, Elting JW, Staal MJ, Absalom AR (2013) Sympathetic regulation of cerebral blood flow in humans: a review. *BrJAnaesth* 111 (3):361-367
67. Purkayastha S, Saxena A, Eubank WL, Hoxha B, Raven PB (2013) alpha1-Adrenergic receptor control of the cerebral vasculature in humans at rest and during exercise. *ExpPhysiol* 98 (2):451-461
68. Ogoh S, Hirasawa A, Raven PB, Rebuffat T, Denise P, Lericollais R, Sugawara J, Normand H (2015) Effect of an acute increase in central blood volume on cerebral hemodynamics. *Am J Physiol Regul Integr Comp Physiol* 309 (8):R902-911. doi:10.1152/ajpregu.00137.2015
69. Immink RV, van den Born BJ, van Montfrans GA, Koopmans RP, Karemaker JM, van Lieshout JJ (2004) Impaired cerebral autoregulation in patients with malignant hypertension. *Circulation* 110 (15):2241-2245. doi:10.1161/01.CIR.0000144472.08647.40
70. Immink RV, van den Born BJ, van Montfrans GA, Kim YS, Hollmann MW, van Lieshout JJ (2008) Cerebral hemodynamics during treatment with sodium nitroprusside versus labetalol in malignant hypertension. *Hypertension* 52 (2):236-240. doi:10.1161/HYPERTENSIONAHA.108.110395
71. Seifert T, Fisher JP, Young CN, D. H, Fadel PJ, Secher NH (2010) Indication for cholinergically mediated cerebral vasodilatation during static exercise in humans. *FASEB* 24:979.977
72. Fox PT, Raichle ME (1986) Focal physiological uncoupling of cerebral blood flow and oxidative metabolism during somatosensory stimulation in human subjects. *Proceedings of the National Academy of Sciences of the United States of America* 83 (4):1140-1144
73. Fox PT, Raichle ME, Mintun MA, Dence C (1988) Nonoxidative glucose consumption during focal physiologic neural activity. *Science* 241 (4864):462-464
74. Quistorff B, Secher NH, Van Lieshout JJ (2008) Lactate fuels the human brain during exercise. *FASEB J* 22 (10):3443-3449. doi:10.1096/fj.08-106104
75. Filosa JA, Iddings JA (2013) Astrocyte regulation of cerebral vascular tone. *AmJPhysiol Heart CircPhysiol* 305 (5):H609-H619. doi:ajpheart.003359.2013 [pii];10.1152/ajpheart.003359.2013 [doi]
76. Pellerin L, Magistretti PJ (1994) Glutamate uptake into astrocytes stimulates aerobic glycolysis: a mechanism coupling neuronal activity to glucose utilization. *ProcNatlAcadSciUSA* 91 (22):10625-10629
77. Magistretti PJ, Pellerin L (1999) Astrocytes couple synaptic activity to glucose utilization in the brain. *News Physiol Sci* 14:177-182
78. Magistretti PJ, Pellerin L, Rothman DL, Shulman RG (1999) Energy on demand. *Science* 283 (5401):496-497
79. Peñáz J (1992) Criteria for set point estimation in the volume clamp method of blood pressure measurement. *Physiol Res* 41 (1):5-10
80. Wesseling KH, De Wit B, Van der Hoeven GMA, Van Goudoever J, Settels JJ (1995) Physiological, calibrating finger vascular physiology for Finapres. *Homeostasis* 36 (2-3):67-82
81. Guelen I, Westerhof BE, Van Der Sar GL, Van Montfrans GA, Kiemeneij F, Wesseling KH, Bos WJ (2008) Validation of brachial artery pressure reconstruction from finger arterial pressure. *J Hypertension* 26 (7):1321-1327
82. Bogert LW, Wesseling KH, Schraa O, Van Lieshout EJ, de Mol BA, van Goudoever J, Westerhof BE, van Lieshout JJ (2010) Pulse contour cardiac output derived from non-invasive arterial pressure in cardiovascular disease. *Anaesthesia* 65 (11):1119-1125. doi:10.1111/j.1365-2044.2010.06511.x
83. Ameloot K, Van De Vijver K, Broch O, Van Regenmortel N, De Laet I, Schoonheydt K, Dits H, Bein B, Malbrain ML (2013) Nexfin noninvasive continuous hemodynamic monitoring: validation against continuous pulse contour and intermittent transpulmonary thermodilution derived cardiac output in critically ill patients. *Scientific World Journal* 2013:519080. doi:10.1155/2013/519080
84. Gabrielsen A, Videbæk R, Schou M, Damgaard M, Kastrop J, Norsk P (2002) Non-invasive measurement of cardiac output in heart failure patients using a new foreign gas rebreathing technique. *Clin Sci (Lond)* 102 (2):247-252

85. Bartels SA, Stok WJ, Bezemer R, Boksem RJ, van Goudoever J, Cherpanath TG, van Lieshout JJ, Westerhof BE, Karemaker JM, Ince C (2011) Noninvasive cardiac output monitoring during exercise testing: Nexfin pulse contour analysis compared to an inert gas rebreathing method and respired gas analysis. *J Clin Monit Comput* 25 (5):315-321. doi:10.1007/s10877-011-9310-4
86. Triebwasser JH, Johnson RL, Burpo RP, Campbell JC, Reardon WC, Blomqvist CG (1977) Noninvasive determination of cardiac output by a modified acetylene rebreathing procedure utilizing mass spectrometer measurements. *AviatSpace EnvironMed* 48 (3):203-209
87. Aaslid R, Markwalder TM, Nornes H (1982) Noninvasive transcranial Doppler ultrasound recording of flow velocity in basal cerebral arteries. *J Neurosurg* 57 (6):769-774
88. Moppett IK, Mahajan RP (2004) Transcranial Doppler ultrasonography in anaesthesia and intensive care. *British journal of anaesthesia* 93 (5):710-724. doi:10.1093/bja/ae205
89. Secher NH, Seifert T, Van Lieshout JJ (2008) Cerebral blood flow and metabolism during exercise: implications for fatigue. *J Appl Physiol* 104 (1):306-314. doi:10.1152/jappphysiol.00853.2007
90. Van Lieshout JJ (2005) Cerebrale perfusie en oxygenatie. In: Büller HR, Kastelein JJP, Stroes ESG (eds) *Vasculaire geneeskunde*. 2 edn. Van Zuiden Communications, Alphen aan den Rijn, pp 329-362
91. Giller CA, Bowman G, Dyer H, Mootz L, Krippner W (1993) Cerebral arterial diameters during changes in blood pressure and carbon dioxide during craniotomy. *Neurosurgery* 32 (5):737-741
92. Serrador JM, Picot PA, Rutt BK, Shoemaker JK, Bondar RL (2000) MRI measures of middle cerebral artery diameter in conscious humans during simulated orthostasis. *Stroke* 31 (7):1672-1678
93. Detre JA, Leigh JS, Williams DS, Koretsky AP (1992) Perfusion imaging. *Magnetic resonance in medicine* 23 (1):37-45
94. Aguirre GK, Detre JA, Wang J (2005) Perfusion fMRI for functional neuroimaging. *International review of neurobiology* 66:213-236. doi:10.1016/S0074-7742(05)66007-2
95. Chalela JA, Alsop DC, Gonzalez-Atavales JB, Maldjian JA, Kasner SE, Detre JA (2000) Magnetic resonance perfusion imaging in acute ischemic stroke using continuous arterial spin labeling. *Stroke* 31 (3):680-687
96. Alsop DC, Detre JA, Golay X, Gunther M, Hendrikse J, Hernandez-Garcia L, Lu H, MacIntosh BJ, Parkes LM, Smits M, van Osch MJ, Wang DJ, Wong EC, Zaharchuk G (2015) Recommended implementation of arterial spin-labeled perfusion MRI for clinical applications: A consensus of the ISMRM perfusion study group and the European consortium for ASL in dementia. *Magnetic resonance in medicine : official journal of the Society of Magnetic Resonance in Medicine / Society of Magnetic Resonance in Medicine* 73 (1):102-116. doi:10.1002/mrm.25197
97. Heijtel DF, Mutsaerts HJ, Bakker E, Schober P, Stevens MF, Petersen ET, van Berckel BN, Majoie CB, Booi J, van Osch MJ, Vanbavel E, Boellaard R, Lammertsma AA, Nederveen AJ (2014) Accuracy and precision of pseudo-continuous arterial spin labeling perfusion during baseline and hypercapnia: a head-to-head comparison with (1)(5)OH(2)O positron emission tomography. *NeuroImage* 92:182-192. doi:10.1016/j.neuroimage.2014.02.011
98. Ghariq E, Chappell MA, Schmid S, Teeuwisse WM, van Osch MJ (2014) Effects of background suppression on the sensitivity of dual-echo arterial spin labeling MRI for BOLD and CBF signal changes. *NeuroImage* 103:316-322. doi:10.1016/j.neuroimage.2014.09.051
99. Detre JA, Wang J (2002) Technical aspects and utility of fMRI using BOLD and ASL. *Clinical neurophysiology : official journal of the International Federation of Clinical Neurophysiology* 113 (5):621-634
100. Secher NH, Van Lieshout JJ (2005) Normovolaemia defined by central blood volume and venous oxygen saturation. *Clin Exp Pharmacol Physiol* 32 (11):901-910. doi:10.1111/j.1440-1681.2005.04283.x
101. Perko G, Payne G, Secher NH (1993) An indifference point for electrical impedance in humans. *Acta Physiologica Scandinavica* 148 (2):125-129
102. Shapiro MD, Nicholls KM, Groves BM, Kluge R, Chung HM, Bichet DG, Schrier RW (1985) Interrelationship between cardiac output and vascular resistance as determinants of effective arterial blood volume in cirrhotic patients. *Kidney Int* 28 (2):206-211
103. Kirsch K, Merke J, Hinghofer-Szalkay H (1980) Fluid volume distribution within superficial shell tissues along body axis during changes of body posture in man: the application of a new miniature plethysmographic method. *Pflügers Arch* 383 (3):195-201

104. Smith JJ, Ebert J (1990) General response to orthostatic stress. CRC Press, Boca Raton, Florida
105. Lundvall J, Bjerkhoel P, Quittenbaum S, Lindgren P (1996) Rapid plasma volume decline upon quiet standing reflects large filtration capacity in dependent limbs. *Acta Physiol Scand* 158 (2):161-167
106. Goswami N, Grasser E, Roessler A, Schneditz D, Hinghofer-Szalkay H (2009) The cardiovascular response to lower body negative pressure in humans depends on seal location. *Physiol Res* 58 (3):311-318
107. Wieling W (1988) Standing, orthostatic stress, and autonomic function. In: Bannister R (ed) *Autonomic failure. A textbook of clinical disorders of the autonomic nervous system*. Oxford University Press, Oxford, pp 308-320
108. Lewis SL, Taylor WF, Bastian BC, Graham RM, Pettinger WA, Blomqvist CG (1983) Haemodynamic responses to static and dynamic handgrip in normal subjects and after autonomic blockade. *Clin Sci* 64:593-599

CHAPTER

4

Assessment of middle cerebral artery diameter during hypocapnia and hypercapnia in humans using ultra high-field MRI

Jasper Verbree

Anne-Sophie G.T. Bronzwaer

Eidrees Ghariq

Maarten J. Versluis

Mat J. Daemen

Mark A. van Buchem

Albert Dahan

Johannes J. van Lieshout

Matthias J.P. van Osch

J Appl Physiol 117: 1084–1089, 2014.

DOI:10.1152/jappphysiol.00651.2014.

ABSTRACT

In the evaluation of cerebrovascular CO₂ reactivity measurements, it is often assumed that the diameter of the large intracranial arteries insonated by Transcranial Doppler (TCD) remains unaffected by changes in arterial CO₂ partial pressure. However, the strong cerebral vasodilatory capacity of CO₂ challenges this assumption, suggesting that there should be some changes in diameter, even if very small. Data from previous studies on effects of CO₂ on cerebral artery diameter (MCA) have been inconsistent.

In this study, we examined ten healthy subjects (5 female, 5 male, age 21–30 years). High resolution (0.2 mm in-plane) MRI scans at 7 Tesla were used for direct observation of the MCA diameter during hypocapnia: -1 kPa (-7.5 mmHg), normocapnia: 0 kPa (0 mmHg) and two levels of hypercapnia: +1 and +2 kPa (7.5 and 15 mmHg) with respect to baseline. The vessel lumen was manually delineated by two independent observers.

The results showed that the MCA diameter increased by $6.8 \pm 2.9\%$ in response to 2 kPa PetCO₂ above baseline. However, no significant changes in diameter were observed at the -1kPa ($-1.2 \pm 2.4\%$), and +1kPa ($+1.4 \pm 3.2\%$) levels relative to normocapnia. The non-linear response of the MCA diameter to CO₂ was fitted as a continuous calibration curve. Cerebral blood flow-changes measured by TCD could be corrected by this calibration curve using concomitant PetCO₂ measurements. In conclusion, the MCA diameter remains constant during small deviations of the end-tidal CO₂ pressures from normocapnia, but increases at higher PetCO₂ values.

Keywords

Transcranial Doppler; MRI; Hypocapnia; Hypercapnia; Angiography; Cerebral blood flow measurement.

INTRODUCTION

Over the past three decades, Transcranial Doppler (TCD) has been extensively used in clinical and research settings for non-invasive assessment of the vasodilatory capacity of the cerebral vasculature [1]. The cerebrovascular reactivity, defined as the change in cerebral blood flow (CBF) in response to a carbon dioxide (CO_2) challenge [2], represents the vasodilatory capacity of the cerebral vasculature to changes in arterial CO_2 partial pressure. It is often assumed that the diameter of the large insonated intracranial arteries remains unaffected by changes in arterial CO_2 partial pressure [3]. Based on this assumption, changes in blood flow velocity measured with TCD in response to a CO_2 challenge are considered directly proportional to the change in CBF. However, due to the quadratic dependency of the vessel cross-section area on the diameter, even small changes in diameter would translate to considerable errors in the measurement of CBF changes by TCD. Therefore the validity of this assumption is extremely important.

To test this fundamental assumption, various techniques have been employed to assess the effect of substances, such as CO_2 and acetazolamide, which are known to change the CBF, on the diameter of the middle cerebral artery (MCA). Angiographic studies [4-6] and intraoperative measurements [7] of the MCA demonstrated that arteries smaller than the MCA, but not the MCA itself, exhibit vasodilation in response to increases in arterial partial pressures of CO_2 . In contrast, comparisons of the blood flow velocity in the MCA with SPECT CBF measurements [8] or venous outflow [9] indicated an increase in MCA diameter during administration of CO_2 . However, these methods are indirect measures of the MCA diameter and it is unclear whether the data reflect true changes in diameter. Direct observations using MRI-based measurements in conscious humans did not show changes in MCA diameter during hypocapnia [3,10] nor during hypercapnia [3]. In addition, results from studies with the carbonic anhydrase inhibitor acetazolamide were also contradictory. Administration of acetazolamide leads to a decreased pulmonary removal of CO_2 from the blood leading to lower blood pH. One MRI study did not detect an increase in MCA diameter following acetazolamide administration [11], while a more recent study did report an increase in MCA diameter [12]. In summary, the results from the literature on the effects of arterial CO_2 partial pressure on MCA diameter are inconsistent.

One explanation for the contradictory findings might be the limited spatial resolution of the techniques used in the aforementioned studies in terms of detecting small changes in the MCA diameter. Another explanation might be the narrow CO_2 range used.

The purpose of the present study was to measure the MCA diameter for a wide range of end-tidal CO_2 pressures with high resolution MRI at 7 Tesla and, if changes are present, to use these data to construct a calibration curve for TCD-based blood flow velocity measurements.

METHODS

Subjects

Ten healthy subjects (5 female, 5 male), aged 21–30 years, were scanned and written informed consent was obtained. Subjects refrained from drinking caffeinated beverages and eating for at least two hours prior to the experiment. The protocol was approved by the Medical Ethics Committee of the Leiden University Medical Center.

Measurements

A gas mixture containing 21% oxygen, 79–71% nitrogen and 0–8% CO₂ was administered to the subject through a silicone face mask. End-tidal CO₂ pressure (PetCO₂) was measured through a cannula attached to the mask and connected to a capnograph (Capnomac Ultima, Datex, Helsinki, Finland) located outside the MRI scanner room. Heart rate and oxygen saturation were continuously monitored and blood pressure measurements were taken every 2–4 minutes using an inflatable arm-cuff (Magnitude, In-Vivo, Orlando, Florida, USA).

Protocol

Baseline PetCO₂ was measured during 5 minutes of rest inside the MRI scanner. Subsequently, four levels of PetCO₂ were applied in random order. PetCO₂ was varied by inhalation of CO₂ and/or hyperventilation. The target PetCO₂ levels consisted of -1 kPa (-7.5 mmHg), 0 kPa (0 mmHg), +1 kPa and +2 kPa (+7.5 and +15 mmHg) relative to the subject's baseline PetCO₂. The PetCO₂ was kept constant during the high resolution scans by manually adjusting the CO₂ concentration of the inspired air [13]. The desired level of PetCO₂ was established for at least 30 seconds prior to the scan to ensure that a steady state level had been reached before the start of acquisition. Subjects were asked to breathe deeply and keep a constant breathing frequency aided by visual and auditory stimuli inside the scanner.

MRI acquisition

All experiments were performed on a 7 Tesla whole body Philips Achieva MRI system (Philips Healthcare, Best, The Netherlands). The MCA was identified on orthogonally reconstructed axial 3D T₁-weighted scans. The parameters for the 3D T₁-weighted were: repetition time / echo time = 4.1 / 1.84 ms, flip angle = 7°, field-of-view = 246 x 246 x 174 mm³, voxel size = 1 x 1 x 1 mm³, scan duration 2 min. The high resolution 2D-scan was planned perpendicular to the MCA and had the following parameters: black blood T₂-weighted Turbo Spin Echo (TSE), repetition time / echo time = 2000/116 ms, refocusing angle = 110°, field-of-view = 240 x 180 x 5 mm³, acquisition matrix = 1200 x 900, voxel size = 0.2 x 0.2 x 5 mm³, TSE factor = 12 with additional 4 startup echoes, dynamics = 2, total scan duration = 5 min.

Data analysis

Two independent observers (JV & AGTB), blinded to subject and PetCO₂ level, manually delineated the MCA lumen on the high resolution MRI scan. Within- and between observer agreement was

assessed by the Intraclass Correlation Coefficient (ICC_{2,1}, SPSS v20, SPSS Inc., Chicago, Illinois, USA). The average value of all observations per vessel was used in subsequent analysis. Data analysis was performed offline using MATLAB (vR2012a, Mathworks, Natick, Massachusetts, USA). The absolute translation and rotation with respect to the first scan of each subject were assessed using the FSL FLIRT routine (v5.0, fMRIB, Oxford, United Kingdom) with three degrees of freedom.

For each subject the MCA diameter (D) was determined from the lumen area (A), using: $D = \sqrt{4A / \pi}$. Additionally, the lumen area was expressed relative to the lumen area during normocapnia using: $A_{\text{normalized}} = A / A_{\text{normocapnia}} \cdot 100\%$, with $A_{\text{normocapnia}}$ the lumen area during normocapnia. The ΔPetCO_2 was defined for each subject as the absolute difference with respect to normocapnia.

The effect of PetCO_2 level on vessel diameter was assessed using a mixed-effects model with post-hoc comparisons (SPSS v20, SPSS Inc., Chicago, Illinois, USA). All multiple comparisons were Bonferroni-corrected and a p-value less than 0.05 was considered significant.

The normalized vessel area was fitted using a third order polynomial curve and compared to a linear model. Goodness-of-fit was assessed with the R-square (R^2) statistic adjusted for the number of degrees-of-freedom.

RESULTS

All ten subjects successfully completed the entire protocol and a total of 40 scans were acquired. Three subjects reported slight discomfort at +2 kPa, upon which the highest PetCO_2 level was lowered. In one of these subjects the PetCO_2 had to be lowered to values which were not appropriate to the study, and this scan was excluded from analysis. One further scan was excluded by both observers because of severe motion artefacts at the highest PetCO_2 level. The remaining 38 scans were included in the full analysis.

The effects of PetCO_2 on MCA diameter, heart rate and mean arterial pressure are given in Table 4.1. Four distinct levels of PetCO_2 were achieved ($p < 0.01$) with a minor increase in PetCO_2 during normocapnia compared to baseline (0.17 kPa; $p = 0.014$). Varying the PetCO_2 did not affect heart rate ($p = 0.187$) or mean arterial pressure ($p = 0.078$). The image quality was sufficient to be able to visualize and outline the vessel lumen for all PetCO_2 conditions (Figure 4.1). The absolute displacements of the head relative to the first scan were 1.6 mm and 2.3 mm in the x and y directions, respectively, with a small in-plane rotation of 0.7° . Within-observer agreement was very high for both observers, ICC = 0.94 and 0.97 for JV and AGTB respectively. Measurements were also consistent between observers, ICC = 0.86, albeit with a significant mean difference of 0.16 mm ($p < 0.001$, paired t -test).

Table 4.1 | Effects of PetCO₂ on hemodynamic variables and middle cerebral artery diameter.

	Diameter (mm)	PetCO ₂ (kPa)	HR (bpm)	MAP (mmHg)
Baseline		4.9±0.5	67.5±11.7	81.7±4.7
Hypocapnia	3.19±0.27	3.8±0.5 [†]	69.0±12.9	83.9±7.0
Normocapnia	3.23±0.26	5.1±0.5 [†]	67.1±12.4	83.4±7.0
Mild hypercapnia	3.28±0.33	6.0±0.5 [†]	67.3±12.5	84.1±6.2
Moderate hypercapnia (N=8)	3.42±0.33*	6.8±0.6 [†]	70.2±12.3	88.0±6.3

Data (N=10) are represented as mean ± SD. *p<0.001 vs hypo- (-1 kPa), normo- (+0 kPa), and hypercapnia (-1 kPa). [†]p<0.001 vs baseline condition. (Bonferroni-corrected)

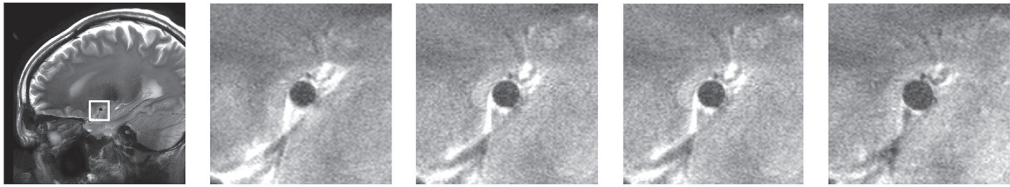


Figure 4.1 | Representative example of high resolution MRI scans planned perpendicular to the MCA. From left to right: the white square depicts the location of the zoomed images; zoomed image at hypocapnia (-1 kPa), baseline normocapnia (0 kPa), and hypercapnia (+1 and +2 kPa end-tidal CO₂) respectively.

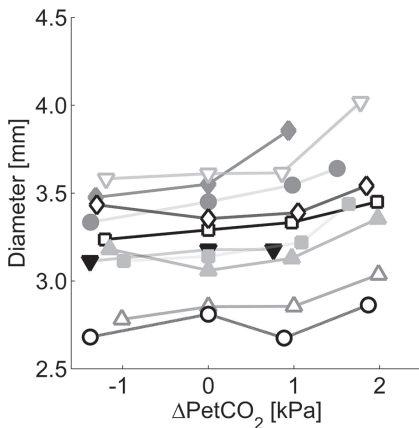


Figure 4.2 | Effect of Δ PetCO₂ (kPa) on absolute middle cerebral artery diameter (MCA). The Δ PetCO₂ is relative to the subject's resting baseline in the scanner. Variation in MCA diameter can be observed between subjects. Different subjects are indicated with distinct symbol and color.

There was a significant effect of PetCO₂ level on MCA diameter ($p < 0.001$, Figure 4.2) with a $6.8 \pm 2.9\%$ increase in vessel diameter at +2 kPa hypercapnia. No significant differences were observed at -1 kPa hypocapnia ($-1.2 \pm 2.4\%$), or +1 kPa hypercapnia ($+1.4 \pm 3.2\%$) compared to normocapnia. The effect of Δ PetCO₂ on normalized vessel area is depicted in Figure 4.3. The normalized lumen areas for the -1, +1 and +2 kPa PetCO₂ levels relative to normocapnia were $98 \pm 5\%$, $103 \pm 6\%$ and $114 \pm 6\%$, respectively. A non-linear PetCO₂ – MCA cross-sectional area relationship was established using a third-order model (R^2_{adj} of 0.51 versus a R^2_{adj} of 0.44 for a linear relation) with the normalized MCA area (y) approximated by: $y = 0.93x^3 + 1.22x^2 + 1.99x + 99.64$, where x denotes Δ PetCO₂ in kPa.

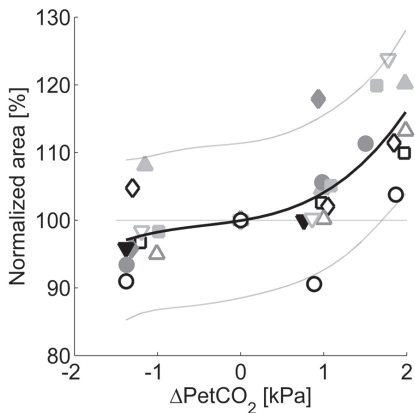


Figure 4.3 | Effect of Δ PetCO₂ (kPa) on middle cerebral artery (MCA) area relative to normocapnia. The MCA area is expressed as a percentage of normocapnia and the Δ PetCO₂ is relative to the subject's resting baseline in the scanner. The data is modeled with a 3rd order polynomial (thick-line) and 95% confidence interval (dotted-lines). Identical symbols as in Figure 4.2 are used.

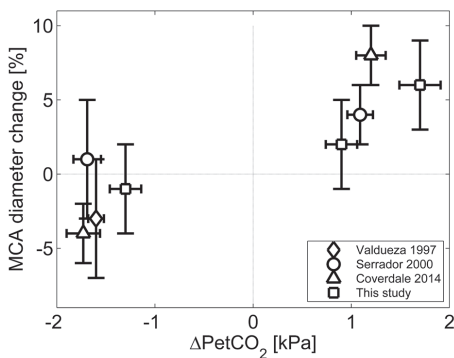


Figure 4.4 | Graphical summary of MRI studies directly observing the MCA during CO₂ challenges [3,10,17]. Data are presented as percentage change in diameter as function of PetCO₂ (mean \pm SEM). Data from Serrador et al. [3] are derived from their Figure 4.3. All studies employed PetCO₂ measurements with exception of Valdueza et al. [10] that used PaCO₂. PaCO₂ is comparable to PetCO₂ during hypocapnia [23].

DISCUSSION

The major finding of the present study is the non-linear behavior of the MCA in response to hypercapnia with (proximal) vasodilatation at a PetCO_2 level of +2 kPa above normocapnia, and constancy of the MCA diameter in the lower PetCO_2 range (-1 to +1 kPa). The clinical implication is that the often-assumed constant value of the MCA diameter linking TCD blood flow velocity measurements to CBF is not valid for PetCO_2 levels between +1 and +2 kPa, leading to underestimation of the underlying CBF response.

The present data complements those from Serrador et al. [3] by extending the PetCO_2 range to +2 kPa hypercapnia. Data from the present study confirm their earlier observations that the MCA diameter does not change in the lower PetCO_2 range up to 1 kPa above baseline. This result has also been confirmed using a variety of methodologies, including angiography [4,6,5], surgical microscopy [7], TCD [9,14-16] and MRI [3,10]. A recent MRI study by Coverdale et al. [17], investigated the MCA diameter response to 6% CO_2 inhalation. Whereas the present study detected a significant difference in MCA diameter of 6.8% at the highest PetCO_2 level (+2kPa), they observed an 8% increase at a lower PetCO_2 of +1.2 kPa. Moreover, they indicated a significant decrease in diameter of -4% during hypocapnia (-1.7 kPa), whereas the present study observed a non-significant decrease of -1.2% at a slightly milder hypocapnia level of -1.3 kPa. To reduce the subject dependent reaction to a fixed CO_2 step (e.g. inhalation of 6% CO_2), the present study employed controlled PetCO_2 levels relative to the baseline of each subject. Together with a higher resolution and larger observed mean diameter in the present study this might explain the differences in the observed MCA diameter changes between the two studies. Both studies used similar subject population and MRI acquisition technique, suggesting strongly that the MCA diameter is responsive to PetCO_2 levels above +1 kPa. This is in line with a previous observation in the +2 kPa PetCO_2 range using color Doppler [18], which found an increase in the carotid artery diameter, in turn suggesting that the vasoactive effects of $P_a\text{CO}_2$ are not limited to the smaller cerebral arteries [4-7].

In order to place the MCA diameter changes observed in the present study into context, the results from the present study and previous literature are graphically depicted in Figure 4.4. Data are taken from those studies that directly observed the MCA using MRI [3,10,17]. During hypercapnia all studies observed an increased diameter, although this was not statistically significant in all studies. During hypocapnia the observations are more variable, suggesting that the diameter changes, if present, might be small compared to changes observed during hypercapnia. Based on physiological principles, it might be expected that the MCA diameter – PetCO_2 relation would be sigmoidal [19]. However, an upper and lower bound to the MCA diameter changes are not established by the current data.

The cerebrovascular reactivity is defined as the increase in CBF per unit CO_2 [2]. Inhalation of 5–6% CO_2 is a common method to quantify the cerebrovascular reactivity, and increases the PetCO_2

by 1 to 2 kPa [8,20], with a 3.8%/mmHg increase in CBF in healthy subjects [19]. This implies a CBF increase of 57% at +2 kPa, which should be compared to an underestimation of 14% of the CBF-change by TCD due to the increase in MCA diameter (6.8%). The accuracy of such TCD measurements is diminished if this bias is not accounted for. Clinical guidelines currently do not correct for diameter changes at higher levels of PetCO₂ and the new data on the PetCO₂ – MCA diameter relation may be of particular importance for cerebrovascular reactivity measurements in a multi-modal setting.

Among the strengths of the present study is the relatively high in-plane resolution of 0.2 mm that enabled the detection of a mean increase in MCA diameter of 6.8%. The physical resolution of previous studies ranges from 0.27 mm [11] to up 0.7 mm [4,10], which, based on our diameter measurements, corresponds to a detection limit of 8.5%–22%. The sensitivity and limited range of PetCO₂ levels in previous studies may have prevented the detection of small changes in diameter. In the present study no changes in MCA diameter between -1 to +1 kPa PetCO₂ compared to baseline levels were identified. This may well be in agreement with other studies, but we cannot exclude that conclusion that the absence of an observed diameter change in the lower PetCO₂ ranges could still be related to technical limitations, such as the spatial resolution of 0.2 mm.

The calibration curve, as presented in Figure 4.3, can directly be related to an over- or underestimation of the CBF-change measured by TCD. For practical purposes the non-linear relationship between arterial cross-sectional area and PetCO₂ was approximated by a third order polynomial curve without prior physiological assumptions, enabling the possibility to correct TCD measurements by concurrent PetCO₂ measurements. This assumes that a smooth fit to all available data points best approximates the underlying physiological response, even though only at the highest PetCO₂ level was a significant difference in MCA diameter found. The variation observed between subjects in relative area changes might suggest that the sensitivity to PetCO₂ is subject-specific. This variation gives rise to the large confidence intervals of the calibration curve.

Whether (small) MCA diameter changes are of practical value depends on the precision of the TCD and PetCO₂ measurements and the change in CBF that is considered relevant in a clinical or scientific context. Continuous TCD measurements are quite stable during rest, provided that the probe is adequately fixed to the head. The uncertainty (standard error of the mean) of TCD flow velocity measurements during 3 consecutive 1-minute recordings is, on average, 1% [10 subjects, unpublished data]. An underestimate of 1% in the CBF determination, due to the concomitant increase in MCA diameter, corresponds to the Δ PetCO₂ being higher than +0.4 kPa according to the calibration curve. This value should be compared to the typical precision of PetCO₂ measurements of 0.24 kPa [present study, unpublished data]. At a Δ PetCO₂ of +0.4 kPa and a precision of 0.48 kPa (2 times standard deviation) the calibration curve gives a 1% uncertainty in the vessel cross-sectional area. Therefore, without more precise PetCO₂ measurements area, changes smaller than 1% do not improve the accuracy of CBF-changes measured by TCD. However, an underestimation of 1% is one order magnitude smaller than the flow-changes expected in clinical practice.

Several limitations exist in this study. First, the sensitivity of the MRI contrast to in- or outflow of blood might affect the apparent diameter of the MCA. In the current study black-blood imaging was used, which is inherently dependent on the outflow of blood and gives a complete signal void in the vessel lumen when the blood flow velocity is sufficiently high [21]. The use of four startup echoes and long echo time further reduces the value of the minimum blood flow velocity for which a signal void occurs. Additionally, the observed contrast of the vessel lumen in the present study is consistent for all PetCO₂ levels. Therefore, it can be assumed that the effect of blood flow on the diameter measurements was negligible. It should be noted that some earlier studies [10-12] used time-of-flight (TOF) imaging to assess the vessel diameter. In TOF imaging the brightness and extent of the vessel depends on the inflow of blood [22]. Hence, the apparent diameter of the vessel is influenced by the blood flow through the vessel, which is strongly dependent on the PetCO₂ level. Therefore, black-blood imaging, as used in the current study, should be considered more suitable to measure vessel diameter during PetCO₂ variation.

During normocapnia and hypercapnia a difference exists between the measured PetCO₂ and the arterial CO₂ partial pressure (PaCO₂) [23], which could have introduced some variation in the MCA diameter measurements. In a fixed body position, the PetCO₂ – PaCO₂ relation is linear [23-25]. In the present study the subjects remained in the supine position and breathing rate and depth was controlled by visual and auditory stimuli. Therefore, a linear relation between PaCO₂ and PetCO₂ was assumed. Little or no influence of the PaCO₂ – PetCO₂ difference is expected on the variability of the MCA diameter measurements. In most applications PetCO₂ is readily available, making it a more suitable parameter for accounting for the effect of CO₂ on flow-change measurements by TCD.

Subject head-motion between individual scans could introduce errors in the lumen area measurements. This motion would lead to a non-perpendicular intersection of the imaging slice with the MCA, leading to an overestimation of the lumen area. This study used a 2D-scan planned perpendicular to the MCA. Therefore it was not possible to assess the head motion for any out-of-plane translations and rotations. To estimate the potential impact of such motions, the extent of in-plane motion was used as a proxy for the out-of-plane translation and rotations. Limited in-plane translation and rotation was observed. Therefore, by extension, overall head motion and out-of-plane movement between scans was deemed to be small. Moreover, the image quality was consistent between dynamics and only one out of total 40 scans was excluded due to poor image quality caused by movement artefacts. Therefore, head motion is considered only a minor concern for this study.

This study was performed in a relatively small number (N=10) of young healthy subjects. Increased age has been associated with cardiovascular degradation including atherosclerotic changes and arterial stiffening [26], which reduces the ability of the arteries to vasoconstrict and vasodilate. Therefore, the vasodilatory response of the MCA to CO₂ might be reduced in an older population compared to the young subjects measured in the present study. This might be one of the

explanations for the discrepancy between the results obtained by Schreiber [11] in a population with internal carotid stenosis with mean age of 62 years compared to the present study with a mean age of 23 years. Finally, only the MCA was considered in the present study. The protocol was limited to one artery due to constraints on the total examination time per subject. The MCA is a common target for TCD insonation as it supplies a large part of the cerebral hemisphere. It is currently unknown whether the observed diameter changes of the MCA could be extrapolated to other cerebral arteries, such as the anterior- and posterior cerebral arteries.

CONCLUSION

This study found a non-linear vasodilatory response of the middle cerebral artery diameter under hypercapnic conditions. High resolution MR imaging at 7 Tesla in combination with CO₂ inhalation was able to measure the vasodilatory effect at a PetCO₂ level of +2 kPa above baseline, but not during -1 kPa (hypocapnia) or +1 kPa (hypercapnia). This indicates that the blood flow velocity changes measured with TCD underestimate underlying changes in CBF under high hypercapnic conditions. The proposed calibration curve can be used to correct such underestimations of CBF changes measured by TCD.

Acknowledgements

The authors would like to thank Dr. Erik Olofsen (Department of Anesthesiology, LUMC) and Mr. R. Gips (Department of Instrumentation, LUMC) for their help with the set-up of the MRI-compatible gas delivery system, and Mr. H.J.F. Van de Stadt (Department of Instrumentation, LUMC) for creating the MRI-compatible gas delivery masks.

REFERENCES LIST

1. Ringelstein EB, Sievers C, Ecker S, Schneider PA, Otis SM (1988) Noninvasive assessment of CO₂-induced cerebral vasomotor response in normal individuals and patients with internal carotid artery occlusions. *Stroke* 19:963-969
2. Markwalder TM, Grolimund P, Seiler RW, Roth F, Aaslid R (1984) Dependency of blood flow velocity in the middle cerebral artery on end-tidal carbon dioxide partial pressure—a transcranial ultrasound Doppler study. *J Cereb Blood Flow Metab* 4:368-372
3. Serrador JM, Picot PA, Rutt BK, Shoemaker JK, Bondar RL (2000) MRI measures of middle cerebral artery diameter in conscious humans during simulated orthostasis. *Stroke* 31 (7):1672-1678
4. Djurberg HG, Seed RF, Evans DA, Brohi FA, Pyper DL, Tjan GT, al Moutaery KR (1998) Lack of effect of CO₂ on cerebral arterial diameter in man. *Journal of Clinical Anesthesia* 10:646-651
5. Bradac GB, Simon RS, Heidsieck CH (1976) Angiographically verified transient alteration of the intracranial arteries and veins in dependence of different CO₂ tensions. *Neuroradiology* 10 (5):257-262
6. Huber P, Handa J (1967) Effect of contrast material, hypercapnia, hyperventilation, hypertonic glucose and papaverine on the diameter of the cerebral arteries. Angiographic determination in man. *Invest Radiol* 2 (1):17-32
7. Giller CA, Bowman G, Dyer H, Mootz L, Krippner W (1993) Cerebral arterial diameters during changes in blood pressure and carbon dioxide during craniotomy. *Neurosurgery* 32 (5):737-741
8. Sorteberg W, Lindegaard KF, Rootwelt K, Dahl A, Nyberg-Hansen R, Russell D, Nornes H (1989) Effect of acetazolamide on cerebral artery blood velocity and regional cerebral blood flow in normal subjects. *Acta Neurochir (Wien)* 97 (3-4):139-145
9. Valdueza JM, Draganski B, Hoffmann O, Dirnagl U, Einhaupl KM (1999) Analysis of CO₂ vasomotor reactivity and vessel diameter changes by simultaneous venous and arterial Doppler recordings. *Stroke* 30:81-86
10. Valdueza JM, Balzer JO, Villringer A, Vogl TJ, Kutter R, Einhaupl KM (1997) Changes in blood flow velocity and diameter of the middle cerebral artery during hyperventilation: assessment with MR and transcranial Doppler sonography. *AJNR Am J Neuroradiol* 18 (10):1929-1934
11. Schreiber SJ, Gottschalk S, Weih M, Villringer A, Valdueza JM (2000) Assessment of blood flow velocity and diameter of the middle cerebral artery during the acetazolamide provocation test by use of transcranial Doppler sonography and MR imaging. *Am J Neuroradiol* 21 (7):1207-1211
12. Bokkers RP, Wessels FJ, van der Worp HB, Zwanenburg JJ, Mali WP, Hendrikse J (2011) Vasodilatory capacity of the cerebral vasculature in patients with carotid artery stenosis. *AJNR Am J Neuroradiol* 32 (6):1030-1033
13. Dahan A, Nieuwenhuijs D, Teppema L (2007) Plasticity of central chemoreceptors: effect of bilateral carotid body resection on central CO₂ sensitivity. *PLoS medicine* 4 (7):e239. doi:10.1371/journal.pmed.0040239
14. Aaslid R, Lindegaard KF, Sorteberg W, Nornes H (1989) Cerebral autoregulation dynamics in humans. *Stroke* 20 (1):45-52
15. Poulin MJ, Liang PJ, Robbins PA (1996) Dynamics of the cerebral blood flow response to step changes in end-tidal PCO₂ and PO₂ in humans. *Journal of Applied Physiology* 81 (3):1084-1095
16. Poulin MJ, Robbins PA (1996) Indexes of flow and cross-sectional area of the middle cerebral artery using doppler ultrasound during hypoxia and hypercapnia in humans. *Stroke* 27 (12):2244-2250
17. Coverdale NS, Gati JS, Opalevych O, Perrotta A, Shoemaker JK (2014) Cerebral blood flow velocity underestimates cerebral blood flow during modest hypercapnia and hypocapnia. *Journal of applied physiology* (Bethesda, Md : 1985) 117 (10):1090-1096. doi:10.1152/jappphysiol.00285.2014
18. Willie CK, Macleod DB, Shaw AD, Smith KJ, Tzeng YC, Eves ND, Ikeda K, Graham J, Lewis NC, Day TA, Ainslie PN (2012) Regional brain blood flow in man during acute changes in arterial blood gases. *J Physiol* 590 (Pt 14):3261-3275. doi:10.1113/jphysiol.2012.228551
19. Ainslie PN, Duffin J (2009) Integration of cerebrovascular CO₂ reactivity and chemoreflex control of breathing: mechanisms of regulation, measurement, and interpretation. *Am J Physiol Regul Integr Comp Physiol* 296 (5):R1473-R1495

20. Kastrup A, Kruger G, Neumann-Haefelin T, Moseley ME (2001) Assessment of cerebrovascular reactivity with functional magnetic resonance imaging: comparison of CO₂ and breath holding. *Magn Reson Imaging* 19 (1):13-20
21. Jara H, Yu BC, Caruthers SD, Melhem ER, Yucel EK (1999) Voxel sensitivity function description of flow-induced signal loss in MR imaging: implications for black-blood MR angiography with turbo spin-echo sequences. *Magnetic resonance in medicine: official journal of the Society of Magnetic Resonance in Medicine / Society of Magnetic Resonance in Medicine* 41 (3):575-590
22. Parker DL, Yuan C, Blatter DD (1991) MR angiography by multiple thin slab 3D acquisition. *Magnetic resonance in medicine : official journal of the Society of Magnetic Resonance in Medicine / Society of Magnetic Resonance in Medicine* 17 (2):434-451
23. Peebles K, Celi L, McGrattan K, Murrell C, Thomas K, Ainslie PN (2007) Human cerebrovascular and ventilatory CO₂ reactivity to end-tidal, arterial and internal jugular vein PCO₂. *J Physiol* 584 (Pt 1):347-357. doi:10.1113/jphysiol.2007.137075
24. Immink RV, Pott FC, Secher NH, van Lieshout JJ (2014) Hyperventilation, cerebral perfusion, and syncope. *J Appl Physiol* 116 (7):844-851. doi:10.1152/jappphysiol.00637.2013
25. Immink RV, Truijen J, Secher NH, Van Lieshout JJ (2009) Transient influence of end-tidal carbon dioxide tension on the postural restraint in cerebral perfusion. *Journal of applied physiology (Bethesda, Md : 1985)* 107 (3):816-823. doi:10.1152/jappphysiol.91198.2008
26. Mitchell GF (2008) Effects of central arterial aging on the structure and function of the peripheral vasculature: implications for end-organ damage. *J Appl Physiol* 105 (5):1652-1660

CHAPTER

5

Using high field magnetic resonance imaging to estimate distensibility of the middle cerebral artery

Esther A.H. Warnert

Jasper Verbree

Richard G. Wise

Matthias J.P. van Osch

Neurodegener Dis 2016; 16:407–410

DOI: 10.1159/000446397

ABSTRACT

Background: Although cerebral arterial stiffness may be an important marker for cerebrovascular health, there is not yet a measurement that accurately reflects the distensibility of major intracranial arteries. Herein we aim to non-invasively measure distension of the human middle cerebral artery (MCA).

Methods: Ten healthy volunteers (age: 30.3 ± 10.8 years) underwent ultra-high field (7 Tesla) MRI scanning. Time of flight angiography and phase contrast flow imaging were used to locate the M1 segment of the middle cerebral artery (MCA) and to determine the occurrence of systole and diastole. High resolution cross-sectional cardiac triggered T_2 -weighted images of the M1 segment of the MCA were acquired in systole and diastole.

Results: The average distension of the middle cerebral artery area from diastole to systole was 2.58% [min-max range: 0.08%–6.48%]. There was no significant correlation between MCA distension and the pulsatility index, calculated from the phase contrast flow velocity profiles.

Conclusion: These results lead to the first non-invasive image-based estimation of distensibility of the MCA (approximately $3 \times 10^{-4} \text{ mmHg}^{-1}$) and demonstrate that ultra-high field MRI could be a promising tool for investigating distensibility of intracranial arteries in relation to cerebrovascular pathology.

Key words

Arterial Stiffness; Arterial Structure and Compliance; Cerebral Small Vessel Disease; Ultra-high field MRI; Middle Cerebral Artery

INTRODUCTION

Healthy cerebral arteries are able to smooth out the pulsatile blood flow originating from the heart into an almost continuous flow into the capillary bed of the brain [1]. If the cerebral arteries stiffen, the pulsatile blood flow propagates further into the arterial tree, where the pulsatile shear stress can induce damage to the walls of the small vessels [2,3]. This process has been linked to severe pathologies, including cerebral small vessel disease (SVD) and vascular cognitive decline [2,3], and highlights the potential value of a measure of cerebral arterial stiffness as a marker of cerebrovascular health.

Measuring stiffness (or its inverse: distensibility) in extracranial arteries is commonly done by assessing changes in diameter occurring with changes in pressure occurring at the same site [4]. The skull complicates such measurements for intracranial arteries, and therefore explains the absence of an accurate measurement of cerebral arterial stiffness. However, volume changes of approximately 5% occurring throughout the cardiac cycle in the middle cerebral artery (MCA) have recently been measured with computed tomography (CT) angiography [5].

In contrast to CT, magnetic resonance imaging (MRI) can be used non-invasively to measure the cross-sectional area of the MCA.[6] Based on the volume changes found by CT angiography [5], distention of the MCA through the cardiac cycle is expected to be small (0.05–0.1 mm). Non-invasive imaging of such small geometrical changes requires high resolution measurements, which currently is only feasible with ultra-high field MRI [6].

In this proof-of-principle experiment we aimed to measure distension of the MCA by using ultra-high field MRI and by synchronizing the image acquisition to the cardiac cycle. In addition, we assessed the pulsatility index as a combined measure of cerebrovascular resistance and stiffness. To the best of our knowledge, this is the first non-invasive assessment of cerebral arterial distension in humans.

MATERIAL AND METHODS

Ten healthy participants were recruited for this experiment (6 females, all non-smoking, average age 30.3 ± 10.8 years). Informed consent was obtained from all volunteers. This study was performed under approval of the institutional review board of the Leiden University Medical Center according to the Declaration of Helsinki and in accordance with the guidelines for Good Clinical Practice (CPMP/ICH/135/95).

Image acquisition

MRI scans were performed at 7 Tesla (whole body Philips Achieva, Philips Healthcare, Best, The Netherlands) and similar to a previously described protocol[6]. All image acquisition parameters

are stated in the online data supplement. A 3-dimensional time-of-flight (TOF) angiogram was performed to identify the MCA and for planning of an imaging plane perpendicular to the M1 segment. Care was taken to select a straight portion of the MCA and exclude branching arteries. Planning of this imaging plane was guided by additional reconstructions of the TOF scan to better visualize the course of the MCA in all directions. The position and orientation of the imaging plane were copied to the quantitative flow scan to assess the flow velocity waveform through the MCA. Directly after acquisition, a circular region of interest in the centre of the MCA was used to determine the flow velocity profile at the level of M1, which was used to determine the time points at which peak-diastole and peak-systole occurred and to calculate the post-trigger acquisition delay times for the cardiac triggered T2-weighted images. High resolution and cardiac triggered T2-weighted images were acquired at 4 time points in the cardiac cycle in pseudo-random order: 200 (t_1) and 100ms (t_2) preceding peak-diastole, and 50 ms before (t_3) and 50 ms after (t_4) peak-systole. These time points were chosen because in the carotid artery peak flow velocities have been shown to closely follow systolic and diastolic pressure [7]. An example of a high resolution structural image can be seen in Figure 5.1a. Throughout all scans pulse oximetry at the finger was used to measure the cardiac pulse.

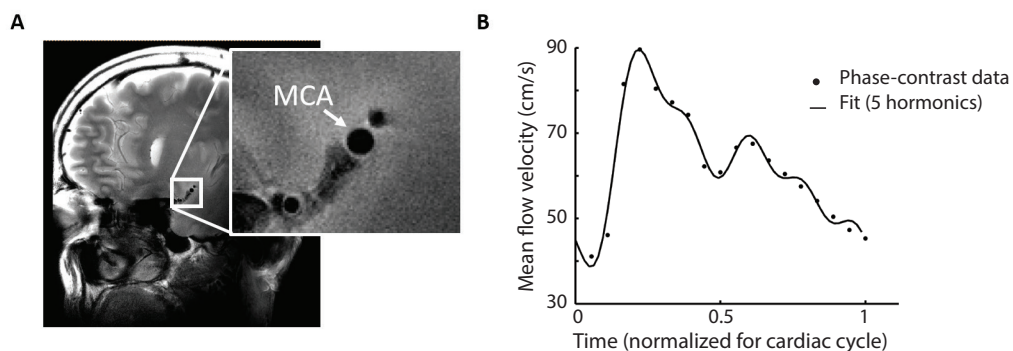


Figure 5.1 | **A.** Example of T₂-weighted high-resolution structural image of the cross-sectional area of the M1 segment of the MCA. **B.** Example of phase contrast flow velocity data (dots) measured at the same location as A. The flow velocity waveform was approximated by fitting the first five harmonics of a Fourier sequence (solid line), from which the pulsatility index was calculated. MCA = middle cerebral artery, Sys = systole, Dia = diastole.

Image analysis

Two observers, blinded to participant and cardiac phase of the images, manually drew elliptical regions of interests on the T₂-weighted images to delineate the internal wall of the MCA. Each observer repeated this process once, and the average of all 8 measurements (two scans per time point and two observers who delineated the MCA twice) per time point was used to calculate MCA cross-sectional area. Paired t-tests were used to investigate whether the MCA area at time points t_1 , t_3 , and t_4 were significantly different than at t_2 (triggered closest to peak-diastolic velocity).

To investigate the consistency within and between observers the intraclass coefficient of correlation for consistency (ICC(C,1), ICC(C,k)) was calculated with Matlab (R2012b, MathWorks, Natick, Massachusetts, USA).

The quantitative flow scan was also used to calculate a commonly used cerebral arterial stiffness index based on the blood flow velocity waveform through the MCA, the pulsatility index (PI) [8]. A linear regression was performed (*robustfit* in Matlab) between the distention of the MCA between peak-diastole and peak-systole (t_2 and t_3) and the PI.

RESULTS

There was high consistency in MCA area measurements within observer ($ICC(C,1)_{Obs.1} = 0.89$, $ICC(C,1)_{Obs.2} = 0.92$) and between observers ($ICC(C,k) = 0.91$), justifying the averaging of all 8 MCA area measurements per time point.

There was a significant increase in MCA area between diastole and systole of 2.58% [min-max range: 0.08%–6.48%] (*t*-test, $p < 0.01$), see Figure 5.2a.

The group average PI was 0.80 ± 0.12 , and was not significantly correlated with the change in MCA area between systole and diastole ($r^2 = 0.13$, $p = 0.35$), see Figure 5.2b.

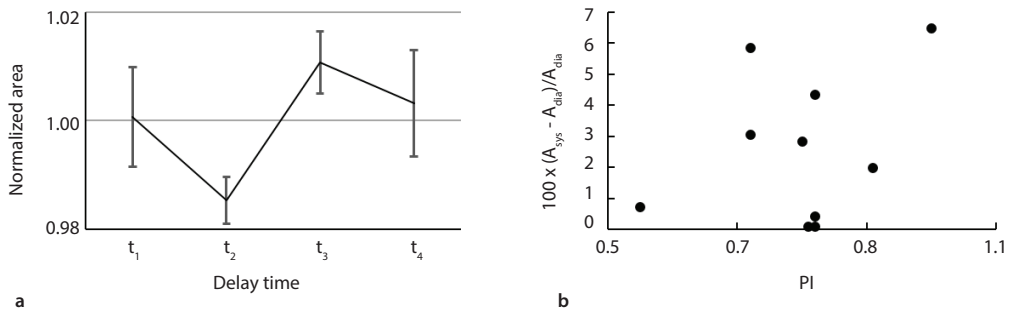


Figure 5.2 | A. Group average ($N = 10$) cross-sectional area of the MCA for 4 different delay times. Data was normalized per participant by dividing by the average MCA cross-sectional area of each individual. Note that t_2 is the delay time closest to peak-diastole and t_3 the delay time closest to peak-systole. There was a significant difference ($* p < 0.05$, paired *t*-test) between the diastolic and systolic area. The errorbars indicate the standard error of the mean. **B.** The increase in area from diastole to systole plotted against the pulsatility index for all 10 participants. (No significant correlation, $r^2 = 0.13$, $p = 0.35$). MCA = middle cerebral artery.

DISCUSSION

In the current study it is shown for the first time that ultra-high field MRI can be used to non-invasively measure distention of the MCA occurring through the cardiac cycle, which is a prerequisite for measurement of cerebral arterial stiffness. When combined with reference values for central pulse pressure in healthy participants (45 mmHg [9]), the estimated average MCA distensibility is approximately $3.0 \times 10^{-4} \text{ mmHg}^{-1}$.

This level of distensibility in the MCA is plausible, as the significant change in MCA area of $2.58\% \pm 2.4\%$ through the cardiac cycle falls within the range of volume changes in the MCA measured with CT.[5] Furthermore, the resulting estimation of MCA distensibility follows the expectation that intracranial arteries are less distensible than extracranial arteries, e.g. reported distensibility in the carotid artery ranges from 0.5×10^{-3} to $5.8 \times 10^{-3} \text{ mmHg}^{-1}$ [4].

There was no correlation between the distention of the MCA cross-sectional area and PI. Although in a small cohort, this finding highlights that in addition to local arterial stiffness, other factors such as stiffness and resistance of the downstream vascular bed shape the blood flow velocity waveform [10]. Furthermore, this illustrates the need for investigation of the relationship between cerebral arterial distensibility and the formation of blood flow velocity waveforms, which is an important step in understanding the mechanisms that link increased arterial stiffness to cerebrovascular pathologies, such as SVD [11] and vascular cognitive decline [3]. Future studies investigating these mechanisms should include participants with a wide range of expected cerebral arterial distensibilities, e.g. young and elderly individuals or patients with SVD.

A limitation of this study is that no blood pressure measurements were included and therefore only an estimation of MCA distensibility was feasible. However, underlying pulse pressures are not expected to show large deviations from reference values [9], because only healthy and non-smoking volunteers were recruited. Future work should include blood pressure measurements, such that cerebral arterial stiffness can be quantified in terms of distensibility or compliance [1,12]. Although measuring local pulse pressure would be a requirement for accurate estimation of arterial distensibility [4], we recommend using a non-invasive measurement of blood pressure (e.g. brachial blood pressure [12]) in studies for which it is not feasible to invasively assess intracranial blood pressure.

In summary, we have shown that ultra-high field MRI can be used to non-invasively measure cerebral arterial distensibility and that this is a promising tool for future research into the relationship between cerebral arterial stiffness and cerebrovascular pathology.

REFERENCE LIST

1. Hall JE, Guyton AC (2006) Vascular distensibility and functions of the arterial and venous systems. Textbook of medical physiology, 11th edn. Elsevier Inc, Philadelphia
2. Mitchell GF, van Buchem Ma, Sigurdsson S, Gotal JD, Jonsdottir MK, Kjartansson O, Garcia M, Aspelund T, Harris TB, Gudnason V, Launer LJ (2011) Arterial stiffness, pressure and flow pulsatility and brain structure and function: the Age, Gene/Environment Susceptibility - Reykjavik Study. *Brain* 134:3398-3407. doi:10.1093/brain/awr253
3. O'Rourke MF, Safar ME (2005) Relationship Between Aortic Stiffening and Microvascular Disease in Brain and Kidney: Cause and Logic of Therapy. *Hypertension* 46:200-204. doi:10.1161/01.HYP.0000168052.00426.65
4. O'Rourke MF, Staessen JA, Vlachopoulos C, Duprez D, Plante GE (2002) Clinical applications of arterial stiffness; definitions and reference values. *Am J Hypertens* 15:426-444. doi:S0895706101023196 [pii]
5. Kuroda J, Kinoshita M, Tanaka H, Nishida T, Nakamura H, Watanabe Y, Tomiyama N, Fujinaka T, Yoshimine T (2012) Cardiac Cycle-Related Volume Change in Unruptured Cerebral Aneurysms: A Detailed Volume Quantification Study Using 4-Dimensional CT Angiography. *Stroke*, vol 43. doi:10.1161/STROKEAHA.111.626846
6. Verbree J, Bronzwaer A, van Buchem M, Daemen M, van Lieshout J, van Osch M (2016) Middle cerebral artery diameter changes during rhythmic handgrip exercise in humans. *Journal of Cerebral Blood Flow & Metabolism*:0271678X16679419. doi:10.1177/0271678X16679419
7. Hirata K, Yaginuma T, O'Rourke MF, Kawakami M (2006) Age-related changes in carotid artery flow and pressure pulses: Possible implications for cerebral microvascular disease. *Stroke* 37:2552-2556. doi:10.1161/01.STR.0000242289.20381.f4
8. Bouvy WH, Geurts LJ, Kuijff HJ, Luijten PR, Kappelle LJ, Biessels GJ, Zwanenburg JJM (2015) Assessment of blood flow velocity and pulsatility in cerebral perforating arteries with 7-T quantitative flow MRI. *NMR in biomedicine*. doi:10.1002/nbm.3306
9. Mitchell GF, Parise H, Benjamin EJ, Larson MG, Keyes MJ, Vita JA, Vasan RS, Levy D (2004) Changes in arterial stiffness and wave reflection with advancing age in healthy men and women: The Framingham Heart Study. *Hypertension* 43:1239-1245. doi:10.1161/01.HYP.0000128420.01881.aa
10. Bude RO, Rubin JM (1999) Relationship between the resistive index and vascular compliance and resistance. *Radiology* 211:411-417. doi:10.1148/radiology.211.2.r99ma48411
11. Webb AJS, Simoni M, Mazzucco S, Kuker W, Schulz U, Rothwell PM (2012) Increased Cerebral Arterial Pulsatility in Patients With Leukoaraiosis: Arterial Stiffness Enhances Transmission of Aortic Pulsatility. *Stroke* 43:2631-2636. doi:10.1161/STROKEAHA.112.655837
12. Warnert EAH, Murphy K, Hall JE, Wise RG (2015) Noninvasive assessment of arterial compliance of human cerebral arteries with short inversion time arterial spin labeling. *Journal of Cerebral Blood Flow & Metabolism* 35:461-468. doi:10.1038/jcbfm.2014.219

CHAPTER

6

Middle cerebral artery diameter changes during rhythmic handgrip exercise in humans

J. Verbree*

A.G.T. Bronzwaer*

M.A. van Buchem

M.J.A.P. Daemen

J.J. van Lieshout

M.J.P. van Osch1

*) These authors contributed equally to this work.

J Cereb Blood Flow Metab. 2017 Aug;37(8):2921-2927

DOI: 10.1177/0271678X16679419

ABSTRACT

Transcranial Doppler sonography (TCD) is a frequently employed technique for quantifying cerebral blood flow by assuming a constant arterial diameter. Given that exercise increases arterial pressure by sympathetic activation, we hypothesized that exercise might induce a change in the diameter of large cerebral arteries. Middle cerebral artery (MCA) cross-sectional area was assessed in response to handgrip exercise by direct MRI observations. 20 healthy subjects (11 female) performed three 5 minutes bouts of rhythmic handgrip exercise at 60% maximum voluntary contraction, alternated with 5 minutes of rest. High-resolution 7-Tesla MRI scans were acquired perpendicular to the MCA. Two blinded observers manually determined the MCA cross-sectional area. Sufficient image quality was obtained in 101 MCA-scans of 19 subjects (age-range 20–59 years). Mixed Effects modeling showed that the MCA cross-sectional area decreased by $2.1 \pm 0.8\%$ ($p = 0.01$) during handgrip, while the heart rate increased by $11 \pm 2\%$ ($p < 0.001$) at constant end-tidal CO₂ ($p = 0.10$). In conclusion, the present study showed a 2% decrease in MCA cross-sectional area during rhythmic handgrip exercise. This further strengthens the current concept of sympathetic control of large cerebral arteries, showing in-vivo vasoconstriction during exercise-induced sympathetic activation. Moreover, care must be taken when interpreting TCD exercise studies as diameter constancy cannot be assumed.

Keywords

Transcranial Doppler; Exercise; Cerebral Blood Flow; MRI; MR Angiography; Cerebral Blood Flow Measurement.

INTRODUCTION

The regulation of cerebral blood flow (CBF) is critical for the maintenance of oxygen and nutrient supply to the metabolically active brain. CBF control is multifactorial, influenced largely by the partial pressure of arterial carbon dioxide, mean arterial pressure and cerebral metabolism [1]. Despite the abundance of sympathetic nerve fibers emanating from the cervical and stellate ganglia that innervate the cerebral arteries, the role of the autonomic nervous system in the control of cerebral blood flow (CBF) in humans has remained contentious for decades [2-10].

In peripheral circulations arterioles rather than large arteries are the main site of vascular resistance. However, for the brain, large vessels contribute ~50% to vascular resistance [11]. This noticeable contribution of large arteries in vascular resistance is most likely of importance in defending the cerebral microcirculation against surges in blood pressure by limiting fluctuations in microcirculatory pressure and cerebral perfusion [12-14]. Several observations have been put forward as an argument for sympathetic influence on the human cerebral vasculature [6,15]. At first, blocking sympathetic outflow to the human cerebral vasculature increases CBF, suggesting a sympathetically mediated restraint of cerebrovascular perfusion [15]. Second, systemic agents that impair sympathetic signaling (alpha-adrenergic) reduce measures of cerebral pressure autoregulation [15,16]. Finally, in healthy subjects, spillover of sympathetic neurotransmitters in the jugular vein is increased during sympathetic activation independently from neurotransmitters released in the brain [17]. These observations suggest that the cerebral vasculature is under sympathetic control, leaving the challenge to identify changes in human brain artery diameter during sympathetic activation, especially when these would impact interpretation of physiological measurements, such as Transcranial Doppler (TCD).

In humans, changes in CBF are commonly evaluated non-invasively by measuring the CBF-velocity (CBFv) by transcranial Doppler sonography (TCD) in the large cerebral arteries with real-time resolution [18]. A limitation of the majority of studies is that a constant diameter of the insonated brain artery is assumed to directly link changes in CBFv to changes in regional CBF. This assumption of constancy of brain artery diameter has been evidenced to be violated by high levels of PaCO₂ [19,20] and pressure pulsatility [21,22], but it is as yet unknown whether the assumed constancy of brain artery diameter holds true during exercise. Given that functional activation increases CBF and that sympathetic activation and arterial pressure increase with exercise, we hypothesized that exercise affects the diameter of large cerebral arteries. To that purpose we set out to quantify the middle cerebral artery (MCA) cross-sectional area in rest and in response to rhythmic handgrip exercise using high resolution 7 Tesla MRI.

MATERIALS AND METHODS

Subjects

Twenty healthy, non-smoking, non-diabetic, right handed subjects (9 males, 11 females) without history of cardiovascular disease underwent MRI during rhythmic handgrip exercise. No information about the active or chronic use of vasoactive medication or painkillers was obtained. One subject used a beta-adrenergic blocking agent for mild hypertension which was considered not to have an effect on the cardiovascular response to handgrip exercise [23]. Written informed consent was obtained from all participants prior to examination. The protocol was performed in accordance with the Helsinki protocol, as approved by the institutional Medical Ethics Committee of the Leiden University Medical Center.

Measurements

MRI measurements were performed on a 7 Tesla Philips MRI system. Image acquisition parameters have been described previously [24] and are listed in Table 6.1. The MCA contralateral to the exercise hand was located on an orthogonally reconstructed axial Time-Of-Flight angiogram. Additional sagittal reconstruction was created along the course of the MCA to aid the planning procedure. Subsequently, the high resolution 2D scan based on the black-blood approach and with a voxel-size of $0.2 \times 0.2 \times 5 \text{ mm}^3$ was positioned perpendicular to the MCA. This scan will be referred to as “MCA-scan” for the remainder of this article. Care was taken to select a straight part of the proximal MCA and exclude small branches whenever possible. Image blurring due to variations in vessel lumen across the cardiac cycle was minimized by prospectively triggering the acquisition to the subject’s heart beat using the finger pulse-oximetry unit of the scanner [22]. Acquisition duration was 2.5 to 3.5 minutes, depending on the heart rate (HR) of the subject. End-tidal CO_2 (Pet CO_2) was continuously monitored via a nasal cannula connected to a capnograph (Capnomac Ultima, Datex), located in the control room adjacent to the scanner. Heart rate (HR) was obtained from the finger pulse-oximetry unit of the MRI scanner. After 10–15 minutes of preparatory scans, a brachial blood pressure measurement was performed on the right arm (Invivo Magnitude, Orlando, FL).

Protocol

A graphical representation of the protocol is illustrated in Figure 6.1. Exercise consisted of 5 minutes of dynamic handgripping, i.e. repeated 2 sec hand contractions alternated with 2 sec of relaxation. Prior to scanning the subjects were familiarized with the protocol and handgrip-device (Gripforce 500N, Curdes, Philadelphia PA, USA). Maximum voluntary contraction (MVC) of the dominant hand was assessed by taking the maximum of 3 attempts. To achieve and maintain a steady state, rhythmic handgrip started the first minute at 80% MVC to be directly followed by 60% MVC for 4 minutes. Pilot-studies proofed that this approach results in a robust and steady response for the complete duration of the exercise bout. Graphical representations of the imposed exercise rhythm as well as the force applied by the volunteer were displayed onto a screen in the scanner to provide visual feedback to the subject. The exercise protocol started with 5 minutes of

rest followed by 5 minutes of handgrip. This was repeated three times to facilitate the detection of small differences in cross-sectional area. Acquisition of the MCA-scan was started 90 seconds after start of the rest or exercise bout. A total of 6 MCA scans (3 at rest and 3 during exercise) were obtained per subject.

Table 6.1 | MRI scan parameters.

	Time-of-Flight Angiogram	Black blood T2-weighted (MCA-scan)
Planning orientation	3D acquisition covering the circle of Willis	Single slice, perpendicular to the MCA
Scan Technique	Fast Field Echo	Spin Echo
Acceleration type	none	Turbo spin echo; factor 12 + 4 dummy
Repetition time/echo time	12.6 / 3.7 ms	2 heart beats / 86 ms
Flip/ Refocusing angle	20° / –	110° / 105°
Field of view	180 x 170 x 40 mm ³	240 x 180 x 5 mm ³
Acquisition matrix	544 x 540	1200 x 900
Scan duration	4 min	2.5–3.5 min, depending on heart rate
Additional parameters	–	Trigger delay 50ms

The time-of-Flight angiogram was used to locate the MCA and additional reconstructions ensured perpendicular planning of the high-resolution black blood T2 MCA-scan. The MCA-scan was used to determine the cross-sectional area of the MCA.

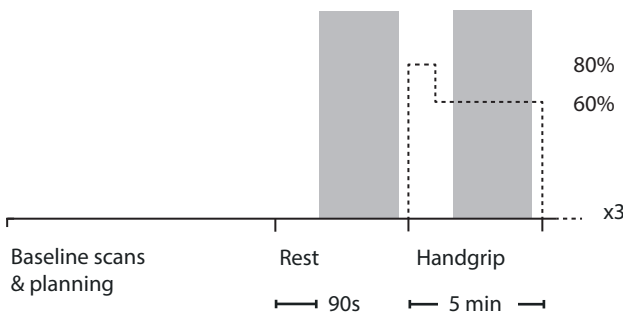


Figure 6.1 | Graphical representation of the exercise protocol. Relative timing of the MCA-scan is indicated by the gray area and the relative force level by a dashed line.

Data processing

The MCA-scans were anonymized and viewed in proprietary Philips viewing software. Two observers blinded to subject-number and condition (JV, AGTB) manually drew elliptical regions of interests to determine the MCA cross-sectional area twice. Quality of the MCA-scans was visually assessed, and scans with visible motion artefacts or a badly discernable vessel wall were

excluded from analysis. All PetCO₂ recordings and HR data were visually inspected and artifacts were manually removed. Values during rest and exercise were averaged per subject. Relative (percentage) change was calculated by normalizing with respect to the resting condition: relative = 100% · (handgrip–rest) / rest.

Statistics

The Intraclass Correlation Coefficient assessed the consistency within- and between observers (ICC C-k, SPSS v23). The effect of handgrip was assessed with a Mixed-effect model (Statistics Toolbox, Matlab v2015b) taking the percentage change in vessel cross-sectional area, HR and PetCO₂ as dependent variable. A fixed intercept with subjects as random intercept was used to model the change in cross-sectional area. The possible effects of time, age, and gender and change in PetCO₂ on the cross-sectional area change were investigated in separate models, using a fixed effect analysis. Normality of the residuals was assessed using Lilliefors test. Based on a sample-variance of 8.19±1.32 mm² as measured during normocapnia in a previous study [19], the a-priori power was set to 0.9 to detect a difference of 5% in cross-sectional area resulting in a sample size of n = 20. Significance threshold was set at 0.05. Values are mean±SE except when stated otherwise.

RESULTS

Sufficient image quality was achieved in 101 of 120 scans, such that 19 subjects entered final analysis. The median (range) age was 30 (20–59) years and resting systolic- and diastolic arterial pressures were 112±9 and 69±10 mmHg (mean±SD) respectively.

During exercise HR increased 11.2±1.7% (p<0.001), without change in PetCO₂ (-0.9±0.5%, p<0.10, see Table 6.2).

Table 6.2 | Average response to rhythmic handgrip exercise.

	Rest (mean ± SD)	Handgrip (mean ± SD)	Effect Estimate (mean ± SE)	
Area (mm ²)	7.47±1.18	7.31±1.15	-2.1±0.81%	p = 0.01
HR (bpm)	62.0±12.5	68.4±12.5	11.2±1.7%	p<0.001
PetCO ₂ (kPa)	5.06±0.36	5.02±0.36	-0.9±0.5%	p = 0.10

Fixed effect estimates determined by corresponding Mixed Effects model. Area: cross-sectional area of the middle cerebral artery; HR: heart rate; PetCO₂: end-tidal carbon dioxide.

Both the consistency of MCA area measurements within- (ICC A-k = 0.978 and 0.977 for JV and AGTB respectively) and between observers (ICC C-k = 0.981) were considered sufficient to accept the reliability of the average MCA cross-sectional area measurement. A representative example of the image quality of the MCA-scan is depicted in Figure 6.2.

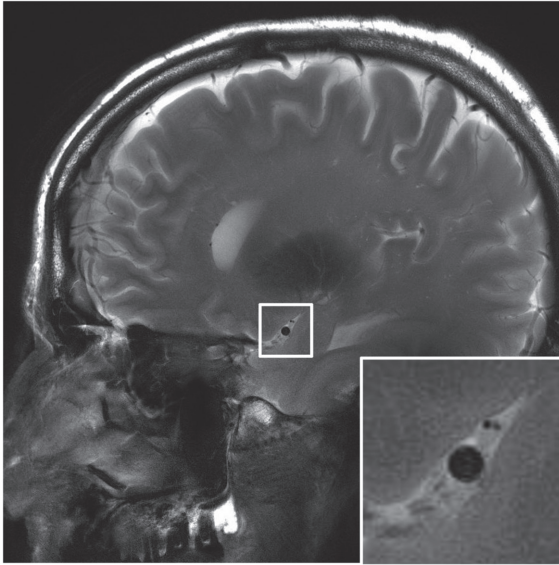


Figure 6.2 | Example of a high resolution cardiac triggered MRI scan of the MCA; based on the black blood principle. The white box indicates the zoomed area showing the lumen of the MCA.

The mean cross-sectional area during rest was $7.47 \pm 1.18 \text{ mm}^2$ (diameter of 3.1 mm), which decreased during handgrip exercise by 0.16 mm^2 to $7.31 \pm 1.15 \text{ mm}^2$, see Figure 6.3. The change in cross-sectional area was $-2.11 \pm 0.81\%$ (95% confidence interval: -3.74%, -0.49%, $p = 0.01$), see Figure 6.4, corresponding to a decrease in diameter of $1.1 \pm 0.4\%$ (0.033 mm). Repeated exercise challenges (time-effect) did not have an effect on this relation ($p = 0.07$).

The age of the participants was strongly clustered into two groups. Therefore, the effect of age was assessed by splitting the population into a group below- (3 males, 8 females) and above 40 years of age (5 males, 3 females). There was no relation between age and the change in cross-sectional area in response to exercise ($p = 0.76$). The change in PetCO_2 did not have a relation to the change in cross-sectional area ($p = 0.51$). There was a larger reduction in cross-sectional area in males compared to females ($\beta_{\text{male}} = -3.46 \pm 1.47$, $p = 0.02$).

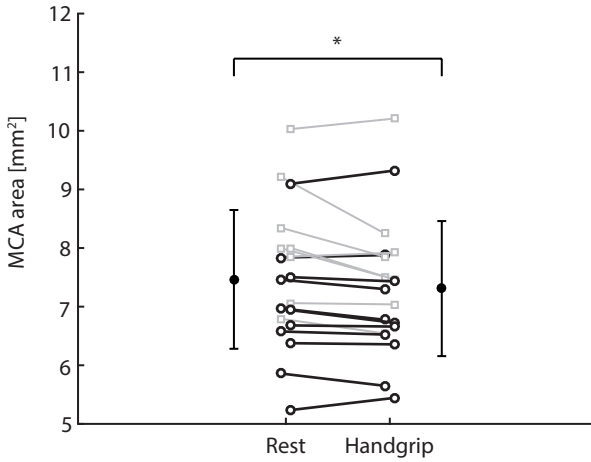


Figure 6.3 | Effect of dynamic handgrip exercise on the average MCA cross-sectional area. Black error-bars indicate mean and standard deviation. Squares represent males and circles females. Corresponding measurements of a subject are connected by a line. * $p < 0.05$ rest vs. handgrip.

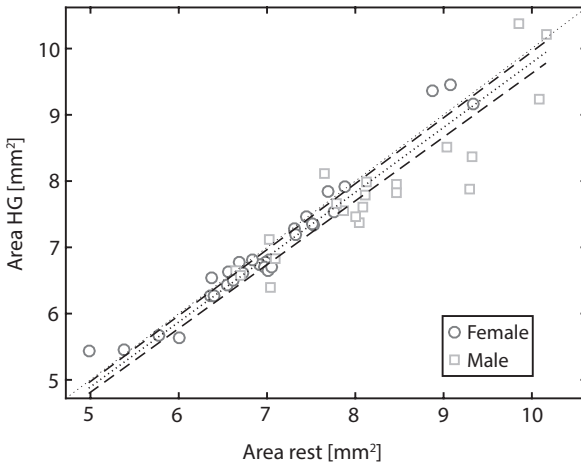


Figure 6.4 | Scatterplot of the cross-sectional area during rest and handgrip. All 57 data pairs are plotted for male (square) and female (circle) subjects. The Mixed Model Estimate is indicated by the dotted line with 95% confidence intervals (dashed lines). The line of identify (dotted line) is added for visual reference.

DISCUSSION

The main finding of the present study is that a 2% reduction in the contralateral MCA cross-sectional area in response to rhythmic handgrip. This suggests that vasoconstriction occurs in a large brain artery during exercise induced sympathetic activation. This falsifies the hitherto assumed constancy of cerebral artery diameter.

Regarding the evaluation of cerebral perfusion with TCD, the concern has been raised whether the diameter of the basal cerebral arteries remains constant during sympathetic activation, specifically exercise [8,9,25]. To our knowledge this is the first study to directly observe a MCA lumen change during exercise with high resolution MRI. To date a single study estimated the change in MCA cross-sectional area specifically during rhythmic handgrip [8]. Their estimate of 21% change was indirect, i.e. by comparing the regular TCD signal with the spectrally averaged Doppler signal, and therefore not easily comparable with the present findings. A study, assessing the effect of sympathetic activation on arterial diameter did not find a change in a small peripheral artery of the foot as assessed with ultrasound [7]. Moreover, direct MRI observations of the MCA during sympathetic stimulation by lower body negative pressure [26] also did not find a diameter change. The absence of observable changes in these studies suggest that, the magnitude of any changes can be considered minor. Moreover, changes in MCA cross-sectional during CO₂ inhalation and pressure pulsatility can also be considered small [19,20,22]. This is in line with the current finding of 2% vasoconstriction, indicate that MCA cross-sectional area changes are small when induced by sympathetic activation by moderate exercise.

The extent in MCA diameter response to exercise and sympathetic activation could differ depending on factors such as age and gender. Findings of the present study suggest a larger change in MCA cross-sectional area in males compared to females in response to rhythmic handgrip. This finding coincides with the observation that premenopausal females exhibit lower sympathetic outflow in response to static handgrip exercise [27] and lower cerebrovascular reactivity [28,29] as a marker for brain vessel dilatatory capacity. Contrary, with age, no relation with the degree of MCA vasoconstriction was observed in present study. This is in line with preserved sympathetic response to autonomic challenges [30,31] and preserved carbon dioxide cerebrovascular reactivity [32,33] in aging. We consider that the limited sample size of the gender and age groups precludes proper inference of possible differences.

Small changes in vessel lumen can have profound influence on the estimation of CBF by relative velocity measurements. A decrease in vessel lumen proportionally increases the flow velocity even at constant blood flow. However, with exercise both the lumen and blood flow are changing. For example, during handgrip the CBF_v increases from 50 cm/s to 55 cm/s, corresponding to an apparent 10% increase in CBF. However, a concurrent decrease in cross-sectional area of 2.1% reduces the underlying CBF change to 7.9% rather than the 10%, as would be estimated from the velocity only. Moreover, the variation in the cross-sectional area change ranged (mean±STD)

from $-10.4 \pm 4.7\%$ (subject 3, male, $n = 3$) to $4.3 \pm 5.3\%$ (subject 16, female, $n = 2$), respectively overestimating and underestimating the underlying CBF response to handgrip exercise by 10.5% and by 5.3% in these subjects. Given a measured 10% change in velocity, the corresponding change in CBF, corrected for the change in lumen area of these subjects, would be +0.5% and +15.3%, respectively. While the change in lumen seems slight, it constitutes a sizable part of the TCD determined cerebral hemodynamic response during handgrip exercise.

Measuring small changes in vessel lumen requires high precision measurements. The acquisition resolution of the employed MCA-scan was $0.2 \times 0.2 \text{ mm}^2$, therefore the average change in MCA cross-sectional area of 0.16 mm^2 constitutes ~ 4 pixels, providing for sufficient statistical power in the current study to infer these changes. The determination of the cross-sectional area can be dependent on the effective contrast of the acquisition as well as on the observer accuracy. Reliability of the cross-sectional area assessments was augmented by excluding scans with poorly discernable MCA vessel wall (e.g. subject motion), as well as by averaging the observations of two observers, who were blinded to participant number and condition.

High resolution scanning was complemented with cardiac triggering that stabilized the imaging by timing the acquisition with respect to the cardiac cycle. Although this approach prolongs scan time, it mitigates blurring effects and imaging artifacts. In addition, the sensitivity of the MCA-scan to variations in blood flow has been minimized by the application of dummy echoes, thereby creating a clear signal void within the vessel lumen [19]. Although some dependency of the intravascular signal on the blood flow velocity may persist, an increase in flow velocity near the vessel wall would make the lumen appear larger rather than smaller. This effect can therefore not explain the observed decrease in cross-sectional area as found in the current study, it might only have resulted in an underestimation of the actual decrease in MCA cross-sectional area.

A potential limitation of the present study is the application of concurrent visual feedback to maintain the desired exercise level. Stimulation of the visual cortex by the visual feedback is associated regional increases in CBF [34]. However, the visual cortex is supplied by the posterior cerebral circulation rather than by the MCA, rendering an effect of visual stimulation on the MCA cross-sectional area negligible. Another limitation of the present study is that the level of sympathetic activation was not directly determined. This could have contributed to the large between-subject variation. However, the exercise protocol was setup to provide a consistent response within- and between-subjects, by scaling the prescribed force to the individually maximal voluntary contraction. Currently no data exist how the level of (rhythmic handgrip) exercise impacts sympathetic activation, and we can therefore not exclude an effect of the level of sympathetic activation on the large between-subject variation. In the present study arterial pressure was not monitored during exercise, as brachial pressure measurements would occlude either the handgripping arm or disrupt blood flow in the finger used for triggering the MCA-scan. However, it has been well documented that the arterial pressure increases in response to rhythmic handgrip exercise [35,36]. This increase in pressure is required to provide the work to counteract

the higher vascular resistance and actually increase the blood flow velocity. Without an increase in pressure the blood flow would decrease with a constant flow velocity. Therefore, given that the arterial pressure increases during handgrip exercise, then the observed vasoconstriction in the MCA can be considered to modulate the blood flow velocity and lead to an overestimation when using TCD to assess CBF changes.

CONCLUSION

In conclusion, the present study observed a 2% decrease in MCA cross-sectional area with MRI during rhythmic handgrip exercise in healthy subjects. This further strengthens the current concept of sympathetic control of large cerebral arteries, showing in-vivo vasoconstriction during exercise induced sympathetic activation. Finally, the assumption of constancy vessel diameter is falsified. Therefore, care must be taken when interpreting TCD measurements of the cerebral circulation in exercise studies.

REFERENCE LIST

1. Ainslie PN, Bailey DM (2013) Your ageing brain: the lows and highs of cerebral metabolism. *J Physiol* 591 (Pt 7):1591-1592
2. Strandgaard S, Sigurdsson ST (2008) Point:Counterpoint: Sympathetic activity does/does not influence cerebral blood flow. Counterpoint: Sympathetic nerve activity does not influence cerebral blood flow. *J Appl Physiol* 105 (4):1366-1367
3. Purkayastha S, Saxena A, Eubank WL, Hoxha B, Raven PB (2013) alpha1-Adrenergic receptor control of the cerebral vasculature in humans at rest and during exercise. *ExpPhysiol* 98 (2):451-461
4. Van Lieshout JJ, Secher NH (2008) Point: Counterpoint: Sympathetic activity does/does not influence cerebral blood flow. *Journal of Applied Physiology* 105 (4):1364-1366. doi:10.1152/jappphysiol.90597.2008
5. Strandgaard S, MacKenzie ET, Sengupta D, Rowan JO, Lassen NA, Harper AM (1974) Upper limit of autoregulation of cerebral blood flow in the baboon. *CircRes* 34 (4):435-440
6. Willie CK, Tzeng YC, Fisher JA, Ainslie PN (2014) Integrative regulation of human brain blood flow. *J Physiol* 592 (Pt 5):841-859. doi:10.1113/jphysiol.2013.268953
7. Pott F, Ray CA, Olesen HL, Ide K, Secher NH (1997) Middle cerebral artery blood velocity, arterial diameter and muscle sympathetic nerve activity during post-exercise muscle ischaemia. *Acta Physiologica Scandinavica* 160 (1):43-47
8. Giller CA, Giller AM, Cooper CR, Hatab MR (2000) Evaluation of the cerebral hemodynamic response to rhythmic handgrip. *J Appl Physiol* 88:2205-2213
9. Giller CA (2003) The Emperor has no clothes: velocity, flow, and the use of TCD. *J Neuroimaging* 13 (2):97-98
10. Seifert T, Secher NH (2011) Sympathetic influence on cerebral blood flow and metabolism during exercise in humans. *Prog Neurobiol* 95 (3):406-426. doi:10.1016/j.pneurobio.2011.09.008
11. Faraci FM, Heistad DD (1990) Regulation of large cerebral arteries and cerebral microvascular pressure. *CircRes* 66 (1):8-17
12. Cassaglia PA, Griffiths RI, Walker AM (2008) Sympathetic nerve activity in the superior cervical ganglia increases in response to imposed increases in arterial pressure. *Am J Physiol RegulIntegrComp Physiol* 294 (4):R1255-R1261
13. Ainslie PN, Brassard P (2014) Why is the neural control of cerebral autoregulation so controversial? *F1000prime reports* 6:14. doi:10.12703/P6-14
14. Hamel E (2006) Perivascular nerves and the regulation of cerebrovascular tone. *Journal of applied physiology* (Bethesda, Md : 1985) 100 (3):1059-1064. doi:10.1152/jappphysiol.00954.2005
15. ter Laan M, van Dijk JM, Elting JW, Staal MJ, Absalom AR (2013) Sympathetic regulation of cerebral blood flow in humans: a review. *BrJAnaesth* 111 (3):361-367
16. Zhang R, Zuckerman JH, Iwasaki K, Wilson TE, Crandall CG, Levine BD (2002) Autonomic neural control of dynamic cerebral autoregulation in humans. *Circulation* 106 (14):1814-1820
17. Mitchell DA, Lambert G, Secher NH, Raven PB, van Lieshout J, Esler MD (2009) Jugular venous overflow of noradrenaline from the brain: a neurochemical indicator of cerebrovascular sympathetic nerve activity in humans. *J Physiol* 587 (Pt 11):2589-2597. doi:10.1113/jphysiol.2008.167999
18. Aaslid R, Markwalder TM, Nornes H (1982) Noninvasive transcranial Doppler ultrasound recording of flow velocity in basal cerebral arteries. *J Neurosurg* 57 (6):769-774
19. Verbree J, Bronzwaer AS, Ghariq E, Versluis MJ, Daemen MJ, van Buchem MA, Dahan A, van Lieshout JJ, van Osch MJ (2014) Assessment of middle cerebral artery diameter during hypocapnia and hypercapnia in humans using ultra-high-field MRI. *J Appl Physiol* 117 (10):1084-1089. doi:10.1152/jappphysiol.00651.2014
20. Coverdale NS, Gati JS, Opalevych O, Perrotta A, Shoemaker JK (2014) Cerebral blood flow velocity underestimates cerebral blood flow during modest hypercapnia and hypocapnia. *Journal of applied physiology* (Bethesda, Md : 1985) 117 (10):1090-1096. doi:10.1152/jappphysiol.00285.2014
21. Kuroda J, Kinoshita M, Tanaka H, Nishida T, Nakamura H, Watanabe Y, Tomiyama N, Fujinaka T, Yoshimine T (2012) Cardiac cycle-related volume change in unruptured cerebral aneurysms: a detailed volume quantification study using 4-dimensional CT angiography. *Stroke* 43 (1):61-66. doi:10.1161/strokeaha.111.626846

22. Warnert EA, Verbree J, Wise RG, van Osch MJP (2016) Imaging changes in cross-sectional area of the middle cerebral artery through the cardiac cycle at 7 tesla. *Neurodegenerative Diseases*
23. Nyberg G (1976) Blood pressure and heart rate response to isometric exercise and mental arithmetic in normotensive and hypertensive subjects. *Clinical science and molecular medicine Supplement* 3:681s-685s
24. Warnert EA, Verbree J, Wise RG, van Osch MJ (2016) Using High-Field Magnetic Resonance Imaging to Estimate Distensibility of the Middle Cerebral Artery. *Neuro-degenerative diseases* 16 (5-6):407-410. doi:10.1159/000446397
25. Secher NH, Seifert T, Van Lieshout JJ (2008) Cerebral blood flow and metabolism during exercise: implications for fatigue. *J Appl Physiol* 104 (1):306-314. doi:10.1152/jappphysiol.00853.2007
26. Serrador JM, Picot PA, Rutt BK, Shoemaker JK, Bondar RL (2000) MRI measures of middle cerebral artery diameter in conscious humans during simulated orthostasis. *Stroke* 31 (7):1672-1678
27. Ettinger SM, Silber DH, Collins BG, Gray KS, Sutliff G, Whisler SK, McClain JM, Smith MB, Yang QX, Sinoway LI (1996) Influences of gender on sympathetic nerve responses to static exercise. *Journal of applied physiology* (Bethesda, Md : 1985) 80 (1):245-251
28. Conijn MM, Hoogduin JM, van der Graaf Y, Hendrikse J, Luijten PR, Geerlings MI (2012) Microbleeds, lacunar infarcts, white matter lesions and cerebrovascular reactivity -- a 7 T study. *NeuroImage* 59 (2):950-956. doi:10.1016/j.neuroimage.2011.08.059
29. Kassner A, Winter JD, Poublanc J, Mikulis DJ, Crawley AP (2010) Blood-oxygen level dependent MRI measures of cerebrovascular reactivity using a controlled respiratory challenge: reproducibility and gender differences. *Journal of magnetic resonance imaging : JMRI* 31 (2):298-304. doi:10.1002/jmri.22044
30. Ng AV, Callister R, Johnson DG, Seals DR (1994) Sympathetic neural reactivity to stress does not increase with age in healthy humans. *Am J Physiol* 267:Pt 2:H344-353
31. Gagnon D, Schlader ZJ, Crandall CG (2015) Sympathetic activity during passive heat stress in healthy aged humans. *J Physiol* 593 (9):2225-2235. doi:10.1113/jp270162
32. Kastrup A, Dichgans J, Niemeier M, Schabet M (1998) Changes of cerebrovascular CO2 reactivity during normal aging. *Stroke* 29 (7):1311-1314
33. Zhou Y, Rodgers ZB, Kuo AH (2015) Cerebrovascular reactivity measured with arterial spin labeling and blood oxygen level dependent techniques. *Magnetic resonance imaging* 33 (5):566-576. doi:10.1016/j.mri.2015.02.018
34. Wang J, Aguirre GK, Kimberg DY, Roc AC, Li L, Detre JA (2003) Arterial spin labeling perfusion fMRI with very low task frequency. *Magnetic resonance in medicine : official journal of the Society of Magnetic Resonance in Medicine / Society of Magnetic Resonance in Medicine* 49 (5):796-802. doi:10.1002/mrm.10437
35. Shoemaker JK, MacDonald MJ, Hughson RL (1997) Time course of brachial artery diameter responses to rhythmic handgrip exercise in humans. *Cardiovasc Res* 1997Jul 35:125-131
36. Hartwich D, Fowler KL, Wynn LJ, Fisher JP (2010) Differential responses to sympathetic stimulation in the cerebral and brachial circulations during rhythmic handgrip exercise in humans. *Exp Physiol* 95 (11):1089-1097. doi:10.1113/expphysiol.2010.054387

CHAPTER

7

Transcranial Doppler determined middle cerebral artery blood flow velocity does not match MRI global or regional cerebral tissue perfusion during handgrip exercise

Jasper Verbree*

Anne-Sophie G.T. Bronzwaer*

Mark A. van Buchem

M.A.A. van Walderveen

Mat J.A.P. Daemen

Johannes J. van Lieshout

Matthias J.P. van Osch

* These authors contributed equally

Submitted

ABSTRACT

Changes in Transcranial Doppler (TCD) determined cerebral blood flow velocity (CBFv) are regularly considered to reflect (proportional) changes in cerebral blood flow (CBF), for instance during exercise. However, neuroimaging studies indicated a localized and smaller CBF increase compared to the CBFv changes. The aim of this study was to validate this interpretation by comparing the TCD measured velocity response to rhythmic handgrip exercise with the regional CBF response assessed with Arterial Spin Labeling (ASL) MRI. Thirty-eight healthy subjects completed an exercise protocol of three times 5 minutes of rhythmic handgrip. In the first session, the cerebral hemodynamic response to handgrip was assessed by TCD and during the second session by ASL-MRI. No difference in heart-rate response was observed between TCD and MRI sessions and PetCO₂ remained unchanged. During handgrip CBFv increased by $10.7 \pm 11.7\%$, whereas no change in CBF in the MCA flow territory was detected by ASL MRI ($-1.2 \pm 10.4\%$, $p = 0.18$); regional CBF increased by $7.8 \pm 10.1\%$ in the precentral region. Therefore, changes in CBFv do not reflect changes in the underlying flow territory CBF and/or regional CBF. These findings call into question the nature or the disparity between large artery flow velocity and brain tissue flow in response to rhythmic handgrip.

Keywords

Arterial spin labeling; cerebral blood flow; rhythmic handgrip; MRI; transcranial Doppler

INTRODUCTION

During exercise the brain is activated [1-3], and locally enhanced neuronal activity and energy demand [4,5] increase cerebral blood flow (CBF) in specific areas of the brain [6-8]. Transcranial Doppler (TCD) determined cerebral blood flow velocity (CBFv) in large brain-feeding arteries is commonly used as proxy for CBF [9]. During dynamic exercise with large muscle groups (e.g. cycling exercise) CBFv varies in parallel with ^{133}Xe clearance measures of CBF [10,11], with Fick-determined CBF [12], and with internal [13,14] and common carotid artery flow [15]. In contrast, high spatial resolution neuroimaging studies evidenced that upon static handgrip [16,17], rhythmic handgrip [18] and cycling [19-21] increases CBF in specific cortical regions only. This increase in regional CBF (rCBF) occurs in only a small sub-region of the flow territory of the artery in which TCD measures the velocity. The much smaller volume sub-region involved in neuronal activation during exercise suggests that the change in flow territory CBF (ftCBF) is much smaller than the CBFv increase in large brain arteries.

For example, the CBF change upon mild to moderate exercise of 10–15% [17-19] is limited to the motor cortex, which comprises only 3% of the entire MCA flow territory [22]. Combining these numbers suggests that the ftCBF increases by 0.3–0.5%. However, TCD observations during dynamic handgrip exercise showed that MCAv increases by 8–19% [23-31]. Depending on the location of measurement either the ftCBF increases negligible (<1%) using spatially resolved CBF or substantial (~10%) when assessed with CBFv. We therefore question whether CBFv is a valid proxy for CBF during small muscle group exercise. This study addressed whether the increase in CBFv during exercise matches the CBF-change within the corresponding flow territory or within the activated brain region. To that purpose the study compared CBFv and MRI-determined CBF in healthy subjects during dynamic handgrip exercise.

MATERIALS AND METHODS

Subjects

57 non-smoking subjects were included in the study. The study was performed in accordance with the Helsinki protocol, as approved by the institutional Medical Ethics Committee of the Academic Medical Center in Amsterdam. Written informed consent was obtained from all participants prior to the medical screening. All subjects underwent a medical screening on a separate day prior to the experiment consisting of a medical interview, fasting blood sampling (including plasma hemoglobin, hematocrit, HbA1C, creatinine, glucose, total-, HDL- and LDL-cholesterol), urine-testing and a 12-lead electrocardiogram (ECG). Subjects were excluded from participation in case of cardiovascular disease, hypertension, diabetes mellitus and/or neurological disease, use of vasoactive medication, abnormal lab-results, abnormal ECG and/or smoking or having smoked <10 years ago. Subjects were instructed to abstain from alcoholic and caffeinated beverages for at least 4 hours prior to the experiment.

Sessions

All subjects performed the same exercise protocol in two measurement sessions in fixed order, separated by 8 ± 4 days. During the first (TCD) session, continuous CBFv, non-invasive blood pressure (BP), heart rate (HR) and end-tidal CO_2 (Pet CO_2) responses to small muscle group exercise (dynamic handgrip) were determined. In the second (MRI) session, the spatial distribution of CBF during dynamic handgrip was assessed.

Exercise protocol

Three bouts of 5-minute rhythmic handgrip exercise were alternated with 5 minutes of rest. Prior to the measurements, maximum voluntary contraction (MVC) was measured using an MRI compatible handgrip device (Gripforce 500N, Curdes design, Philadelphia PA, USA). The highest value of three measurements was set as MVC for the duration of the experiment. To achieve and maintain a steady state hemodynamic response to exercise, one minute of rhythmic handgripping at 80% MVC was followed by 60% MVC for 4 minutes. Visual feedback of the exercise rhythm (2 seconds contraction, 2 seconds rest) and the force applied by the volunteer were displayed either on a laptop (TCD session) or onto a screen in the MRI scanner.

TCD session

Subjects were in the supine position with the head supported by a pillow. Changes in CBFv were monitored in the proximal segment of the MCA by means of transcranial Doppler ultrasonography (DWL Multidop X4, Sipplingen, Germany) using a pulsed 2 MHz TCD probe at a depth of 45–55 mm [9]. The MCA contralateral to the handgripping hand was insonated through the temporal-window above the zygomatic arch at a depth of 40–60 mm. After signal optimization [24], the probe was immobilized by a head-band. Continuous BP and heart rate (HR) was measured non-invasively by finger plethysmography with an inflatable cuff placed around the middle finger of the non-dominant hand (Nexfin, Edwards Lifesciences BMEYE, the Netherlands). End-tidal CO_2 (Pet CO_2) was continuously monitored by a nasal cannula connected to a capnograph (Datex Normocap 200, Helsinki, Finland).

MRI session

Changes in CBF were measured with a 3 Tesla Philips Achieva TX MR system (Philips, Best, The Netherlands), using a commercial 32-channel head coil. Subjects were instructed not to move their head and additional foam padding next to the head minimized motion.

A detailed listing of scanning parameters is given in Table 7.1. The MRI protocol included a whole-brain T_1 -weighted anatomical scan for anatomical depiction and gray matter segmentation, FLAIR of the brain and 3D Phase-Contrast angiography of the brain-feeding arteries. An experienced neuroradiologist (MvW) evaluated these images for structural abnormalities and the presence of carotid stenosis.

Table 7.1 | Summary of MRI scan parameters for anatomical and CBF measurements.

	Anatomical T1-weighted	Dual Echo pCASL	M0	Phase Contrast angiogram	FLAIR
Planning orientation	Transverse	Transverse	Transverse	Coronal, covering neck arteries	Transverse
Scan Technique	3D Fast Field Echo	Multi Slice Gradient Echo	Multi Slice Gradient Echo	3D Fast Field Echo	Multi slice, Inversion Recovery
Acceleration type	TFE factor 179, SENSE 1.8 RL	SENSE factor 3, EPI factor 25	SENSE factor 3, EPI factor 25	SENSE 2 RL 3 AP, Halfscan 0.85	SENS 1.75 RL, TSE factor 41
Repetition time/echo time	9.8 / 4.6 ms	4500 ms / 11 & 28.5 ms	2000 ms / 11 & 28.5 ms	10 / 6.2 ms	11000 / 120 ms
Flip / Refocusing angle	8° / -	90° / -	90° / -	10° / -	- / 120°
Field of view	224 x 176 x 168 mm ³	220 x 220 x 102 mm ³	220 x 220 x 102 mm ³	230 x 170 x 180 mm ³	230 x 184 x 119 mm ³
Acquisition voxel size	1.19 / 1.21 / 1.20 mm ³	2.75 x 2.75 x 6 mm ³	2.75 x 2.75 x 6 mm ³	0.99 / 1.00 / 2.00	0.96 / 1.33 / 4.00 mm ³
Acquisition matrix	188 x 146	72 x 69	72 x 69	232 x 170	240 x 138
Scan duration	2:47 min	30 min (400 dynamics)	22 sec (10 averages)	1:45 min	01:39 min
Labeling / PLD duration	-	1800 ms / 1800 ms	no labeling	-	-
Additional parameters	Inversion delay 935 ms	BGS pulses 1850 & 3175 ms	No BGS pulses	VENC 80 cm/s (uniform)	Inversion time 2800 ms
TFE dur. shot / acq	1938 / 1757 ms	-	-	-	-

TFE: Turbo Field Echo; BGS Background suppression; VENC: velocity encoding; SENSE: parallel imaging technique

CBF was assessed continuously during the exercise protocol using pseudo-continuous arterial spin labeling (pCASL) [32] with similar settings as in Ghariq et al. [33]. The ASL imaging volume was positioned to cover the cerebrum, and the labeling plane was planned perpendicular to the internal carotid arteries at the level of the basilar artery. Two background suppression pulses were applied after labeling to improve signal to noise ratio [34,33]. Finally, a separate M_0 scan was acquired to enable quantification of CBF ($TR_{M_0} = 2000\text{ms}$).

Heart rate was derived from the finger pulse oximetry plethysmogram, either by the build-in scanner unit, or by a patient monitoring device (Magnitude, In-Vivo, Philadelphia, California). $PetCO_2$ was sampled with a nasal cannula connected to a capnograph located outside the scanner (Capnomac Ultima, Datex, Helsinki, Finland), or the patient monitoring device. In a subset of subjects, blood pressure was monitored during resting conditions using the patient monitoring device. All signals were synchronized to the acquisition of the ASL scan.

MRI post-processing

The ASL images were preprocessed to obtain CBF values according to the procedures laid out in the consensus paper [32]. All preprocessing steps were done within the Matlab 2016a coding environment (Mathworks, Natick, Massachusetts, U.S.A) using SPM12 (<http://www.fil.ion.ucl.ac.uk/spm/>), ASLtbx [35], and AAL [36] toolboxes. The anatomical T1-weighted scan was segmented into CSF, white- and gray matter probability maps. Motion correction of the ASL series was performed using ASLtbx, taking into account the signal intensity gradient introduced by background suppression [33]. The motion corrected ASL image volumes were pairwise subtracted (control – label) and converted to units of flow according to the consensus model [32]:

$$CBF = \frac{6000 \cdot e^{\frac{PLD}{T_{1,blood}}}}{2 \cdot \alpha \cdot T_{1,blood} \cdot (1 - e^{\frac{-lbdur}{T_{1,blood}}})} \cdot \frac{SI_{control} - SI_{label}}{M_0}$$

where SI represents the spatially varying ASL signal intensity during control and label conditions. Reported values in literature for $T_{1,blood}$ (1665 ms) and labeling efficiency ($\alpha = 0.85$) were assumed. The PLD was corrected for the time-difference of the readout of the slices, starting at 1800 ms for the first slice increasing by 48 ms for subsequent slices. The M_0 -image was calculated from the M_0 scan by smoothing with a 5 mm FWHM 3D kernel, thresholded to limit the scan to brain tissue, and was corrected for finite TR with $(1 - \exp(-TR_{M_0}/T_{1,gm}))^{-1}$, with $T_{1,gm}$ assumed to be 1260 ms. The temporal mean of the CBF-series was co-registered to the gray matter probability map (SPM, Intensity Normalization metric).

MRI regions of interest

Regions of interest (ROIs) were defined to calculate the rCBF at multiple locations in the brain. For each subject, the single-subject AAL atlas [36] (Figure 7.1) was non-linearly deformed (warped) to the T_1 -weighted anatomical scan using the inverse transform obtained during the segmentation

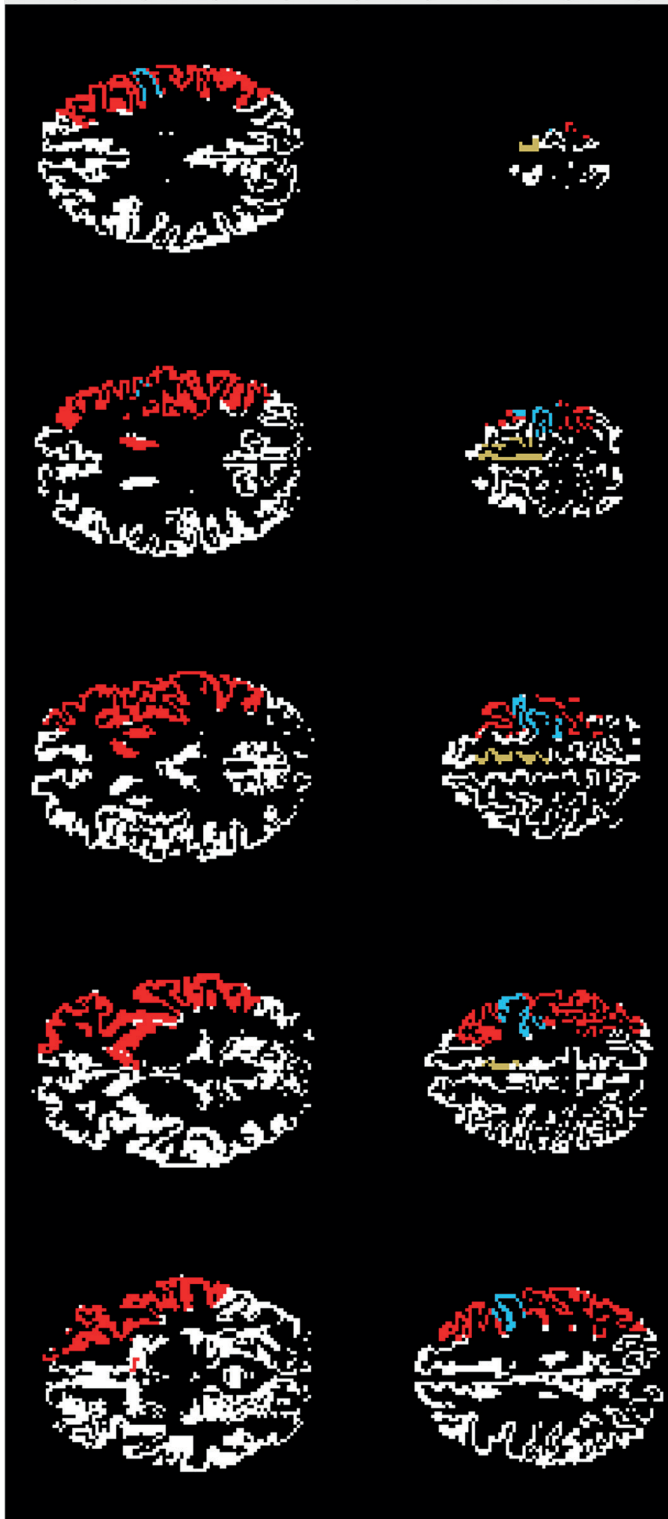


Figure 7.1 | Illustration of the grey matter mask of a representative subject. Regions of interest are indicated with color, showing MCA (red), precentral cortex (blue) and supplementary motor area (yellow).

step. The resulting subject-specific atlas was visually checked by overlaying the ROIs on the anatomical scan. All ROIs were masked by the gray matter probability map (threshold >0.9). Relative volumes of the ROI were calculated individually (in native space) by counting the number of voxels and converting to mL. ROIs were subsequently transferred to the CBF-maps, which were co-registered to the T_1 -weighted anatomical scan during the MRI post-processing steps (see above). Lower regions in the brain, e.g. vermis, brainstem and cerebellum were excluded from analysis due to a limited field-of-view of the ASL imaging module in the feet-head direction. The remaining ROIs of the AAL atlas were grouped in ACA, MCA and PCA flow territories [37]. The extent and overlap of flow territories can differ substantially between individuals, therefore next to the nominal MCA flow territory, a conservative and a liberal estimate of the MCA-territory were defined based on a surgical-anatomical atlas [37]. Specific regional CBF changes were investigated in the precentral and supplementary motor area (SMA) ROI as these regionals are generally associated with motor function. The MRI data of left handed subjects ($n = 4$) were mirrored before further analysis. To quantify the effect of visual feedback, a visual cortex ROI was defined by combining the calcarine and superior-, middle- and inferior occipital cortex.

Statistics and data analysis

Data from the TCD and MRI sessions were visually inspected and images with artifacts were excluded from analysis. The signals of BP, the envelope curve of the transcranial Doppler spectrum from the MCA and $PETCO_2$ were A/D converted at 200 Hz and stored. Mean arterial pressure (MAP), HR and the mean CBFv were calculated per heart-beat. Data were averaged over the three runs and the averaged values over the last 3 minutes of each episode of both rest or handgrip were used as steady-state values. Statistical analysis was performed using the Statistics toolbox of Matlab (v2016a). Differences within and between sessions (TCD and MRI) were inferred using paired *t*-test and ANOVA after confirming a normal distribution of the data using the Lilliefors test). The relation between the change in CBFv and CBF in predefined ROI's was investigated by regression analysis. Levene's test was used to assess the assumption of equal variances and normality of the residuals was inspected.

RESULTS

Subjects

Seven subjects were excluded based on the results of medical screening, and one subject declined participation after the screening process. Technical issues resulted in incomplete data in 10 subjects, and one additional subject had a structural abnormality on the MRI scans. The final analysis was performed on the data of the remaining 38 subjects (13 female) with a median age of 55 years (range: 19–79).

Systemic response

Resting values and responses to handgrip for both sessions are summarized in Table 7.2. Resting HR, PetCO₂ and MAP were similar for the TCD and MRI sessions. During handgrip, HR increased similarly in TCD (10±5%, p<0.01) and MRI (9±7%, p<0.01) sessions (between sessions p = 0.23). No change in PetCO₂ was detected in either session (p = 0.10 and p = 0.08 for TCD and MRI respectively). MAP increased in the TCD session by 10±5% (p<0.01) during handgrip (MAP response was not assessed during the MRI session).

Table 7.2 | Systemic response to rhythmic handgrip in the TCD and MRI sessions.

		TCD		MRI	
		Rest	Handgrip (%Delta)	Rest	Handgrip (%Delta)
HR	(bpm)	59±7	10±5%**	60±8 [†]	9±7%**
PetCO ₂	(mmHg)	39.9±3.5	1.5±4.8%	40.3±4.5 [†]	-0.9±3.6%§
MAP	(mmHg)	9±9	10±5%**	94±11 [†]	–
CBFv / CBFmca	(cm/s / ml/100g/min)	60±14	11±12%**	46±10	-1±10%

HR: heart rate; MAP: mean arterial pressure; CBFv: cerebral blood flow velocity measured by TCD; CBFmca: CBF in the MCA flow territory measured by MRI. *) p<0.05, **) p<0.01 vs. Rest; [†]) p = n.s. vs. TCD Rest; §) p<0.05, §§) p<0.01 vs. %Delta TCD; Values are means±SD.

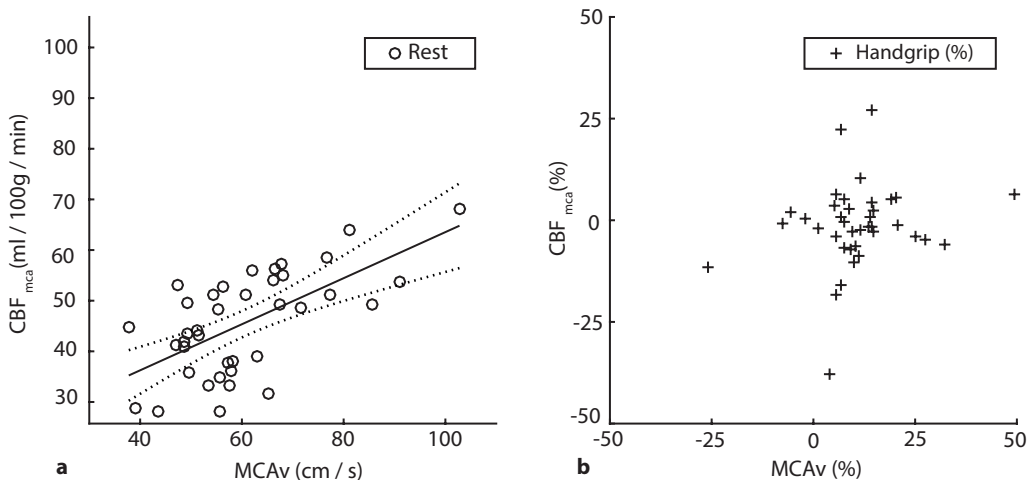


Figure 7.2 | Comparison of CBFv and CBF averaged over the MCA ROI (CBF_{mca}). **a**) Absolute values during rest with regression line $CBF_{mca} = 17.8 + 0.46 \cdot CBFv$ (p<0.001) (solid line) and 95% confidence interval (dotted line); **b**) relative response to handgrip.

Flow territory CBF versus CBFv

Both CBFv and ftCBF in the MCA flow territory ROI responses were measured in the hemisphere contralateral to the exercising hand (see Figure 7.2). During rhythmic handgrip, CBFv increased ($11 \pm 12\%$, $p < 0.01$), while no change was found in ftCBF ($-1 \pm 10\%$, $p = 0.15$). The absence of CBF change in the normal MCA flow territory definition was confirmed for both the conservative ($-0.0 \pm 10\%$) as well as for the liberal definition ($+0.1 \pm 10\%$) of the ROI. During rest CBFv was linearly related to ftCBF ($p < 0.001$), with a non-zero offset ($p < 0.01$), see Figure 7.2a.

Regional CBF versus CBFv

In Figure 7.3 the relative change rCBF in the precentral ROI is depicted against the change in CBFv. During handgrip exercise rCBF increased in the contralateral ($8 \pm 10\%$; $p < 0.01$), but not in the ipsilateral precentral ROI ($6 \pm 18\%$; $p = 0.12$). The increase in CBFv was not correlated to the regional CBF increase in the precentral ROI ($r = 0.16$, $p = 0.35$).

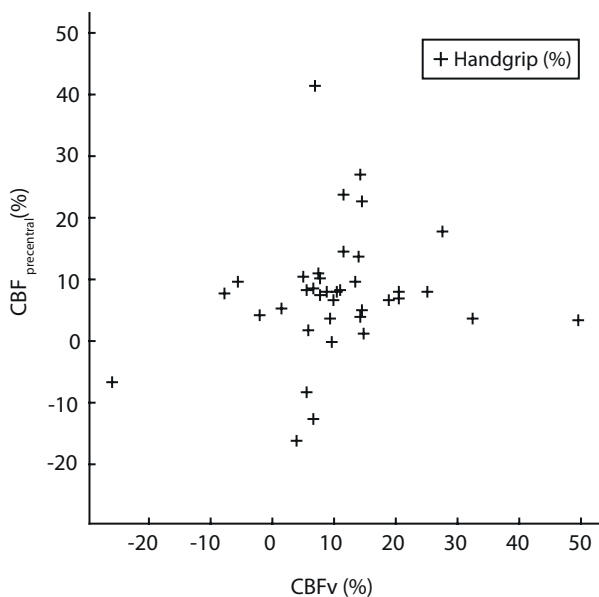


Figure 7.3 | Relative changes in CBFv and regional CBF (Precentral ROI) upon handgrip.

CBF in the contralateral SMA ROI increased ($8 \pm 13\%$; $p < 0.01$), but did not change in the ipsilateral ROI ($\pm 13\%$, $p = 0.13$). rCBF in the visual cortex ROI increased by $9 \pm 11\%$ ($p < 0.01$).

ROI Volume Estimates

Volume estimates of the MCA-, Precentral- and SMA ROIs are given in Table 7.3. The relative total volume of the precentral ROI was $10 \pm 1\%$ of the total MCA ROI, whereas the precentral gray matter volume was $7 \pm 1\%$ relative to the MCA gray matter volume.

Table 7.3 | Volume estimates of regions of interest.

	Total (mL)	GM (mL)	Relative Total (% MCA)	Relative GM (% MCA)
MCA flow territory	156±14	74±12		
Precentral	15±1	5±1	9.5±0.4%	7.0±0.7%
SMA	11±1	4±1	6.8±0.3%	5.7±0.4%

ROIs are contralateral to the side handgripping. GM: gray matter; SMA: supplementary motor area. Values are mean±SD.

DISCUSSION

This study addressed whether the increase in middle cerebral artery (MCA) blood flow velocity as measured by TCD during small muscle group exercise parallels CBF within the relevant area of the brain as measured by ASL-MRI. The main finding is that the CBFv increased by 11%, whereas no change could be detected in the corresponding flow territory CBF, although an 8% increase in rCBF was detected in the functional relevant brain regions. This finding calls into question the use of TCD velocity changes as a proxy for cerebral blood flow changes.

To illustrate this disparity, the locations of the CBFv and CBF measurements are graphically depicted in Figure 7.4. The observed increase in CBFv is well within the range (8–19%) previously reported by studies using rhythmic handgrip [23–31]. Traditionally, an increase in CBFv is assumed to imply a ftCBF response. For example, a hypothetical rCBF increase of 110% in a tenth of the flow territory volume (see Table 7.3) is required to increase ftCBF by 11%, which is much larger than observed in this study or reported in MRI literature. Conversely, the observed 8% increase in rCBF would predict a 0.8% increase in ftCBF, which is clearly at odds with the observed increase in CBFv. Although in-between scenarios can be constructed, these black-and-white scenarios illustrate clearly the order of magnitude discrepancy between the measured CBFv and ftCBF.

Validity of ASL and TCD measurements

Assumptions of both TCD and ASL could attribute to the observed discrepancy. Particularly relevant are the assumptions that affect the percentage change as used in the present study. Factors affecting only the quantitative scaling have been discussed elsewhere for TCD [38] and ASL-MRI [32].

In ASL-MRI, the labeling efficiency is dependent on the blood flow velocity of the arteries at the level of the labeling plane. Simulations showed that the efficiency decreases only by ~1% when velocity is increased by 20% [39,40], therefore it can be assumed that reduced labeling efficiency contributes little to the observed discrepancy. During exercise, faster blood flow shortens the transport time of the labeled blood to the tissue. Theoretically this could lead to an overestimation of the CBF-increase (more labeled blood arrives in the ROI), but could also lead

to an underestimation of the CBF response due to faster decay of the label in the tissue (label stays a shorter time in blood, whereas the T_1 of tissue is smaller than T_1 of blood). Finally, during exercise the T_2^* of the label might be prolonged due to the higher levels of blood oxygenation (BOLD-effect), leading again to an overestimation of the CBF-increase [41]. Therefore, it is difficult to provide a clear explanation why ASL-MRI would severely underestimate the mean CBF increase over the MCA-flow territory.

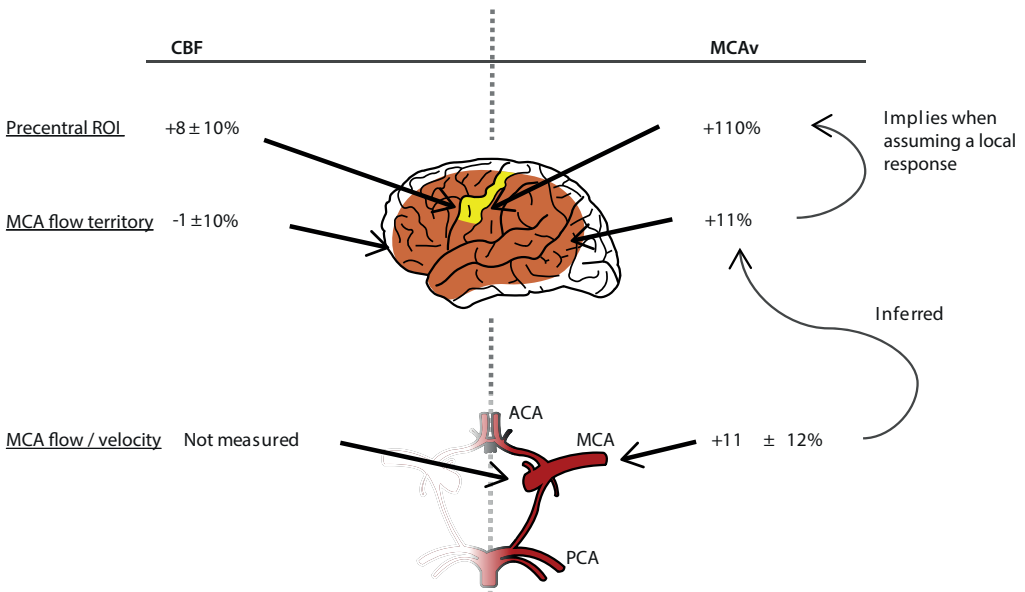


Figure 7.4 | Schematic representation of the location of the regional CBF and CBFv changes observed in the present study. Note that the CBF also increased outside the indicated areas: in particular, the supplementary motor area and visual cortex which are both not supplied by the MCA. Illustrations adapted from Wikimedia under the creative commons license.

An important assumption in TCD is the constancy of the MCA diameter. A decrease in MCA cross-sectional area would inverse-proportionally affect the flow, at constant velocity. In a previous study, we assessed the MCA cross-sectional area response during rhythmic handgrip exercise using high resolution MRI [42]. In that study, the exact same handgrip protocol was used as in the present study, although in a different study population (age range 20–59 years). On average a 2% decrease in cross-sectional area was observed. This difference is small and could maximally explain a fifth of the 11% CBFv increase observed in the present study. Therefore, the minimal change in MCA diameter during handgrip exercise is not the sole contributor to the discrepancy.

In transcranial Doppler ultrasonography, the reported change in CBFv is usually based on the average maximum velocity derived from TCD spectrum of multiple heart beats [9,38]. The maximum velocity is used as a proxy for the cross-sectional average velocity, which physically

defines flow. The relation between the maximum and cross-sectional velocity can be complex in the short and curved MCA (M1 segment), but is assumed stable when comparing beat-to-beat averages. Changes in the flow profile can offset this relation and maximum velocity potentially underestimates the changes in average cross-sectional velocity. However, CBFv matches the flow increase in the internal carotid artery during loaded cycling [43], rendering an important offset between maximum- and cross-sectional velocity unlikely.

In summary, both ASL and TCD both involve assumptions that could potentially under- or overestimate the change in cerebral perfusion upon exercise, but reasonable estimation of the order of magnitude of such errors limit these to a few percentage points. Hence these do not satisfactorily explain the order of magnitude difference between the observed CBFv and CBF changes. Therefore, without clear evidence of the invalidity of either of the two modalities, other explanations need to be considered.

Possible explanation

Shunting of arterial blood directly to the venous side through arteriovenous anastomosis, or to other tissues than the brain is a straightforward explanation for the discrepancy between TCD and MRI flow. For example, shunting would increase MCA flow while bypassing brain-tissue, hence leaving ftCBF unchanged. However, multiple arguments make this concept unlikely. For instance, it is currently accepted that the MCA is an end-artery, hence it contains no shunts and feeds exclusively brain-tissue. However, quantitative data on variability and functional consequences of shunts (leptomeningeal anastomoses) in humans are virtually lacking [44]. Moreover, the presence of pre-capillary arteriovenous-shunts in the brain has not been evidenced [45]. In ASL, shunting would be expected to show residual signal in venous compartments, as was observed in patients with an arterio-venous malformation [46], but not seen in healthy volunteers nor in our participants. Moreover, such assumed shunts would have to be “recruited” during exercise to accommodate an 11% increase in CBFv. Therefore, the shunting of blood flow seems an unlikely explanation and further research would be required to determine how bulk flow and tissue perfusion are related during the degree of neural recruitment involved at this type of exercise.

Correlation CBFv with rCBF

Although the interpretation of CBFv as a proxy of CBF changes in the flow territory might be difficult based on our results, TCD measurements during exercise might be considered of practical use if changes in CBFv would be directly associated with the increase in rCBF. However, no correlation between the change in CBFv and change in CBF in the precentral ROI was observed (see Figure 7.3). The present study is considered limited to assess a possible correlation between rCBF and CBFv as it employed only one intensity of exercise, and the absence of correlation should be verified with graded exercise intensities or by employing exercise with different levels of complexity. Even if such an association would be confirmed, the current observations would still introduce several conceptual difficulties.

Limitations of the present study

Some limitations pertaining to the present study must be considered. The exercise protocol in the present study was part of a larger research program, which might have influenced the present results. Prior to the handgrip exercise all subjects participated in a lower body negative pressure LBNP experiment at -50 mmHg. The LBNP exposure was performed in both the TCD and MRI session and was well tolerated by all subjects. Furthermore, minimally 15 minutes of supine rest was allowed before the start of the handgrip protocol and therefore the effect on the response to exercise was assumed to be negligible. The MRI table was modified to accommodate the LBNP box necessitating to raise subjects and head coil by 75 mm, therefore creating an offset with the magnet iso-center. This did not lead to visible decrease in image quality or artifacts; furthermore, any possible effect would impact both the CBF measurement in rest as well as the exercise-measurement, making it unlikely that the relative increase would be severely underestimated. The experiments were divided between two sessions in fixed order. Our pilot studies (unpublished data) and previous research [47,48] showed that the cardiovascular response upon exercise is highly similar when performed one week later. In the present study, comparable HR response was observed between sessions in addition to similar baseline parameters for HR, MAP and PetCO₂. This suggests a comparable cardiovascular response during both sessions and we therefore assume a similar cerebral hemodynamic response.

A-priori defined regions of interest (ROIs) were used to calculate the regional CBF increases. However, due to the heterogeneity of the CBF-response and the uncertainty in the exact location of the CBF response, this ROI might be sub-optimally defined. This could either result in an overestimation or an underestimation of the CBF response. An alternative approach would be the use of voxel-based statistics to define and search for clusters of significant increased CBF upon exercise. This would, however, make the ROI definition dependent on the CBF response itself and the employed threshold and it could result in large differences in ROI-volume between subjects. Therefore, the present study used an atlas to consistently define and evaluate regional CBF increase in predefined ROIs, therefore preventing a potential bias.

Visual feedback was used during the handgrip session, which could be considered a limitation of the present study. Visual stimulation is a potent stimulus and we observed a corresponding increase of 8.7% in the visual cortex ROI. The visual cortex is normally supplied by the PCA [37] and this was not investigated using TCD in the present study. The same software was used for visual feedback during both sessions, therefore a possible influence of visual stimulation on the response in the MCA territory was considered unlikely and it is assumed not to have impacted the results of this study.

CONCLUSION

During handgrip exercise ASL determined CBF does not support the claim that TCD determined changes in CBFv are a proxy for CBF changes in the relevant brain areas. The results suggest an order of magnitude difference in the measured hemodynamic response upon exercise between the two modalities. Shunting of MCA blood flow during exercise bypassing the brain tissue could be an explanation for this discrepancy. However, evidence for such a mechanism is currently lacking. Implications could be far reaching for either or both modalities, indicating the need to further explore the relation of arterial blood flow and tissue perfusion.

Acknowledgement

The authors would like to acknowledge drs. W.J. Stok for assistance in preparing and executing the experiments.

REFERENCE LIST

1. Fox PT, Raichle ME (1986) Focal physiological uncoupling of cerebral blood flow and oxidative metabolism during somatosensory stimulation in human subjects. *Proceedings of the National Academy of Sciences of the United States of America* 83 (4):1140-1144
2. Ide K, Horn A, Secher NH (1999) Cerebral metabolic response to submaximal exercise. *J Appl Physiol* 87 (5):1604-1608
3. Quistorff B, Secher NH, Van Lieshout JJ (2008) Lactate fuels the human brain during exercise. *FASEB J* 22 (10):3443-3449. doi:10.1096/fj.08-106104
4. Raichle ME, Grubb RL, Jr., Gado MH, Eichling JO, Ter Pogossian MM (1976) Correlation between regional cerebral blood flow and oxidative metabolism. In vivo studies in man. *ArchNeurol* 33 (8):523-526
5. Laughlin MH, Davis MJ, Secher NH, van Lieshout JJ, Arce-Esquivel AA, Simmons GH, Bender SB, Padilla J, Bache RJ, Merkus D, Duncker DJ (2012) Peripheral circulation. *Compr Physiol* 2 (1):321-447. doi:10.1002/cphy.c100048
6. Lassen NA, Ingvar DH, Skinhoj E (1978) Brain function and blood flow. *Sci Am* 239 (4):62-71
7. Olesen J (1971) Contralateral focal increase of cerebral blood flow in man during arm work. *Brain* 94 (4):635-646
8. Obrist WD, Thompson HK, Jr., Wang HS, Wilkinson WE (1975) Regional cerebral blood flow estimated by 133-xenon inhalation. *Stroke* 6 (3):245-256
9. Aaslid R, Markwalder TM, Nornes H (1982) Noninvasive transcranial Doppler ultrasound recording of flow velocity in basal cerebral arteries. *J Neurosurg* 57 (6):769-774
10. Jorgensen LG, Perko M, Hanel B, Schroeder TV, Secher NH (1992) Middle cerebral artery flow velocity and blood flow during exercise and muscle ischemia in humans. *J Appl Physiol* 72 (3):1123-1132
11. Jorgensen LG, Perko G, Secher NH (1992) Regional cerebral artery mean flow velocity and blood flow during dynamic exercise in humans. *J Appl Physiol* 73 (5):1825-1830
12. Kim YS, Seifert T, Brassard P, Rasmussen P, Vaag A, Nielsen HB, Secher NH, van Lieshout JJ (2015) Impaired cerebral blood flow and oxygenation during exercise in type 2 diabetic patients. *Physiological reports* 3 (6):1-13. doi:10.14814/phy2.12430
13. Hellstrom G, Fischer-Colbrie W, Wahlgren NG, Jogestrand T (1996) Carotid artery blood flow and middle cerebral artery blood flow velocity during physical exercise. *J Appl Physiol* 81 (1):413-418
14. Sato K, Ogoh S, Hirasawa A, Oue A, Sadamoto T (2011) The distribution of blood flow in the carotid and vertebral arteries during dynamic exercise in humans. *J Physiol* 589 (Pt 11):2847-2856. doi:10.1113/jphysiol.2010.204461
15. Sato K, Moriyama M, Sadamoto T (2009) Influence of central command on cerebral blood flow at the onset of exercise in women. *Exp Physiol* 94 (11):1139-1146
16. Friedman DB, Friberg L, Mitchell JH, Secher NH (1991) Effect of axillary blockade on regional cerebral blood flow during static handgrip. *J Appl Physiol* 71 (2):651-656
17. Williamson JW, McColl R, Mathews D (2003) Evidence for central command activation of the human insular cortex during exercise. *J Appl Physiol* 94 (5):1726-1734
18. Williamson JW, Friedman DB, Mitchell JH, Secher NH, Friberg L (1996) Mechanisms regulating regional cerebral activation during dynamic handgrip in humans. *J Appl Physiol* 81 (5):1884-1890
19. Williamson JW, McColl R, Mathews D, Ginsburg M, Mitchell JH (1999) Activation of the insular cortex is affected by the intensity of exercise. *J Appl Physiol* 87 (3):1213-1219
20. Fontes EB, Okano AH, De Guio F, Schabert EJ, Min LL, Basset FA, Stein DJ, Noakes TD (2015) Brain activity and perceived exertion during cycling exercise: an fMRI study. *Br J Sports Med* 49 (8):556-560. doi:10.1136/bjsports-2012-091924
21. Mehta JP, Verber MD, Wieser JA, Schmit BD, Schindler-Ivens SM (2009) A novel technique for examining human brain activity associated with pedaling using fMRI. *Journal of neuroscience methods* 179 (2):230-239. doi:10.1016/j.jneumeth.2009.01.029

22. King M, Rauch HG, Stein DJ, Brooks SJ (2014) The handyman's brain: a neuroimaging meta-analysis describing the similarities and differences between grip type and pattern in humans. *NeuroImage* 102 Pt 2:923-937. doi:10.1016/j.neuroimage.2014.05.064
23. Jørgensen LG, Perko G, Payne G, Secher NH (1993) Effect of limb anesthesia on middle cerebral response to handgrip. *American journal of physiology Heart and circulatory physiology* 264 (2 Pt 2):H553-H559
24. Pott F, Jensen K, Hansen H, Christensen NJ, Lassen NA, Secher NH (1996) Middle cerebral artery blood velocity and plasma catecholamines during exercise. *Acta Physiol Scand* 158 (4):349-356. doi:10.1046/j.1365-201X.1996.564325000.x
25. Pott F, Ray CA, Olesen HL, Ide K, Secher NH (1997) Middle cerebral artery blood velocity, arterial diameter and muscle sympathetic nerve activity during post-exercise muscle ischaemia. *Acta Physiol Scand* 160 (1):43-47
26. Ide K, Pott F, Van Lieshout JJ, Secher NH (1998) Middle cerebral artery blood velocity depends on cardiac output during exercise with a large muscle mass. *Acta Physiol Scand* 162 (1):13-20. doi:10.1046/j.1365-201X.1998.0280f.x
27. Giller CA, Giller AM, Cooper CR, Hatab MR (2000) Evaluation of the cerebral hemodynamic response to rhythmic handgrip. *J Appl Physiol* 88:2205-2213
28. Rasmussen P, Plomgaard P, Krogh-Madsen R, Kim YS, van Lieshout JJ, Secher NH, Quistorff B (2006) MCA Vmean and the arterial lactate-to-pyruvate ratio correlate during rhythmic handgrip. *J Appl Physiol* 101 (5):1406-1411. doi:10.1152/jappphysiol.00423.2006
29. Kim YS, Krogh-Madsen R, Rasmussen P, Plomgaard P, Ogoh S, Secher NH, van Lieshout JJ (2007) Effects of hyperglycemia on the cerebrovascular response to rhythmic handgrip exercise. *Am J Physiol Heart Circ Physiol* 293 (1):H467-473. doi:10.1152/ajpheart.00045.2007
30. Ono T, Hasegawa Y, Hori K, Nokubi T, Hamasaki T (2007) Task-induced activation and hemispheric dominance in cerebral circulation during gum chewing. *J Neuro* 254 (10):1427-1432. doi:10.1007/s00415-007-0570-3
31. Miyazawa T, Horiuchi M, Ichikawa D, Sato K, Tanaka N, Bailey DM, Ogoh S (2011) Kinetics of exercise-induced neural activation; interpretive dilemma of altered cerebral perfusion. *Exp Physiol*
32. Alsop DC, Detre JA, Golay X, Gunther M, Hendrikse J, Hernandez-Garcia L, Lu H, MacIntosh BJ, Parkes LM, Smits M, van Osch MJ, Wang DJ, Wong EC, Zaharchuk G (2015) Recommended implementation of arterial spin-labeled perfusion MRI for clinical applications: A consensus of the ISMRM perfusion study group and the European consortium for ASL in dementia. *Magnetic resonance in medicine : official journal of the Society of Magnetic Resonance in Medicine / Society of Magnetic Resonance in Medicine* 73 (1):102-116. doi:10.1002/mrm.25197
33. Ghariq E, Chappell MA, Schmid S, Teeuwisse WM, van Osch MJ (2014) Effects of background suppression on the sensitivity of dual-echo arterial spin labeling MRI for BOLD and CBF signal changes. *NeuroImage* 103:316-322. doi:10.1016/j.neuroimage.2014.09.051
34. Ye FQ, Frank JA, Weinberger DR, McLaughlin AC (2000) Noise reduction in 3D perfusion imaging by attenuating the static signal in arterial spin tagging (ASSIST). *Magnetic resonance in medicine : official journal of the Society of Magnetic Resonance in Medicine / Society of Magnetic Resonance in Medicine* 44 (1):92-100
35. Wang Z, Aguirre GK, Rao H, Wang J, Fernandez-Seara MA, Childress AR, Detre JA (2008) Empirical optimization of ASL data analysis using an ASL data processing toolbox: ASLtbx. *Magnetic resonance imaging* 26 (2):261-269. doi:10.1016/j.mri.2007.07.003
36. Tzourio-Mazoyer N, Landeau B, Papathanassiou D, Crivello F, Etard O, Delcroix N, Mazoyer B, Joliot M (2002) Automated anatomical labeling of activations in SPM using a macroscopic anatomical parcellation of the MNI MRI single-subject brain. *NeuroImage* 15 (1):273-289. doi:10.1006/nimg.2001.0978
37. Tatu L, Moulin T, Bogousslavsky J, Duvernoy H (1998) Arterial territories of the human brain: cerebral hemispheres. *Neurology* 50 (6):1699-1708
38. Kontos HA (1989) Validity of cerebral arterial blood flow calculations from velocity measurements. *Stroke* 20 (1):1-3
39. Gevers S, Nederveen AJ, Fijnvandraat K, van den Berg SM, van OP, Heijtel DF, Heijboer H, Nederkoorn PJ, Engelen M, van Osch MJ, Majoie CB (2012) Arterial spin labeling measurement of cerebral perfusion in children with sickle cell disease. *J Magn Reson Imaging* 35 (4):779-787. doi:10.1002/jmri.23505 [doi]
40. Dai W, Garcia D, de BC, Alsop DC (2008) Continuous flow-driven inversion for arterial spin labeling using pulsed radio frequency and gradient fields. *Magnetic resonance in medicine* 60 (6):1488-1497

41. Petersen ET, Zimine I, Ho YC, Golay X (2006) Non-invasive measurement of perfusion: a critical review of arterial spin labelling techniques. *Br J Radiol* 79 (944):688-701. doi:10.1259/bjr/67705974
42. Verbree J, Bronzwaer A, van Buchem MA, Daemen M, van Lieshout JJ, van Osch M (2016) Middle cerebral artery diameter changes during rhythmic handgrip exercise in humans. *J Cereb Blood Flow Metab*. doi:10.1177/0271678X16679419
43. Hellström G, Fischer-Colbrie W, Wahlgren NG, Jøgestrand T (1996) Carotid artery blood flow and middle cerebral artery blood flow velocity during physical exercise. *J Appl Physiol* 81 (1):413-418
44. Brozici M, van der Zwan A, Hillen B (2003) Anatomy and functionality of leptomeningeal anastomoses: a review. *Stroke* 34 (11):2750-2762. doi:10.1161/01.str.0000095791.85737.65
45. Duvernoy HM, Delon S, Vannson JL (1981) Cortical blood vessels of the human brain. *Brain Res Bull* 7 (5):519-579
46. Le TT, Fischbein NJ, Andre JB, Wijman C, Rosenberg J, Zaharchuk G (2012) Identification of venous signal on arterial spin labeling improves diagnosis of dural arteriovenous fistulas and small arteriovenous malformations. *Am J Neuroradiol* 33 (1):61-68. doi:10.3174/ajnr.A2761
47. Sinoway L, Shenberger J, Leaman G, Zelis R, Gray K, Baily R, Leuenberger U (1996) Forearm training attenuates sympathetic responses to prolonged rhythmic forearm exercise. *J Appl Physiol* 81 (4):1778-1784
48. Lopez MG, Silva BM, Joyner MJ, Casey DP (2012) Ischemic exercise hyperemia in the human forearm: reproducibility and roles of adenosine and nitric oxide. *Eur J Appl Physiol* 112 (6):2065-2072. doi:10.1007/s00421-011-2035-8

CHAPTER 8

Influence of the cardiac cycle on pCASL: cardiac triggering of the end-of-labeling

J. Verbree

M.J.P. van Osch

Magn Reson Mater Phy (MAGMA) 2017 Mar 9

DOI: 10.1007/s10334-017-0611-6

ABSTRACT

Object: In arterial spin labeling (ASL), the cardiac cycle might adversely influence signal-stability by varying the amount of label created, labeling efficiency and/or transport times. Due to the long labeling duration in pseudo-Continuous ASL (pCASL), the blood labeled last contributes most to the ASL-signal. The present study investigated, using numerical simulations and in-vivo experiments, the effect of the cardiac cycle on pCASL, thereby focusing on the end-of-labeling.

Materials and Methods: In the in-vivo experiments the end-of-labeling was timed to a specific cardiac phase while a long labeling duration of >7 seconds was used to isolate the influence of the lastly labeled spins on ASL-signal stability.

Results: Simulations showed dependence of the ASL-signal on the cardiac phase of the end-of-labeling, and that the variation in signal was more pronounced at lower heart rates. The ASL-signal variation was small ($\sim 4\%$), but could be effectively reduced by simulated end-of-labeling triggering. In-vivo, no difference in mean CBF ($p = 0.58$) nor in CBF temporal-STD ($p = 0.44$) could be detected between triggered and non-triggered acquisitions.

Conclusion: Influence of the cardiac cycle on pCASL-signal stability is small and triggering the start-of-labeling and end-of-labeling can be considered not to have practical implications to improve stability.

Keywords

Perfusion magnetic resonance imaging; Cerebrovascular circulation; Pulsatile Flow; Cerebral blood flow

INTRODUCTION

Pseudo Continuous Arterial Spin Labeling (pCASL) is the current recommended and validated non-invasive MR technique to image cerebral blood flow (CBF) [1,2]. The pCASL sequence consists of separate label and control acquisitions which are subtracted to yield a CBF measurement. Since labeling efficiency of pCASL depends on the blood flow velocity [3] and the recommended labeling duration is approximately two times the cardiac interval, perturbations of the ASL-signal due to variation in timing of the acquisitions with respect to the cardiac cycle should be expected. Such physiological noise could potentially be reduced by synchronizing the ASL acquisitions to the cardiac cycle. Synchronizing the moment of labeling to the cardiac cycle by means of cardiac triggering has been shown to reduce signal variability over time in pulsed ASL [4,5]. However, pulsed ASL has a much shorter labeling duration (≈ 20 ms) compared to pCASL (1500–2000 ms) and the generation of label is therefore almost instantaneous and can easily be timed to always happen at the same moment within the cardiac cycle. A similar cardiac triggering approach has previously been investigated in continuous ASL by triggering the start of the labeling. However, no improvements in signal stability were observed using this approach [6]. This might be explained by the long labeling duration that will result in asynchronous timing at the end of the labeling and the moment of imaging even when the start of the labeling was triggered.

In ASL, the magnetic labeling of blood decays with the T_1 of arterial blood (at least until the label is exchanged with brain tissue after which it will decay with the T_1 of tissue). Label generated later in the labeling period will be less affected by this decay and will therefore contribute more to the detected signal. For example, at a labeling duration of 1.8 seconds, label generated at the end of the labeling period contributes a factor three more to the totally detected ASL-signal compared to label generated at the start of labeling. Therefore, the largest contribution to the ASL-signal arises from the end of the labeling period. The greatest impact of cardiac triggering on ASL-signal stability should therefore be expected when triggering the end-of-labeling.

Three main effects of flow velocity in the feeding arteries on pCASL signal stability can be expected. First, the amount of label generated is proportional to the volume of spins flowing through the labeling plane and thus on the blood flow velocity. Secondly, the labeling efficiency is known to depend on the velocity of the flowing blood. Finally, the transport time of label to the brain tissue is dependent on the blood flow velocity and will influence the relative time the label spends in the blood versus the tissue compartment. That is, faster delivery (i.e. higher flow velocity) of the label to the tissue will reduce the ASL-signal due to smaller T_1 in tissue compared to the blood compartment. Therefore, in summary, both the generation and the delivery of the label are dependent on the blood flow velocity which varies over the cardiac cycle. Both effects could have an independent, but opposite influence on the pCASL-signal stability. Furthermore, these effects are expected to have a stronger impact on the ASL-signal at the end-of-labeling than at the start of the labeling.

The aim of the present study was to investigate the influence of the cardiac cycle on pCASL-signal by studying the influence of triggering the end-of-labeling on the pCASL-signal stability. By focusing on the end-of-labeling, the moment of the largest influence is isolated, thereby providing a worst-case scenario estimation of the influence of the cardiac cycle on the pCASL-signal and its stability. Simulations were used to assess the influence of pulsatile flow in combination with variations in heart rate on the pCASL-signal stability. Subsequently, in-vivo experiments with end-of-labeling triggering were performed in normal healthy subjects to confirm the findings from these simulations. During the in-vivo experiments impractically long labeling durations were employed to isolate the effect of triggering the end-of-labeling without confounding influences of variation in the total labeling duration.

MATERIALS AND METHODS

Numerical model

A numerical model was implemented in MATLAB 2016a (Mathworks, Natick, MA, USA) to investigate the effect of the cardiac cycle on the ASL-signal, by simulating both label generation and label delivery. The model was subsequently used to investigate the effect of pulsatile flow, heart rate variability and end-of-labeling triggering.

The numerical model simulates the label generation in a single artery and the delivery of the labeled spins into a large tissue compartment, which acts as sink. Fresh blood flows into the artery at the labeling plane according to a typical velocity curve as encountered in the internal carotid artery of an adult person (see Figure 8.1). The arterial compartment consists of a single 300 mm long artery discretized into blocks of 0.01 mm length. Blood flow is simulated by shifting blocks, so that for blood flowing at 24 cm/s a transport time through the arterial compartment of 1250 ms is achieved. Labeling of blood is simulated by introducing blocks with inverted magnetization, while taking into account the labeling efficiency (0.85). When no labeling is applied, the blood magnetization is set to the fully relaxed magnetization ($M_0 = 1.0$). Each iteration (1 ms) the blood is pushed into the artery. Blood at the end of the artery is subsequently pushed into the tissue compartment, which has a size equal to 250.000 blocks. Subsequently, the longitudinal (T_1) magnetization of all blocks in the arterial and tissue compartments is updated according to the Bloch equations [7]:

$$M_z(t+dt) = M_z(t) \cdot e^{-dt/T_1} + M_0 \cdot (1 - e^{-dt/T_1})$$

where the time-step (dt) is taken as 1 ms and the T_1 is set to $T_{1,blood}$ (1664 ms [8]) and $T_{1,tissue}$ (1105 ms, estimate for a voxel containing both gray and white matter [9]) for the arterial- and tissue compartments, respectively.

The control condition of the ASL experiment is not explicitly simulated, but is assumed to be equal to the total sum of blocks making up the tissue compartment. This implies that we assume that the inflowing magnetization is only affected during the label condition and that the control condition is perfect and unaffected by the timing with respect to the cardiac cycle. The blood flow is calculated from the difference (ΔM) between the control condition and simulated label signal and subsequently quantified according to the consensus formula by correcting for the finite labeling duration (LBL) and post labeling delay (PLD) [1]:

$$f = \Delta M \frac{e^{PLD/T_{1,blood}}}{(1 - e^{-LBL/T_{1,blood}})}$$

The flow, or CBF, is the parameter of interest of the simulation and will be referred to as “signal” or “ASL-signal” throughout the manuscript. The recommended timing of 1800 ms for labeling and PLD are used in the initial simulations.

Pulsatile blood flow is simulated by repeating the typical velocity curve (Figure 8.1) to fill the entire duration of the simulation. To isolate the effect of flow pulsatility during labeling (or the PLD), the velocity is set, for some experiments, equal to the mean velocity (i.e. constant velocity, no pulsatility) during certain sub-parts of the ASL sequence. The heart rate was modified by altering the duration of the cardiac cycle, i.e. by linearly scaling the flow velocity curve in the temporal domain. Heart rate variability is achieved in the same way, by randomly altering the duration of each cardiac cycle. Note that the pulsatility (difference between minimum and maximum velocity) is not altered throughout the simulations. The timing of the arrival of label in the tissue compartment is characterized by the bolus arrival time (BAT) and the tail arrival time (TAT). BAT is defined as the first non-zero ASL-signal value arriving in the tissue compartment, whereas TAT is defined as the last non-zero ASL-signal value leaving the arterial compartment.

Labeling efficiency is velocity-dependent and varies between the cardiac phases. The labeling efficiency for a single velocity has been described in a numerical model [10]. However, the flow profile within the vessel varies with the distance from the vessel wall. The data from the numerical model [10] was recalculated assuming parabolic flow profile in the simulated artery (see Figure 8.1b). To isolate the effects of spatially as well as temporally varying labeling efficiencies due to blood velocity differences from other influences on ASL signal stability, labeling efficiency was assumed constant for the other simulations.

The resulting ASL-signal and other variables (e.g. BAT) are expressed relative to the signal as obtained from simulations with a constant mean flow velocity as input. The relative signal (ΔS) is expressed as: $\Delta S = (B - A)/A \cdot 100\%$, where A represents the constant- and B pulsatile flow condition. The cardiac phase is defined as the normalized timing within the cardiac cycle and runs therefore from 0 to 1. Mean and standard deviations of the cardiac phase are calculated by taking into account that the cardiac phase “wraps around” each cardiac cycle, i.e. circular statistics [11].

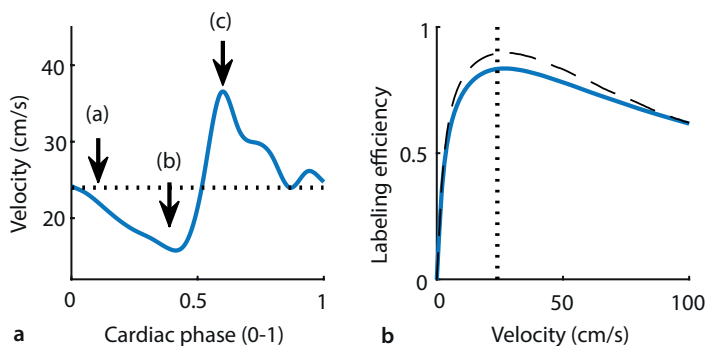


Figure 8.1 | Graphical representation of **a**) a typical velocity curve from a representative subject of the present study in the internal carotid artery, which is used as template in the simulations and **b**) the velocity dependent labeling efficiency as employed in the simulations. The labeling efficiency (dashed line) is adapted from the numerical model described in [10], while assuming parabolic flow profile in the simulated artery (blue line). The dotted line denotes the average velocity (24 cm/s) for visual reference.

In-vivo experiments

Data from eight healthy volunteers (4 female) with a mean age of 30 years (range 23–52), were acquired on a Philips 3T MRI (Achieva, Philips, Best, The Netherlands). All participants were screened for MRI safety compliance and the study protocol was approved by the Ethics Review Board of the Leiden University Medical Center. Prior written informed consent was obtained from all subjects and the study was performed in accordance with the Helsinki protocol.

The vendor supplied pCASL sequence was modified to incorporate both start-of-labeling as well as end-of-labeling triggering. A graphical representation of the ASL sequence in relation to the trigger and the employed trigger-delays is depicted in Figure 8.2. To stop the end-of-labeling in a certain cardiac phase, a delay parameter was set on the scanner that determines the additional labeling duration after receiving a cardiac trigger event. The delay parameter was set by the operator to three distinct cardiac phases (a, b and c) based upon the subject's velocity curve, see Figure 8.1. The velocity curve was obtained prior to the ASL acquisition by means of phase contrast MRA (for acquisition parameters, see Table 8.1). The minimum labeling duration, i.e. the moment after which the scanner will look for the next cardiac trigger, was chosen so that the expected average labeling duration was 7500 ms.

The triggered scan was acquired continuously, cycling through the cardiac phases (a-b-c-a-b-c....) resulting in 20 label and control images for each cardiac phase. In addition to end-of-labeling triggering, both control and label acquisitions were triggered at the start-of-labeling to exclude any residual influence of the start-of-labeling. The control condition was defined to have the same labeling duration as the preceding, end-of-labeling triggered label acquisition, this to ensure equal effects on static tissue magnetization for the control and label condition. A non-triggered reference ASL scan was acquired with the same imaging parameters and a labeling duration of

7500 ms. Total scan time was approximately one hour, exact duration depending on the heart rate.

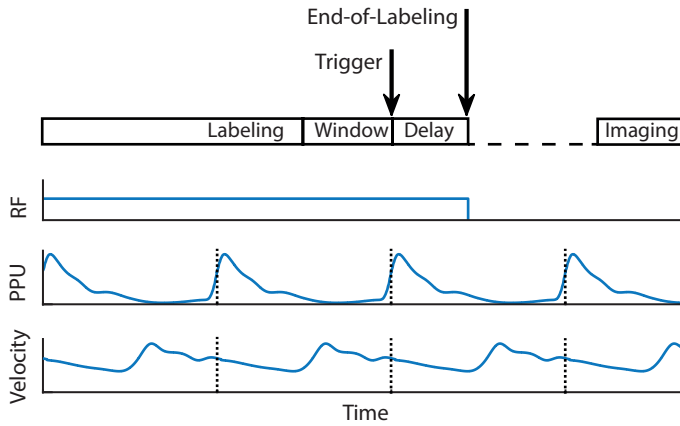


Figure 8.2 | Schematic representation of the modified pCASL sequence (top) with respect to the labeling RF, finger pulse-oxymetry signal (PPU) and blood flow velocity at the labeling plane. “Labeling” indicates the minimum labeling duration (7500 ms – delay). Arrows indicate the cardiac trigger and moment of end-of-labeling. Note the shift between finger PPU trigger and velocity during labeling.

The post-processing of the in-vivo data were performed in MATLAB v2016a (Natick, MA, US) with the SPM12 toolbox. After motion correction, the ASL-images were quantified using the consensus formula, taking into account the increase in PLD for later acquired slices (36 ms inter-slice interval with ascending slice-order, starting from 1800ms) [1]:

$$CBF = \frac{6000 \cdot \lambda \cdot e^{-\frac{PLD}{T_{1,blood}}}}{2 \cdot \alpha \cdot T_{1,blood} \cdot (1 - e^{-\frac{lbldur}{T_{1,blood}}})} \cdot \frac{SI_{control} - SI_{label}}{M_0}$$

The quantification was performed per dynamic to correct for the varying labeling duration while triggering the end-of-labeling. The global scaling factor M_0 was obtained from the maximum “pure water” CSF signal ($M_{0,csf}$) in the lateral ventricles of the non-triggered scan assuming a fully relaxed signal at a repetition time of 8.2 seconds. The $M_{0,csf}$ was corrected for the water content of arterial blood (76%) to obtain the value of fully relaxed spin in blood: $M_{0,blood} = M_{0,csf} \cdot 0.76$ [12]. The average quantified CBF was subsequently calculated by employing a gray matter mask obtained from the segmentation of the T_1 -weighed scan. Differences between the (non)-triggered conditions were assessed using the non-parametric Friedman’s test (Matlab 2016a).

Table 8.1 | Acquisition parameters

	Anatomical T1-weighted	Phase Contrast MRA	Triggered pCASL	Non-Triggered pCASL
Scan Technique	3D Fast Field Echo	2D Fast Field Echo	Multi-slice Gradient Echo	Multi-slice Gradient Echo
Acceleration type	TFE factor 179, SENSE 1.8 RL	–	SENSE factor 2.5, EPI factor 35	SENSE factor 2.5, EPI factor 35
Repetition time/echo time	9.8 / 4.6 ms	13 / 8 ms	variable / 14 ms	8200 ms (fixed) / 14 ms
Flip / Refocusing angle	8° / –	10° / –	90° / –	90° / –
Field of view	224 x 176 x 168 mm ³	150 x 103 x 6 mm ³	240 x 240 x 119 mm ³	240 x 240 x 119 mm ³
Acquisition voxel size	1.19 x 1.21 x 1.20 mm ³	1.17 x 1.17 x 6.00 mm ³	3 x 3 x 7 mm ³	3 x 3 x 7 mm ³
Acquisition matrix	188 x 146	128 x 128	80 x 80	80 x 80
Scan duration	2:47 min	2.5-4 min	Variable	7 min
Labeling duration	–	–	7000 ms (minimum)	7500 ms (fixed)
Post labeling duration	–	–	1800 ms	1800 ms
Additional parameters	Inversion delay 935 ms	Venc 200 cm/s; 2 averages; Retrospective triggering; 15 Cardiac phases	Set trigger delay (0–1000 ms)	–
TFE dur. shot / acq	1938 / 1757 ms			–

TFE: Turbo Field Echo; Venc: phase-encoding velocity; SENSE: parallel imaging technique

RESULTS

Simulations: constant flow

The ASL-signal evolution in the tissue compartment is depicted in Figure 8.3 for three constant flow conditions. Increased flow rate during the PLD (while flow during labeling remained constant) caused the tail of the labeled blood (bolus) to arrive earlier in the tissue compartment. The lower T_1 in the tissue compartment with respect to the blood compartment increased the rate of signal decay. Therefore, a higher flow rate during the PLD resulted in less detected ASL-signal (see inset, Figure 8.3a).

Changing the flow only during labeling had two effects (see Figure 8.3b): first, the ASL-signal increased with the higher flow rate as expected, i.e. more spins are labeled; secondly, the bolus arrival time (BAT) became shorter (horizontal axis, Figure 8.3b). The second effect also leads to faster decay of the ASL-signal similar to the results for increased flow velocity during the PLD due to the shorter T_1 of tissue. Comparing the signal intensity in the insets of Figure 8.3, it can be appreciated that the first (i.e. flow) effect dominates over the compartmental T_1 -effect. Finally, increased flow during both labeling and PLD overlays previous effects (see Figure 8.3c).

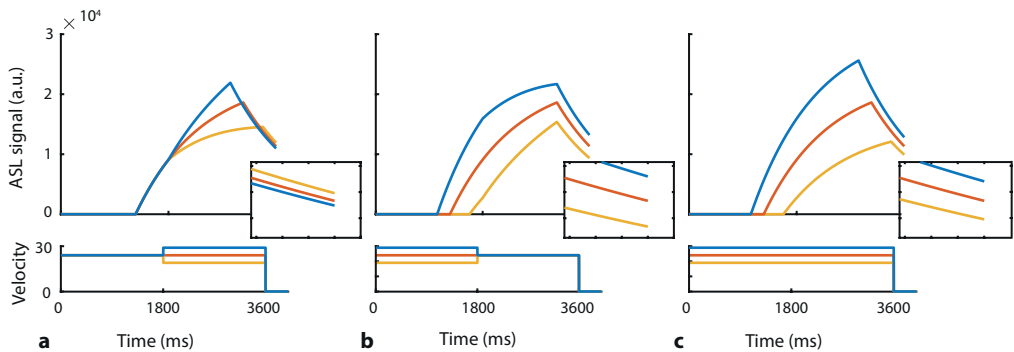


Figure 8.3 | Simulated ASL-signal evolution in the tissue compartment (top panels) during constant flow. Constant velocity increase/decrease during: **a**) PLD only; **b**) labeling only; and **c**) both labeling and PLD. The insets show a close-up of the signals at the moment of imaging (same scale for all insets).

Simulations: pulsatile flow

The effect of pulsatile flow on the signal inflow in the tissue compartment is depicted in Figure 8.4. The labeling duration (1800 ms) was set exactly equal to two cardiac cycles (R-R interval 900 ms) and the velocity of blood during the PLD was set to the average velocity over one cardiac cycle. Therefore, the volume of blood that is labeled was constant for each simulation and thus independent of the cardiac phase of the start-of-labeling.

The pulsatile flow can be seen to influence the ASL-signal relative to the simulation with constant flow (Figure 8.4a), even while the volume of label created was equal and constant. Therefore, differences in the exact timings when label is created (start- versus the end of the labeling) appear to influence the detected signal even after accounting for loss of label due to longitudinal relaxation. Changes in the bolus arrival time (Figure 8.4b) illustrate the variation in timing of label delivery and the influence of compartmental T_1 differences. Setting the same T_1 for both compartments resulted in a very similar signal profile (Figure 8.4a, yellow curve). Finally, adding pulsatile flow during the PLD (Figure 8.4a, red curve) resulted in a slightly stronger influence on the timing of delivery (i.e. of the bolus tail), which induced only small differences in signal fluctuations.

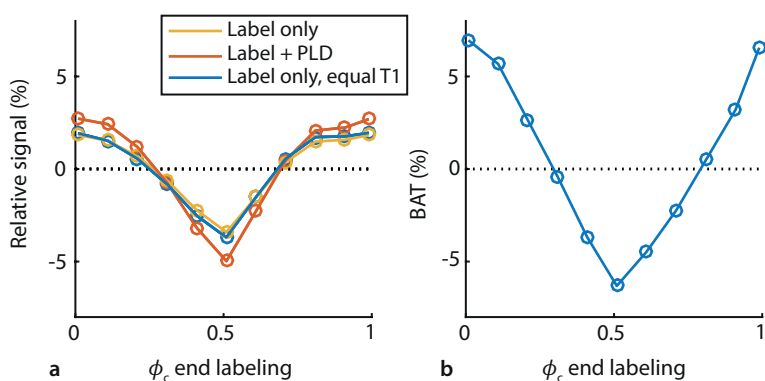


Figure 8.4 | Simulated pulsatile flow of two cardiac cycles during labeling (R-R interval 900 ms = 67 bpm). a) ASL-signal of pulsatile flow during label only (yellow), label only and equal T_1 for blood and tissue compartments (blue) and pulsatile flow during labeling and PLD (red). b) Bolus arrival time (BAT). BAT curve was equal for all three conditions; therefore a single curve is shown. All signals are normalized to the constant flow condition and aligned to the cardiac phase at the end-of-labeling.

Simulations: heart rate

In normal physiological conditions the heart rate will not exactly match the labeling duration and consequently the volume of labeled blood will vary, depending on the cardiac phase of the start- and thus also the end-of-labeling. Multiple fixed heart rates between 40 and 90 bpm were simulated and the phase of the start-of-labeling was varied to cover the entire cardiac cycle. First, the effect of pulsatile flow during labeling was investigated (while flow was constant during the PLD).

The volume of labeled spins (i.e. the number of spins labeled, which should not be confused with the detected ASL-signal at which point the label will have decayed considerably) can be seen to depend on the cardiac phase when labeling stopped (Figure 8.5a) (except for the case when labeling equals exactly 2 cardiac cycles when the labeled volume was, again, constant (Figure 8.5a, 67 bpm yellow)). The relative signal variation over the cardiac cycle (min-max range) was

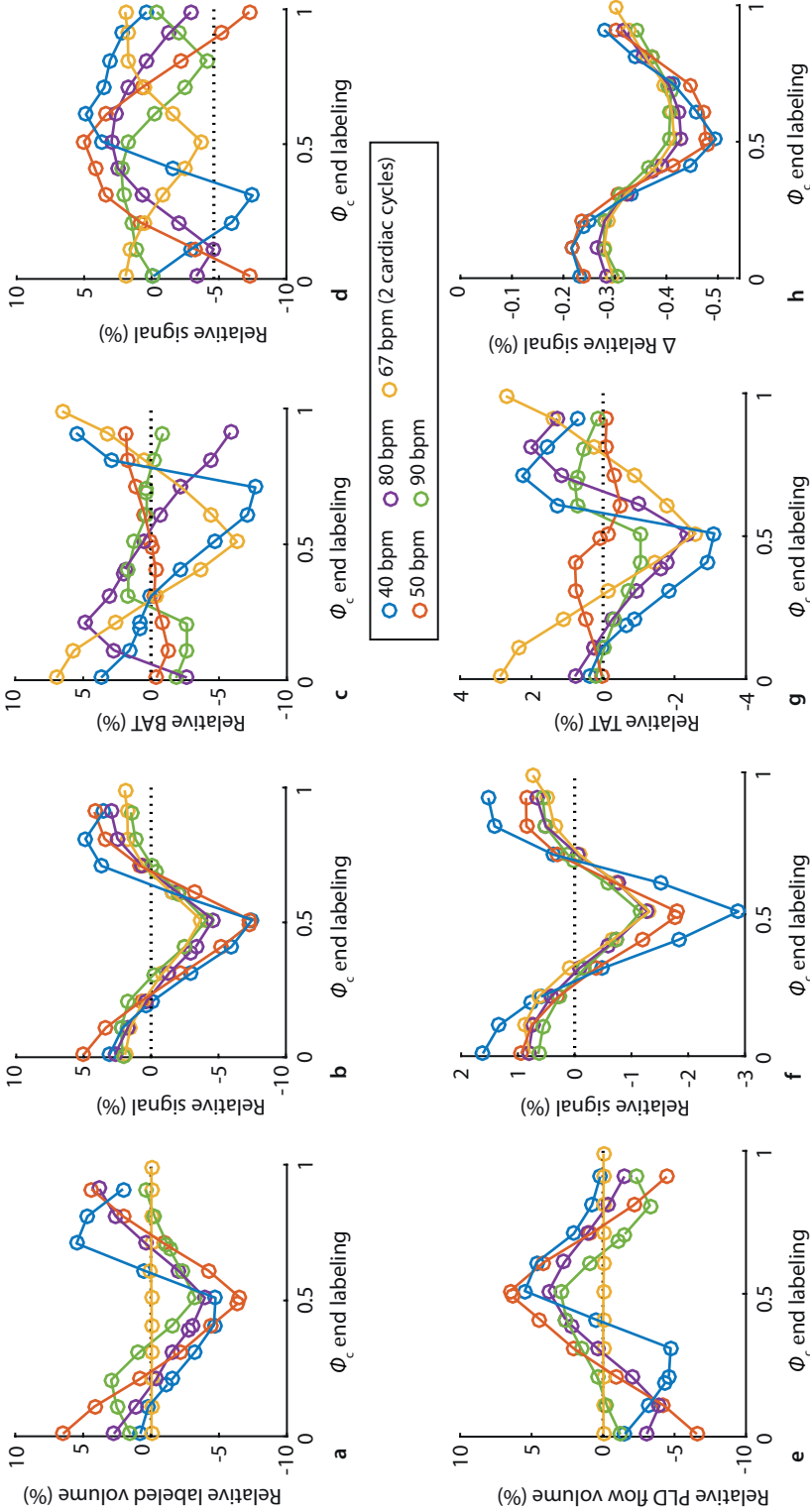


Figure 8.5 | Simulated multiple heart rates with pulsatile flow during labeling and PLD. **a-d**) Pulsatile flow during labeling, while PLD flow was constant. The special condition of exactly two cardiac cycles in the labeling period is shown in yellow (67 bpm), i.e. the situation of Figure 8.4. **e-g**) Simulation of fixed heart rates with pulsatile flow rate during PLD only. Flow during labeling was constant. TAT: tail arrival time of the bolus, with a positive value meaning later arrival in tissue compartment. **d**) Same relative signal as in **b**), only then aligned to the start of the labeling. All values are normalized to the constant flow condition. **h**) Difference in simulated relative signal between constant and velocity dependent labeling efficiency. Difference values are expressed in percentage points.



notably higher at lower heart rates (Figure 8.5b). Although visually there is a strong resemblance between the shape of labeled volume and the ASL-signal, the special case of constant labeling volume (Figure 8.5a, 67 bpm yellow) illustrates that there is a similar amount of signal variation even when there is no variation in labeled volume. Moreover, the curves in Figure 8.5b are all synchronized with respect to the end-of-labeling, whereas after sorting them versus the start of labeling (Figure 8.5d) this coherence is lost. Therefore, the signal variation in Figure 8.5b shows an effect of the end-of-labeling rather than an effect of labeled volume or start-of-labeling.

The effect of pulsatile flow during the PLD (while keeping flow constant during labeling) on the relative signal showed a very similar pattern as the relative signal due to pulsatile flow during labeling (compare Figure 8.5a-c with Figure 8.5e-g). The effect of label generation and delivery will therefore reinforce each other, independent of heart rate.

Simulations: labeling efficiency

Until this moment labeling efficiency was assumed constant over the cardiac cycle, however it is known to be dependent on the velocity of the blood [10,13]. Velocity-dependent labeling efficiency (Figure 8.1) was, therefore, added to the simulations with pulsatile flow during labeling and PLD. Similar curves were obtained as with constant labeling efficiency: the difference between constant and velocity dependent labeling efficiency was only -0.35 ± 0.08 percentage point (95%-confidence interval: -0.37, -0.33%), as shown graphically in Figure 8.5h. The influence of labeling efficiency was more pronounced at higher heart rates.

Simulations: labeling duration

At a very long labeling duration of 7 seconds, increasing the labeling duration by 1 second had no effect on the relative signal within the precision of the simulation (Figure 8.6a). As the cardiac phase of end-of-labeling shifts with increasing labeling duration, the BAT can be seen to shift as well (Figure 8.6b). The relative labeled volume increases with labeling duration as expected (Figure 8.6c).

Simulations: triggering the end-of-labeling

The bridge to the in-vivo experiments was made by simulating the end-of-labeling triggering using the same parameters as during the in-vivo experiments. After labeling for minimally 7 seconds, labeling was continued for an additional labeling period after a trigger; this was dubbed "trigger delay" (see In-vivo experiment Methods sections for details). The normal physiological situation was simulated by adding heart rate variability (HRV) to the cardiac cycle. For this simulation, a pulsatile flow profile with a HRV of 100 ms was generated at two mean heart rates of 40 and 90 bpm as two extreme cases. Due to the stochastic nature of the HRV, each trigger-delay was simulated 33 times. The start-of-labeling was also triggered similarly as done in the in-vivo experiment. The non-triggered case was simulated 33 times with a mean labeling duration of 7500 ms.

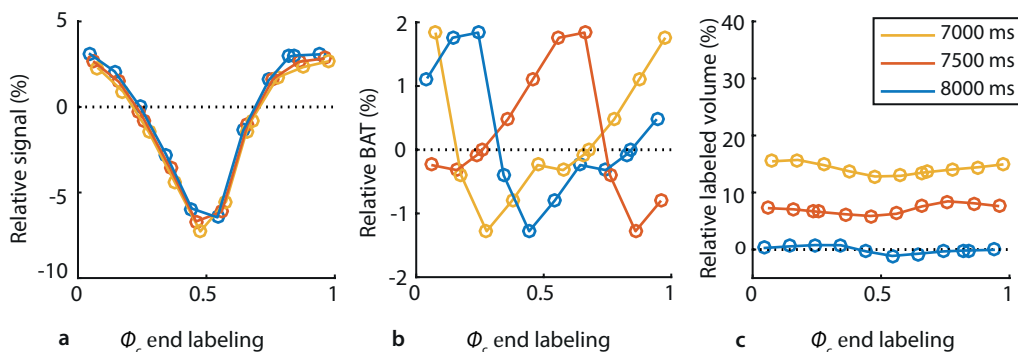


Figure 8.6 | Simulated effect of additional labeling duration on: **a)** relative ASL-signal; **b)** Bolus arrival time and **c)** Labeled volume. Pulsatile flow was simulated during labeling and PLD at a fixed heart rate of 50 bpm. All values are normalized to the constant flow condition with a labeling duration of 7000ms.

From Figure 8.7a it can be appreciated that HRV introduces uncertainty in the determination of the exact phase of the end-of-labeling (i.e. variation in the x-axis). A similar pattern in relative ASL-signal as in Figure 8.5b can be observed. As the variation in ASL-signal due to labeled volume is negligible at these long labeling durations, this is mostly the effect of the end-of-labeling phase. The variation in signal is, again, more pronounced at the lower heart rate both for the triggered (Figure 8.7a) as well as for the non-triggered (Figure 8.7b) case. The standard deviation of the non-triggered ASL-signal averaged over the cardiac cycle was 4.7% and 2.0%, for 40 and 90 bpm respectively (see Figure 8.7b). The standard deviations along the y-axis in Figure 8.7a were plotted separately in Figure 8.7c. A strong reduction in standard deviation can be observed at any end-of-labeling phase when triggering (see Figure 8.7c) compared to the non-triggered (see Figure 8.7b).

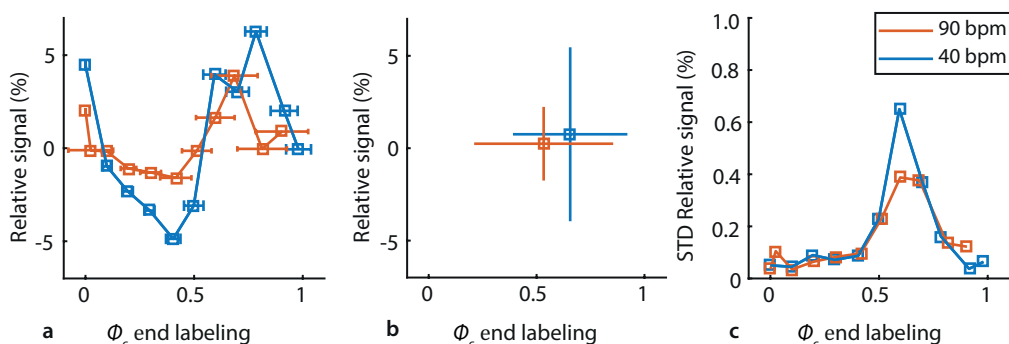


Figure 8.7 | Simulated end-of-labeling triggering at an average heart rate of 40 bpm (blue) and 90 bpm (red) with a heart rate variability of 100 ms. **a)** Relative ASL-signal with triggering. **b)** Relative ASL-signal without triggering (random selection of 33 data points from panel (a)). **c)** Standard deviation of data in panel (a). All values are normalized to the constant flow condition. Error bars indicate the standard deviation.

In-vivo experiments

Physiological parameters as measured during the in-vivo triggered and non-triggered scans are provided in Table 8.2. Heart rate ($p = 0.31$) and mean ($p = 0.65$) and standard deviation ($p = 0.63$) of the labeling duration did not differ significantly between scans or trigger condition. When comparing the phase in the cardiac cycle that we aimed for by setting the post-trigger delay with the actual phase at the end-of-labeling, a close correspondence is found (Table 8.2). The combination of triggering and set delay showed little variation around the intended cardiac phase (5% at longest tested delay (c)).

The mean gray matter CBF was 55.34 ± 21.21 , 53.81 ± 18.85 and 55.80 ± 18.78 ml/100g/min for the triggered conditions a,b, and c and 54.19 ± 19.37 ml/100g/min for the non-triggered scan. No difference in mean CBF between the four conditions could be detected ($p = 0.58$, Friedman's test), see Figure 8.8a. The temporal standard deviation of the CBF (13.59 ± 5.04 , 14.79 ± 4.23 , 15.60 ± 5.38 and 15.04 ± 6.31 ml/100g/min) was comparable between the four conditions ($p = 0.44$), see Figure 8.8b.

Table 8.2 | Physiological values in-vivo experiment

	a)	b)	c)	NT	p-value
Heart rate (bpm)	59±8	59±8	59±8	62±11	0.08
Label duration (ms)	7517±97	7492±140	7475±123	7455±7	0.65
Label duration tSTD (ms)	311±95	284±66	324±74		0.63
Set delay (ms)	70±0	418±78	576±82		
Cardiac phase (0-1)					
End-of-labeling	0.07±0.01	0.40±0.06	0.55±0.07	0.70±0.20	
End-of-labeling tSTD	0.01±0.00	0.03±0.01	0.05±0.02	0.20±0.01	
Imaging	0.71± 0.19	0.03±0.21	0.83±0.22	0.68±0.17	0.78
Imaging tSTD	0.11±0.02	0.13±0.02	0.14±0.03	0.20±0.01	0.54

Values are Mean±STD. tSTD is the temporal standard deviation over 20 dynamics. p-value indicates the repeated-measures ANOVA comparison between the four conditions.

DISCUSSION

The present study investigated the effect of the cardiac cycle on pCASL and especially focused on the effect of end-of-labeling triggering on ASL-signal stability. Simulations showed a clear, although small (on the order of 4% of the ASL-signal) influence of flow pulsations on the ASL-signal, even when the labeling duration spanned multiple cardiac cycles. The timing of the pulsatile flow was shown to influence both the generation- and delivery of the label, and the resulting effect

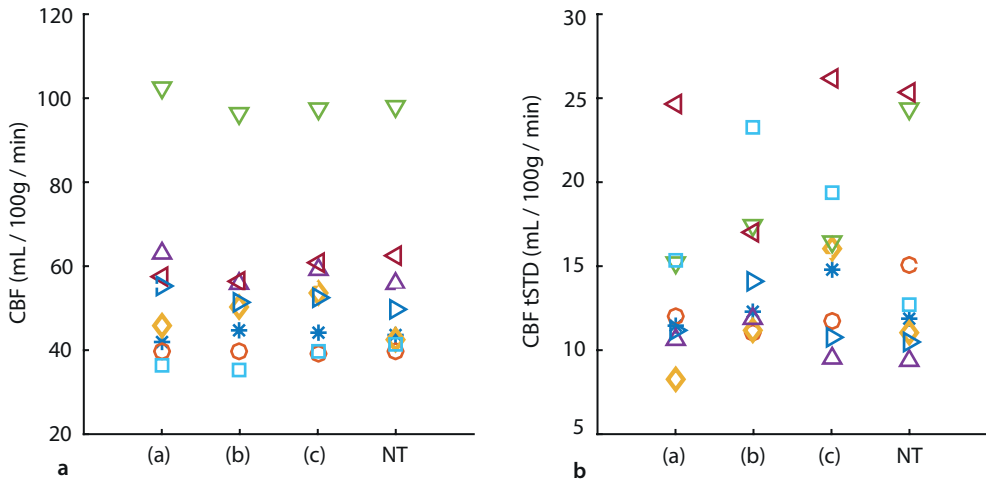


Figure 8.8 | In-vivo measurements of mean gray matter CBF and tSTD of the triggered and non-triggered scans. tSTD is the temporal standard deviation over 20 dynamics. The moment of end-of-labeling in the cardiac cycle a), b) & c) was defined by a set delay and cardiac triggering of the end-of-labeling. The cardiac phase of end-of-labeling varied randomly during the non-triggered scan (NT). Removing the potential outlier (green triangles) reduced the mean CBF to 48.5 ± 8.4 ml/100 g/min, without effect on statistical inferences.

on the ASL-signal was most associated with the end-of-labeling phase. However, the in-vivo experiments could not detect a difference in mean ASL-signal or temporal ASL-signal stability between the cardiac phases of the end-of-labeling triggering and/or with the non-triggered scan.

This study aimed to investigate the influence of the cardiac cycle on pCASL measurements of CBF, particularly during the end-of-labeling, since that timing will affect the ASL-signal stability most. To isolate the influence of cardiac cycle during the end-of-triggering on ASL-signal stability, an impractical long labeling duration was employed and combined with end-of-labeling triggering: by using these very long labeling durations (>7 s) in the in-vivo experiment, the occurrence of additional labeling of e.g. 1 second had little influence on the overall signal as was confirmed by the simulations (see Figure 8.6). When translating this to practical scan properties, triggering the end-of-labeling could be a candidate approach to minimize signal instabilities due to the cardiac cycle, although it might introduce more unwanted effects than solving when employed with commonly employed labeling durations. For instance, at typical heart rate of 60 bpm the additional labeling duration could vary up to 1 second, therefore the ASL-signal change due to the volume of additionally generated label at 2.8 s compared to 1.8 s labeling, could overshadow the potential effect of increased signal stability due to end-of-labeling triggering, while greatly complicating the consistency of CBF quantification. To provide equal quantitative CBF-estimation over such a wide range of labeling durations, it would be crucial to have an accurate estimate of dispersion of the bolus of labeled spins [4] and the exact exchange time of the label from the

intra- to the extravascular compartment [14], which are both difficult to estimate in an individual subject. Therefore, the present study aimed first to study how large the effect of the cardiac cycle is on the signal stability, focusing thereby on the potential benefit and properties of end-of-labeling triggering before moving to solving all the implementation issues that would be encountered when using such an approach in practical clinical applications. The simulation and in vivo results suggest, however, that implementing end-of-labeling triggering does not provide important improvements in signal stability for most pCASL applications. Therefore, it was not deemed useful to solve the aforementioned implementation challenges. It should be noted that during the in vivo experiments, only the label condition was end-of-labeling triggered, whereas the following control condition was acquired with the same 'labeling' duration. Hence the repetition time (TR) was the same for each label and control pair, thereby avoiding that magnetization differences would affect pair-wise subtractions. Even when controlling for these confounding effects, no improvement in signal stability could be proven in the present in-vivo study when using end-of-labeling triggering.

The simulations in the present study showed that signal fluctuations due to cardiac pulsations range between -8% and +5%. Previous work with simulations of continuous ASL showed a similar $\pm 5\%$ range in signal variation for a labeling duration of 1500 ms (see Figure 8.7 of reference [4]). However, their simulations (convolution of the velocity curve with the Buxton model) only took the effects into account that occurred while generating the label. Variation in the transport time of the label due to the cardiac cycle was not part of that continuous ASL study, although it was included in other studies, which investigated pulsed ASL [5,15-17]. Both modeling and in-vivo pulsed ASL data showed earlier arrival of the label with the systolic phase compared to the diastolic phase [5,15-17]. The simulations of the present study extend this concept to pCASL and showed that the delivery of label enhanced the signal fluctuations of labeling generation. In other words, the changes in transport-times during the PLD due to cardiac fluctuations augment the ASL-signal increases and decreases caused by flow pulsations during labeling. Hence, the range in signal variations of the present simulations is slightly larger than earlier predicted in literature. Moreover, this study is the first to show that these signal fluctuation are largely dependent on the phase of end-of-labeling and not to the start-of-labeling. Finally, the influence of the cardiac cycle on the ASL-signal due to the changed transport times and the differences in the amount of generated label, were both greater than changes due to the velocity dependency of the labeling efficiency, which is often cited as a major concern in pCASL.

In the simulations we quoted the influence of the cardiac cycle on ASL-signal by stating the observed signal range (-8 to +5%) to illustrate the maximum range of expected ASL-signal intensities, however, it could also have been expressed as temporal (tSTD), which has the advantage that it can be measured reliably in-vivo. The tSTD of the simulated untriggered case was 4% at the lowest heart rate, which in the simulations reduced to 0.08% tSTD when end-of-labeling triggering was employed. The relative small effect of 4% shows that influence of the

cardiac cycle is probably only a minor factor of observed ASL-signal fluctuations. Therefore, other physiological factors, such as respiration, might play a bigger role in pCASL [6,18].

In the present study, the average coefficient of variation measured in the non-triggered scan coefficient of variation was $28\pm 11\%$ and therefore the number of subjects in the present study can be considered to be too small to be able to show a 4% difference in temporal STD. However, the number of participants was chosen on the ability to proof significant impact on single subject pCASL experiments. When the effect of end-of-triggering could not be proven in a group of eight subjects, it is clear that the total effect of cardiac pulsations can be considered minor in pCASL. Taken together, the simulations and in-vivo experiments suggest that the effect of cardiac pulsations is small and triggering the end-of-labeling (and therefore also the start-of-triggering) provides no consistent improvement in ASL-signal stability on a per-subject basis.

Other methods, besides cardiac triggering, have also been proposed to reduce noise in ASL. Background suppression pulses have been shown to improve the general ASL-signal stability independent of cardiac pulsations [6]. Background suppression is particularly effective when using a read-out option with a single excitation pulse such as 3D-GRACE or 3D FSE stack-of-spirals [1]. Application of background suppression in the present study was not included, because of the high implementation complexity due to the varying TR of each label-control pair. Physiological noise reduction can also be achieved during post-processing, for example by using RETROICOR [6,18] By design, RETROICOR includes the cardiac and respiratory regressor determined at the moment of imaging into account, whereas the influence of the cardiac cycle at the start-of-labeling or end-of-labeling was not considered [4,6,18]. Application of RETROICOR in the present study proofed of limited value due to the low number of dynamics for each condition (20 label-control pairs) and was therefore omitted from the final analysis. Although these post-processing techniques provide a consistent way to reduce (physiological) noise from ASL, it would be beneficial when these noise-sources would be suppressed during the acquisition of the signal. As an extreme variant of triggered ASL, we considered and tested “triple triggered” pCASL (triggering the start- and the end-of-labeling as well as the moment of imaging), which would appear to be more in line with physiology than the independent chosen values as currently employed. Triple triggered ASL leads, however, to ASL-signals that are mainly proportional to the duration cardiac cycle, and should therefore be considered to be not very informative.

The present study modeled the arterial compartment as a rigid vessel without compliance. Arterial compliance is an important mechanical property that gradually reduces the flow pulsatility along the arterial tree toward the tissue compartment. Generation of label at the proximal end of the artery is governed by the typical flow curve (Figure 8.1), which already included the compliance of the arterial tree. The delivery of the label to the tissue was shown in the present study to play a minor role compared to generation. Compliance decreases the flow pulsatility during the delivery phase, which would in turn reduce variations in delivery time and thus increase overall signal

variability. Therefore, the assumption of rigid arterial compartment can be considered to provide a 'worst-case' scenario for the influence of flow pulsations.

The present study used the build-in finger pulse-oxy triggering of the MRI-scanner to synchronize the end-of-labeling with the cardiac cycle, which always lags behind in time compared to ECG-triggering. The present simulations suggest that the optimal moment of triggering lies at the end-systolic phase which corresponds to the finger pulse-oxy trigger with a delay of 0 ms. Although ECG triggering would allow more flexibility in choosing end-of-labeling phases within the systole, the practical application of finger triggering in the present study can be expected not to have influenced the accuracy (see Table 8.2) of the end-of-labeling triggering.

CONCLUSIONS

In summary, simulations showed that flow pulsations can influence the ASL-signal by approximately 4%, and that especially the cardiac cycle at the end-of-labeling is of importance. However, in-vivo experiments provided no difference in mean signal and/or signal stability. Combined with earlier findings concerning cardiac triggering, neither start-of-labeling nor end-of-labeling triggering improves signal stability significantly, suggesting that cardiac triggering is not very beneficial for pCASL. Post-processing methods that include cardiac and/or other physiological regressors (including the timing at the end-of-labeling) could be considered to correct most of the remaining minor influences of the cardiac cycle on pCASL stability.

Acknowledgements

The authors would like to acknowledge ir. J. Wezel for assistance with speed-optimizing the simulations.

REFERENCE LIST

1. Alsop DC, Detre JA, Golay X, Gunther M, Hendrikse J, Hernandez-Garcia L, Lu H, MacIntosh BJ, Parkes LM, Smits M, van Osch MJ, Wang DJ, Wong EC, Zaharchuk G (2015) Recommended implementation of arterial spin-labeled perfusion MRI for clinical applications: A consensus of the ISMRM perfusion study group and the European consortium for ASL in dementia. *Magnetic resonance in medicine : official journal of the Society of Magnetic Resonance in Medicine / Society of Magnetic Resonance in Medicine* 73 (1):102-116. doi:10.1002/mrm.25197
2. Heijtel DF, Mutsaerts HJ, Bakker E, Schober P, Stevens MF, Petersen ET, van Berckel BN, Majoie CB, Booi J, van Osch MJ, Vanbavel E, Boellaard R, Lammertsma AA, Nederveen AJ (2014) Accuracy and precision of pseudo-continuous arterial spin labeling perfusion during baseline and hypercapnia: a head-to-head comparison with $(1)(5)O$ $H(2)O$ positron emission tomography. *Neuroimage* 92:182-192. doi:10.1016/j.neuroimage.2014.02.011
3. Aslan S, Xu F, Wang PL, Uh J, Yezhuvath US, van Osch M, Lu H (2010) Estimation of labeling efficiency in pseudocontinuous arterial spin labeling. *Magn Reson Med* 63 (3):765-771. doi:10.1002/mrm.22245
4. Wu WC, Mazaheri Y, Wong EC (2007) The effects of flow dispersion and cardiac pulsation in arterial spin labeling. *IEEE Trans Med Imaging* 26 (1):84-92. doi:10.1109/TMI.2006.886807
5. Fushimi Y, Okada T, Yamamoto A, Kanagaki M, Fujimoto K, Togashi K (2013) Timing dependence of peripheral pulse-wave-triggered pulsed arterial spin labeling. *NMR Biomed* 26 (11):1527-1533. doi:10.1002/nbm.2986
6. Wu WC, Edlow BL, Elliot MA, Wang J, Detre JA (2009) Physiological modulations in arterial spin labeling perfusion magnetic resonance imaging. *IEEE Trans Med Imaging* 28 (5):703-709. doi:10.1109/TMI.2008.2012020
7. Haacke ME, Brown RW, Thompson MR, R. V (1999) *Magnetic Resonance Imaging: Physical Principles and Sequence Design*. Wiley-Liss, New York
8. Hales PW, Kirkham FJ, Clark CA (2016) A general model to calculate the spin-lattice (T_1) relaxation time of blood, accounting for haematocrit, oxygen saturation and magnetic field strength. *J Cereb Blood Flow Metab* 36 (2):370-374. doi:10.1177/0271678X15605856
9. Wright PJ, Mouglin OE, Totman JJ, Peters AM, Brookes MJ, Coxon R, Morris PE, Clemence M, Francis ST, Bowtell RW, Gowland PA (2008) Water proton T_1 measurements in brain tissue at 7, 3, and 1.5 T using IR-EPI, IR-TSE, and MPRAGE: results and optimization. *MAGMA* 21 (1-2):121-130. doi:10.1007/s10334-008-0104-8
10. Gevers S, Nederveen AJ, Fijnvandraat K, van den Berg SM, van Ooij P, Heijtel DF, Heijboer H, Nederkoorn PJ, Engelen M, van Osch MJ, Majoie CB (2012) Arterial spin labeling measurement of cerebral perfusion in children with sickle cell disease. *J Magn Reson Imaging* 35 (4):779-787. doi:10.1002/jmri.23505
11. Fisher NI (1995) *Statistical analysis of circular data*. Cambridge University Press, Cambridge
12. Herscovitch P, Raichle ME (1985) What is the correct value for the brain-blood partition coefficient for water? *J Cereb Blood Flow Metab* 5 (1):65-69. doi:10.1038/jcbfm.1985.9
13. Dai W, Garcia D, de Bazelaire C, Alsop DC (2008) Continuous flow-driven inversion for arterial spin labeling using pulsed radio frequency and gradient fields. *Magn Reson Med* 60 (6):1488-1497. doi:10.1002/mrm.21790
14. Parkes LM, Tofts PS (2002) Improved accuracy of human cerebral blood perfusion measurements using arterial spin labeling: accounting for capillary water permeability. *Magn Reson Med* 48 (1):27-41. doi:10.1002/mrm.10180
15. Gallichan D, Jezzard P (2008) Modeling the effects of dispersion and pulsatility of blood flow in pulsed arterial spin labeling. *Magn Reson Med* 60 (1):53-63. doi:10.1002/mrm.21654
16. Kazan SM, Chappell MA, Payne SJ (2010) Modelling the effects of cardiac pulsations in arterial spin labeling. *Phys Med Biol* 55 (3):799-816. doi:10.1088/0031-9155/55/3/017
17. Kazan SM, Chappell MA, Payne SJ (2009) Modeling the effects of flow dispersion in arterial spin labeling. *IEEE Trans Biomed Eng* 56 (6):1635-1643. doi:10.1109/TBME.2009.2016977
18. Restom K, Behzadi Y, Liu TT (2006) Physiological noise reduction for arterial spin labeling functional MRI. *Neuroimage* 31 (3):1104-1115. doi:10.1016/j.neuroimage.2006.01.026

CHAPTER

9

Summary

The brain is a metabolically active organ with little capacity for energy storage. This makes it highly dependent on a continuous supply of nutrients and oxygen. Multiple control mechanisms protect the brain against hypo- and hyperperfusion, which is so efficacious that the brain is often considered a hemodynamically separate entity from the rest of the body.

Despite these protective mechanisms, it is known that patients with cardiac dysfunction have a higher prevalence of cognitive dysfunction and higher risk of incident dementia and Alzheimer's disease. Fortuitously, the unfavorable effects of cardiovascular dysfunction on the brain seem reversible as improvement of cardiac function (for example cardiac transplantation or cardiac resynchronization treatment) restores brain perfusion and improves cognition. This suggests a new preventive and therapeutic target for improving cognition by ensuring blood supply to the brain based on improving cardiac function. Not only diseases of the heart are associated with loss of cognitive function, but diseases of the brain can also affect cardiac function. This bidirectional interrelationship is known under the term: heart-brain axis.

Understanding the heart-brain relation might guide future treatment decisions and give incentive for novel therapy development. The primary aim of the project "Go with the flow: the heart-brain axis" was to elucidate the interaction between heart and the brain, across the lifespan. This was done by integration of physiological concepts into the MRI-environment and by monitoring brain perfusion and its regulatory mechanisms at both the macrovascular level (using transcranial Doppler) and the tissue level (using arterial spin labeling MRI). This thesis focused mainly on the comparison and validation of these two modalities used in this project. Expertise from both the fields of cardiovascular physiology and MRI brain perfusion measurements were integrated into synergistic and comprehensive research protocols.

Chapters 1–3 provide a general introduction on the heart-brain axis, offer an overview of the underlying physiology, employed methodologies, and the physiological challenges and techniques applied in this project.

In **chapters 4, 5 & 6**, we considered the trustworthiness of the general assumption of middle cerebral artery diameter constancy. This assumption is applied to relate the TCD-measured cerebral blood flow velocity (CBFv) changes to changes in cerebral blood flow (CBF), i.e. brain perfusion changes. We applied high resolution MRI at 7 Tesla to investigate the middle cerebral artery (MCA) diameter during various environmental challenges. In **chapter 4**, we manipulated the end-tidal CO₂ concentration and showed that the MCA diameter increased at high levels of end-tidal CO₂. In **chapter 5**, high-resolution images of the MCA were obtained synchronized with the cardiac cycle. We found a subtle increase in MCA diameter during systole compared to diastole, suggesting that the diameter is sensitive to the pressure changes that occur within the heartbeat. Subsequently, in **chapter 6**, the effect of handgrip exercise on the MCA diameter was assessed, showing a small decrease in diameter suggestive of sympathetic influence on the

cerebral macrovasculature. These studies challenge the long-held assumption of MCA diameter constancy.

In **chapter 7**, we compared the CBFv response to rhythmic handgrip exercise in the MCA (measured by TCD) to the CBF response in the MCA flow territory (assessed with arterial spin labeling MRI (ASL)). Differences in arterial blood flow velocities are often used as proxy for changes in flow and brain tissue perfusion. We found that during rhythmic handgrip the CBFv increased, whereas no change in the MCA flow territory could be observed. Therefore, whole-brain CBF-measurements by ASL do not support the claim that a change in MCAv measured by TCD can be used as a proxy for regional CBF during rhythmic handgrip exercise. The observed decrease in MCA diameter during handgrip as observed in **chapter 6** can only explain a small part (approximately one fifth) of the observed discrepancy. Shunting of MCA blood flow during exercise (i.e. not feeding the brain tissue) could explain this discrepancy; however, evidence for such a hypothesized mechanism is currently lacking. Implications for understanding the underlying physiological mechanisms could be far reaching for either one or both modalities, indicating the need to further explore the relation of arterial blood flow and tissue perfusion.

In **chapter 8**, we investigated the influence of cardiac pulsations on pseudo-Continuous ASL (pCASL) signal stability. Due to the long labeling duration in pCASL the relative contribution of the label created at the end of labeling to the detected ASL-signal will be the largest, while this could be highly dependent on the moment of the cardiac cycle when labeling stops. Simulations showed only modest influence of the cardiac cycle, with variations both originating from the amount of label created at the end-of-labeling as well as from different transport times of the label to the imaging region during the post-labeling delay. An end-of-labeling triggering scheme was implemented on the scanner to validate these simulation-findings. In-vivo human experiments did also not show measurable effects of triggering on the ASL-signal intensity or stability. Combined with earlier studies on cardiac triggering, it was concluded that cardiac triggering at the start or the end of labeling has little benefit to pCASL signal stability.

CHAPTER 10

General discussion

The studies presented in this thesis laid further groundwork for integrative and multi-disciplinary studies of the Rembrandt Project “Go with the Flow” and the heart-brain connection in general. At the core of the Rembrandt project is the multi-disciplinary approach. This approach allowed us to challenge existing dogma in *TCD as measure for cerebral blood flow changes* and create new opportunities for future research with *Lower Body Negative Pressure in the MRI*. These topics will be discussed in the next paragraphs.

TCD AS MEASURE FOR CEREBRAL BLOOD FLOW CHANGES

The non-invasive nature of TCD, together with its high temporal resolution, portability and affordable setup has made it into a widely-used research and clinical tool [1]. Since the introduction of TCD [2] three decades ago the few basic assumptions of TCD, that couple velocity measurements to cerebral blood flow, have been continuously under discussion [3]. In this thesis, we have aimed to validate two important aspects of TCD: assumption of diameter constancy and whether TCD reflects cerebral blood flow changes.

The first aspect, diameter constancy, assumes that the diameter of the vessel that is insonated by TCD remains constant during physiological challenges. Earlier studies have directly and indirectly measured diameter changes, see e.g. a recent editorial on this topic [3]. In this thesis, we showed with high resolution MRI that this assumption does not hold up during challenges such as: high levels of hypercapnia (**chapter 4**), systolic-diastolic pressure differences (**chapter 5**) and rhythmic handgrip exercise (**chapter 6**). However, these modulations of the velocity are small when compared to differences that are considered clinically relevant. For example, in stroke patients the difference in (TCD measured) cerebrovascular reactivity at three months follow-up between two patient cohorts was approximately 30% [4]. The diameter change observed in our studies would account for approximately one fifth of those CBF-changes as predicted from velocity measurements by TCD, thus potentially overestimating (or underestimating) the differences between groups rather than within groups. This thesis challenges the long-held assumption of diameter constancy, which obscures the interpretation of experimental data as well as the (comparison of) different responses between groups, e.g. patient cohorts.

Measurements obtained with TCD are often interpreted as changes in CBF, i.e. tissue perfusion. TCD is often used to probe CBFv changes at the level of the Circle of Willis, hence obtaining an aggregated measurement over the entire flow territory of the insonated vessel. In **chapter 7** we showed that during handgrip exercise, the ASL CBF did not increase in the flow territory, whereas the TCD CBFv increased by 10% in the corresponding artery. When looking into more detail the ASL determined CBF appeared to increase more locally in the precentral region (motor cortex). This is too small a region to trigger a detectable increase in the mean total MCA flow territory CBF, attributed to neural activation. The expected change in CBFv extrapolated from such a small region (1.5%) still remains within the detection limit of TCD, which is approximately 1%

(unpublished pilot data). However, the change as measured with TCD (10%) overestimates the change as determined with ASL by one order of magnitude. Although, as also stated in the previous paragraph, we did show that during handgrip exercise the MCA-diameter changes significantly (2% area change, **chapter 6**), this is much smaller than the velocity difference (10%). Previous TCD studies have shown significant changes in MCA-velocity occur following emotional or sensory stimulation [1,5], and that hemispheric dominance of hand movement originating in small cortical regions can be detected [6,7]. These results illustrate that TCD does detect velocity changes in response to cognitive or motor challenges, it is as yet uncertain whether these are exclusively related to changes in local or global CBF or whether diameter changes also explains some of these detected velocity changes. This discrepancy between large artery blood flow and tissue perfusion raises fundamental questions (see **chapter 7**) for which present literature does not provide straightforward explanations.

With respect to the question whether we can still apply TCD to measure CBF changes, the results of the present thesis seem to be very clear: i.e. TCD velocity changes are not always a valid proxy for CBF changes at the tissue level for two reasons. First, during physiological challenges constancy of vessel diameter cannot always be assumed, which introduces a level of bias and uncertainty in the TCD determined “perfusion” responses. Second, the coarse spatial resolve TCD obscures localized changes in CBF, and unlikely reflects focal changes in tissue perfusion. This should, however, not be considered as a rejection of TCD for physiological brain research, but more as a strong call to first elucidate these inconsistencies to avoid that misinterpretations on (the control of) cerebral perfusion will enter the scientific literature, thereby obscuring the true mechanisms. Further research and especially more multi-modality studies that combine the strengths of TCD and e.g. ASL-MRI are required to elucidate how cerebral perfusion and blood velocity in large cerebral arteries are related.

LOWER BODY NEGATIVE PRESSURE IN THE MRI

Head-up-tilt (HUT) is the most commonly employed orthostatic challenge for the clinical evaluation of patients with syncope of unknown origin [8,9]. Currently, cerebral hemodynamic responses to HUT are assessed by TCD, which lacks spatial differentiation. Non-invasive MRI CBF-measurements using supine LBNP as challenge might provide insight in the underlying neuronal activation processes and enable identification of areas of hemodynamic impairment during orthostatic stress.

Applying LBNP in the MRI is a challenge, both for practical and safety reasons. A practical concern is that subject motion during the application of pressure during LBNP is inevitable. Such motion occurs in sync with the applied stimulus, i.e. both motion- and stimulus effects overlap each other in time. This creates ambiguity as to whether the measured data reflect an effect of LBNP, is the result of subject motion, or a mixture of these two. In the context of the Rembrandt Project, we

have applied LBNP in the MRI [unpublished data] and observed considerable head movement of 1–2 cm (see Figure 10.1). Head motion during LBNP causes large changes in the raw (i.e. unsubtracted) ASL-signal (see Figure 10.1a). Post-processing software (e.g. SPM, FSL) can be used to correct for head motion. However, the translations and rotations are mostly through-plane (z-direction), complicating the post-processing correction due to the relatively large thickness of the imaging slices. Moreover, motion-induced signal deviations are mostly non-linear, both in (image)-space and time [10], which further complicates corrections by post-processing. Another major concern is that (head) motion will also displace the ASL labeling plane with respect to subjects' anatomy, such that changes in artery anatomy, blood velocities, arterial transit time, main magnetic field (B_0), shimming and coil loading could influence the labeling efficiency and the subsequent CBF quantification. Since ASL relies on the subtraction of label and control images, the CBF calculation would still remain unaffected as long as label and control conditions are being affected by a similar offset in signal intensity. However, due to the effects discussed earlier, this is not the case in reality, and the result is large errors in the measurement of the CBF-response to LBNP. To remedy the subject motion during LBNP, we built and tested, in collaboration with the Instrumental Design Department of the LUMC, a prototype of a compact LBNP box [11]. By restricting the area of negative pressure to the pelvic region and the upper-legs, less downward force is present during the periods of negative pressure, thereby minimizing motion. Using the compact box a strong reduction in head motion was achieved while maintaining similar systemic hemodynamic responses. This could prove to be an important step to bring the LBNP research to the field of MRI. Finally, another solution would be to repeat the survey scans during the different levels of LBNP, to adopt the planning of the ASL scans as well as to repeat the MR-calibration scans during these conditions. Whereas this will make the CBF-measurement by ASL less dependent on the induced motion, it severely limits the time-efficiency of the study-protocol and might lead to unwanted increases in the total time that LBNP is applied.

LBNP in MRI has been used for a variety of experiments, such as assessing muscle metabolism using MR spectroscopy [12,13], for performing cardiac MRI [14-16], assessing the diameter of the large brain-feeding arteries [17] and for probing autonomic and baroreflex function in the brain [18,19]. In the Rembrandt Project, we have applied LBNP to investigate the relation between cardiac output and brain perfusion, leading to the observation that subject motion during moderate levels of LBNP can adversely affect the obtained measurements of the brain [unpublished results]. In contrast, we have successfully applied LBNP in MRI to investigate the effect of sympathetic stimulation on renal perfusion [20]. Nevertheless, the potential of LBNP in the MRI remains to be proven.

In the Rembrandt Project we showed [21] that humans differ in their cardiovascular response patterns to LBNP that are reproducible over time in one and the same individual. Currently, real-time (continuous non-invasive) blood pressure measurements, and especially the derived cardiovascular parameters such as stroke volume and peripheral resistance, are not available in the MRI environment. This hampers the classification of the underlying cardiovascular response

in MRI research. Generally, such real-time cardiovascular monitoring is important for subject safety, as sudden changes in blood pressure or heart rate are suggestive of for the occurrence of (near) syncope. Therefore, both safety and response classification underline the importance of advancing integrative cardiovascular monitoring in an MRI environment, to facilitate correct interpretation of the cerebrovascular response within the framework of the human heart-brain axis.

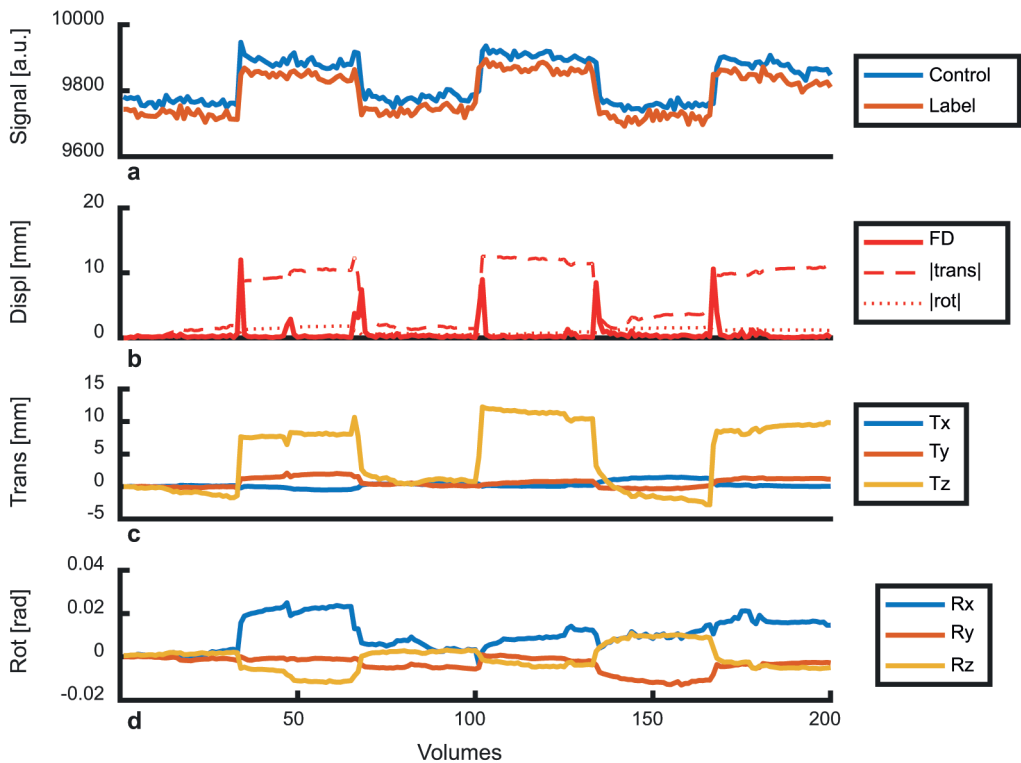


Figure 10.1 | Representative MRI signal and head displacement during three consecutive LBNP challenges in one subject. **a)** Global signal for control and label conditions **b)** Framewise Displacement (FD) and absolute translations and rotation; **c)** Relative Translations along x-, y- and z-axis; z-axis is toward the box **D)** Relative rotations. Global signals are averaged over the entire brain, excluding the skull.

CONCLUDING REMARKS

In the Rembrandt Project “Go with the flow”, we have integrated the fields of cardiovascular physiology and brain MR imaging to investigate the heart-brain axis, and the fruits of the multi-disciplinary approach in this thesis have been plentiful. Learning from other fields of expertise creates insight and challenges traditional assumptions. In this thesis, we have used MRI to verify

an often-debated assumption of TCD (**chapters 4–6**). Moreover, the cardiovascular physiology underscores (to the cerebrovascular MRI community) that the brain does not stop at the neck, but has a body that can respond differently to the same LBNP challenge [21]. This underlines the importance of implementing continuous cardiovascular monitoring in the MRI-scanner to enable the study of the brain and body in an integrated fashion. Also, when bringing physiological challenges, such as LBNP, to the MRI-scanner, limitations of MRI become evident, demanding multi-disciplinary and creative solutions [11]. Combining fields of expertise in the Rembrandt Project has provided fuel to challenge the validity of currently used methods to measure global and regional cerebral blood flow during exercise (**chapter 7**). TCD seems not to reflect changes in tissue perfusion, but on the flip-side, ASL-perfusion MRI fails to explain why a large and obvious increase in blood velocity is observed in the MCA during exercise. This has far-reaching implications for the translation of the concept of cerebral autoregulation (mainly developed in the TCD domain) to the field MRI; i.e. both modalities seem to measure different aspects of cerebral hemodynamics. The observations in our work challenged existing dogma, and gave insight in the assumptions of the employed techniques which contribute to better understanding of underlying (patho-)physiological mechanisms. Also, these findings provide a starting point for evaluating the integrative response of heart and brain which may help guiding future treatment decisions and the development of treatment and interventions strategies in both heart and brain dysfunction.

REFERENCE LIST

1. Willie CK, Colino FL, Bailey DM, Tzeng YC, Binsted G, Jones LW, Haykowsky MJ, Bellapart J, Ogoh S, Smith KJ, Smirl JD, Day TA, Lucas SJ, Eller LK, Ainslie PN (2011) Utility of transcranial Doppler ultrasound for the integrative assessment of cerebrovascular function. *JNeurosciMethods* 196 (2):221-237
2. Aaslid R, Markwalder TM, Normes H (1982) Noninvasive transcranial Doppler ultrasound recording of flow velocity in basal cerebral arteries. *J Neurosurg* 57 (6):769-774
3. Ainslie PN, Hoiland RL (2014) Transcranial Doppler ultrasound: Valid, invalid, or both? *J Appl Physiol* (1985) 117 (10):1081-1083. doi:10.1152/jappphysiol.00854.2014
4. Markus H, Cullinane M (2001) Severely impaired cerebrovascular reactivity predicts stroke and TIA risk in patients with carotid artery stenosis and occlusion. *Brain* 124 (Pt 3):457-467
5. Phillips AA, Chan FH, Zheng MM, Krassioukov AV, Ainslie PN (2015) Neurovascular coupling in humans: Physiology, methodological advances and clinical implications. *Journal of cerebral blood flow and metabolism : official journal of the International Society of Cerebral Blood Flow and Metabolism*. doi:10.1177/0271678x15617954
6. Linkis P, Jørgensen LG, Olesen HL, Madsen PL, Lassen NA, Secher NH (1995) Dynamic exercise enhances regional cerebral artery mean flow velocity. *Journal of Applied Physiology* 78 (1):12-16
7. Ono T, Hasegawa Y, Hori K, Nokubi T, Hamasaki T (2007) Task-induced activation and hemispheric dominance in cerebral circulation during gum chewing. *Journal of neurology* 254 (10):1427-1432. doi:10.1007/s00415-007-0570-3
8. Kenny RA, Ingram A, Bayliss J, Sutton R (1986) Head-up tilt: a useful test for investigating unexplained syncope. *Lancet* ii:1352-1355
9. Moya A, Sutton R, Ammirati F, Blanc JJ, Brignole M, Dahm JB, Deharo JC, Gajek J, Gjesdal K, Krahn A, Massin M, Pepi M, Pezawas T, Ruiz GR, Sarasin F, Ungar A, Van Dijk JG, Walma EP, Wieling W (2009) Guidelines for the diagnosis and management of syncope (version 2009). *EurHeart J* 30 (21):2631-2671
10. Power JD, Schlaggar BL, Petersen SE (2015) Recent progress and outstanding issues in motion correction in resting state fMRI. *NeuroImage* 105:536-551. doi:10.1016/j.neuroimage.2014.10.044
11. Bronzwaer A-SGT, Verbree J, Hoogendoorn SC, Stok WJ, Muller M, Vernooij ASN, Daemen MJAP, van Buchem MA, van Osch MJP, Van Lieshout JJ (2017) Lower body negative pressure in the MRI scanner: a newly designed compact box reduces head motion with preservation of the hemodynamic response. [submitted]
12. Shoemaker JK, Pandey P, Herr MD, Silber DH, Yang QX, Smith MB, Gray K, Sinoway LI (1997) Augmented sympathetic tone alters muscle metabolism with exercise: lack of evidence for functional sympatholysis. *J Appl Physiol* (1985) 82 (6):1932-1938
13. Zange J, Beisteiner M, Muller K, Shushakov V, Maassen N (2008) Energy metabolism in intensively exercising calf muscle under a simulated orthostasis. *Pflugers Arch* 455 (6):1153-1163. doi:10.1007/s00424-007-0361-9
14. Prasad A, Hastings JL, Shibata S, Popovic ZB, Arbab-Zadeh A, Bhella PS, Okazaki K, Fu Q, Berk M, Palmer D, Greenberg NL, Garcia MJ, Thomas JD, Levine BD (2010) Characterization of static and dynamic left ventricular diastolic function in patients with heart failure with a preserved ejection fraction. *Circ Heart Fail* 3 (5):617-626. doi:10.1161/CIRCHEARTFAILURE.109.867044
15. Esch BT, Scott JM, Haykowsky MJ, Paterson I, Warburton DE, Cheng-Baron J, Chow K, Thompson RB (2010) Changes in ventricular twist and untwisting with orthostatic stress: endurance athletes versus normally active individuals. *J Appl Physiol* (1985) 108 (5):1259-1266. doi:10.1152/jappphysiol.01186.2009
16. Taylor JA, Halliwill JR, Brown TE, Hayano J, Eckberg DL (1995) 'Non-hypotensive' hypovolaemia reduces ascending aortic dimensions in humans. *J Physiol* 483 (Pt 1):289-298
17. Serrador JM, Picot PA, Rutt BK, Shoemaker JK, Bondar RL (2000) MRI measures of middle cerebral artery diameter in conscious humans during simulated orthostasis. *Stroke* 31 (7):1672-1678
18. Kimmerly DS, O'Leary DD, Menon RS, Gati JS, Shoemaker JK (2005) Cortical regions associated with autonomic cardiovascular regulation during lower body negative pressure in humans. *J Physiol* 569 (Pt 1):331-345. doi:jphysiol.2005.091637 [pii];10.1113/jphysiol.2005.091637 [doi]

19. Kimmerly DS, Wong S, Menon R, Shoemaker JK (2007) Forebrain neural patterns associated with sex differences in autonomic and cardiovascular function during baroreceptor unloading. *Am J Physiol Regul Integr Comp Physiol* 292 (2):R715-722. doi:10.1152/ajpregu.00366.2006
20. Van der Bel R, Verbree J, Gurney-Champion OJ, Van Osch MJP, Stroes ESG, Nederveen AJ, Krediet CTP (2017) Sympathetic activation by Lower Body Negative Pressure does not affect kidney oxygenation in healthy men
21. Bronzwaer A-SGT, Verbree J, Stok WJ, van Buchem MA, Daemen MJAP, van Osch MJP, van Lieshout JJ (2016) Cardiovascular response patterns to sympathetic stimulation by central hypovolemia. *Frontiers in Physiology* 7. doi:10.3389/fphys.2016.00235

Samenvatting

De hersenen zijn een metabolisch actief orgaan met weinig capaciteit voor energieopslag. Dat maakt de hersenen compleet afhankelijk van een continue toevoer van voedingsstoffen en zuurstof. Meerdere reguleringsystemen beschermen de hersenen tegen hypo- en hyperperfusie. Deze mechanismes houden de perfusie zo effectief constant dat de hersenen vaak worden gezien als een hemodynamisch “los” systeem, separaat van de rest van het lichaam.

Ondanks deze beschermingsmechanismen is het bekend dat de prevalentie van cognitieve dysfunctie in patiënten met cardiale dysfunctie hoger is en dat deze patiënten een hoger risico hebben op het ontstaan van dementie en de ziekte van Alzheimer. Gelukkig lijken de ongunstige effecten van cardiale dysfunctie op het brein in ieder geval gedeeltelijk reversibel. Verbetering van de hartfunctie (door bijvoorbeeld transplantatie of resynchronisatietherapie) herstelt zowel hersenperfusie alsmede het cognitief functioneren. Dit geeft een mogelijk nieuw therapeutisch perspectief voor het herstel van cognitieve functie: zorgen voor adequate hersendoorbloeding door de hartfunctie te verbeteren, bijvoorbeeld door medicatie. Niet alleen ziektes van het hart zijn geassocieerd met verminderde cognitieve functie, maar ziektes van het brein kunnen ook de functie van het hart beïnvloeden. Deze bi-directionele relatie wordt wel de “hart-brein as” genoemd.

Inzicht in de “hart-brein as” zou in de toekomst behandelbeslissingen kunnen ondersteunen en aanzet geven tot ontwikkeling van innovatieve therapieën. De primaire doelstelling van het project “Go with the flow: the heart-brain axis” is het ontrafelen van de interactie tussen het hart en het brein en de veranderingen hierin gedurende de levensduur. Door fysiologische concepten te integreren in de magnetische resonantie (MRI) scanner krijgen we gelijktijdig toegang tot hersenperfusie en de mechanismen die de hersenperfusie regelen en beïnvloeden. De hersenperfusie kan zowel op weefselniveau (met transcraniële Doppler buiten de MRI) als op microvasculair niveau (met arteriële spin labeling MRI) gemeten worden. Dit proefschrift richt zich op het vergelijken en valideren van deze twee modaliteiten. Om dit doel te bereiken worden cardiovasculaire fysiologische en MRI-hersenperfusie technieken geïntegreerd in uitgebreide synergetische onderzoeksprotocollen.

Hoofdstukken 1–3 geven een algemene introductie op de “hart-brein as”, de onderliggende fysiologie en de gebruikte (fysiologische) methoden en technieken.

In **hoofdstukken 4, 5 & 6** wordt de geldigheid onderzocht van de algemeen gebruikte aanname dat de mediale cerebrale arterie (MCA)-diameter constant blijft tijdens fysiologische veranderingen. Deze aanname is voornamelijk van toepassing op het vertalen van TCD-gemeten veranderingen in bloedstroomsnelheid (CBFv) naar bloedvolumestroom (CBF) (ook bekend onder de naam hersenperfusie). Om deze aanname te testen, is gebruik gemaakt van hoge resolutie

7 Tesla MRI om veranderingen in de MCA-diameter te bepalen tijdens een aantal fysiologische manoeuvres. In **hoofdstuk 4** wordt de eindexpiratoire CO₂ concentratie gevarieerd en laten we zien dat bij hogere concentraties CO₂ de MCA-diameter toeneemt. In **hoofdstuk 5** onderzochten we de invloed van bloeddruk op de MCA-diameter door hoge resoluties MRI opnames van de MCA te synchroniseren met de hartslag. Hierbij werd een subtiele toename in MCA-diameter tijdens de systole gevonden in vergelijking met de diastole. Vervolgens hebben we in **hoofdstuk 6** het effect van ritmisch knijpen van de hand op de MCA-diameter bepaald. We laten zien dat door ritmisch knijpen een kleine afname in diameter wordt veroorzaakt, wat indicatief is voor sympathische invloed op de grote hersenvaten. Deze studies dagen de lang-bestaande aanname van constante MCA-diameter uit.

In **hoofdstuk 7** vergelijken we de CBFv response in de MCA gemeten met TCD tijdens ritmisch knijpen van de hand met de respons op dezelfde taak gemeten met ASL in het stroomgebied van de MCA. Verschillen in CBFv worden vaak gebruikt als plaatsvervangend equivalent voor veranderingen in bloedstroomvolume en hersenperfusie. We vonden dat volgens TCD de CBFv sterk toenam tijdens ritmisch knijpen, maar dat er door ASL geen veranderingen in CBF gedetecteerd werd in het MCA-stroomgebied. Deze metingen ondersteunen daarom niet de aanname dat CBFv een plaatsvervangend equivalent is voor regionale CBF-veranderingen. Een afname in MCA-diameter tijdens ritmisch knijpen, zoals gemeten in hoofdstuk 6, kan maar een klein deel (ongeveer één vijfde) verklaren van de discrepantie. Shunts die het bloed om de hersenen heen leiden zouden dit fenomeen kunnen verklaren, maar voor deze hypothese ontbreekt vooralsnog sluitend bewijs. Implicaties voor het begrijpen van de onderliggende fysiologische mechanismen kunnen verstrekkend zijn voor één of zelfs voor beide modaliteiten. Dit geeft aan dat verder onderzoek nodig is om de relatie tussen bloedstroom in de grote vaten en hersenperfusie op weefselniveau te beschrijven.

In **hoofdstuk 8** wordt de invloed van pulsaties van het bloed op de stabiliteit van het pCASL signaal bestudeerd. Door de lange labelingsduur in pCASL is de relatieve bijdrage van het bloed dat als laatste gelabeld is aan het pCASL signaal het grootst. Onze simulaties laten een kleine invloed zien van de fase van de hartcyclus aan het einde van de labelperiode op het ASL-signaal. Deze invloed wordt veroorzaakt door zowel variaties in de hoeveelheid gelabelde bloed dat op het laatst gegenereerd wordt als door (kleine) variaties in transporttijd van het label naar het afbeeldingsgebied tijdens de "post labeling delay". In-vivo experimenten met speciale pCASL hartslag-synchronisatie techniek laten geen meetbaar effect zien van de hartslag-fase op de signaalstabiliteit. We concluderen, mede op basis van eerdere literatuur, dat het synchroniseren van de start of einde van het labelen met de hartslag weinig toegevoegde waarde heeft voor de signaal stabiliteit van pCASL.

List of publications

Influence of the cardiac cycle on pCASL: cardiac triggering of the end-of-labeling. **J Verbree**, MJP van Osch, Magnetic Resonance Materials in Physics, Biology and Medicine, 2017

Aging modifies the effect of cardiac output on middle cerebral artery blood flow velocity. AGT Bronzwaer*, **J Verbree***, WJ Stok, MJAP Daemen, MA van Buchem, MJP van Osch, JJ van Lieshout. *Physiological Reports*, 5 (17), 2017

The cerebrovascular response to lower body negative pressure versus head-up tilt. AGT Bronzwaer*, **J Verbree***, WJ Stok, MJAP Daemen, MA van Buchem, MJP van Osch, JJ van Lieshout. *Journal of Applied Physiology*, 2017; doi: 10.1152/jappphysiol.00797.2016

Cardiovascular response patterns to sympathetic stimulation by central hypovolemia. AGT Bronzwaer*, **J Verbree***, WJ Stok, MA van Buchem, MJAP Daemen, MJP van Osch, JJ van Lieshout. *Frontiers of Physiology* 2016. 7:235. doi: 10.3389/fphys.2016.00235.

Using High-Field Magnetic Resonance Imaging to Estimate Distensibility of the Middle Cerebral Artery. EAH Warnert, **J Verbree**, RG Wise, MJP van Osch. *Neurodegenerative Diseases*, 2016: 16(4-6) p. 407-410

Middle cerebral artery diameter changes during rhythmic handgrip exercise in humans. **J Verbree***, AGT Bronzwaer*, MJAP Daemen, MA van Buchem, JJ van Lieshout, MJP van Osch. *JCBFM*, 2016; doi: 10.1177/0271678X16679419

Assessment of middle cerebral artery diameter during hypocapnia and hypercapnia in humans using ultra-high-field MRI. **J Verbree**, AGT Bronzwaer, E Ghariq, MJ Versluis, MJAP Daemen, MA van Buchem, A Dahan, JJ van Lieshout, MJP van Osch. *J Appl Physiol*, 2014. 117(10): p. 1084-9.

* Shared first / These authors contributed equally to this work.

Dankwoord

Thijs, bedankt voor de begeleiding als copromotor tijdens het hele promotie traject en de afronding. Bedankt voor je scherpe inzicht, de discussies over de betrouwbaarheid van de data en vooral je geduld bij het corrigeren van manuscript versie-zoveel. Hoe je die honderden mailtjes per dag weggewerkt krijgt, is mijn nog steeds een raadsel; als je maar blijft lachen!

BAS, (Beste Anne-Sophie), bedankt voor de fantastische samenwerking op academisch en experimenteel Duct Tape niveau. Ik ben je zeer erkentelijk voor al die keren dat je me tot plannen hebt aangezet. Erg genoten heb ik van onze gezamenlijke congresreizen, eindeloze poster presentaties uitkammen en continue gezelligheid. Ik kon me geen betere partner-in-crime wensen om een PhD mee te doen!

Beste prof. van Lieshout, HH (Ha Han), bedankt voor de overdaad aan fysiologische kennis en het bijbrengen van het juist en bedachtzaam uitvoeren van fysiologische experimenten. Je enthousiasme in wetenschap en fysiologie is erg aanstekelijk.

Beste promotor prof. van Buchem en prof. Daemen, Mark & Mat, bedankt voor jullie nauwe betrokkenheid en interesse in het project. De discussies en jullie kritische vragen tijdens de regelmatige meetings hebben de diverse projecten continue aangescherpt en verbeterd.

Aan alle vrijwilligers die hebben meegedaan aan onze studies: driewerf lof voor jullie belangeloze inzet en vooral jullie tomeloze geduld bij de (best wel) lange, (beste wel) saaie en (best wel) luidruchtige experimenten.

Uiteraard wil ik de promotiecommissie bedanken voor hun wetenschappelijke beoordeling van dit proefschrift. Ik kijk uit naar een interessante gedachtewisseling.

Toppers van C2-195, ook ben ik jullie dankbaar voor de academische discussies, morele ondersteuning en tomeloze gezelligheid. Jullie kunnen de wetenschap laten bloeien en de zon laten schijnen en in een betonnen bunker! Toppers van "Beneden", ook jullie wil ik graag betrekken in bovenstaande lofzang. Bedankt voor het proosten op menig wetenschappelijke overwinning, of gewoon als er niets te vieren viel.

Beste Eidrees, Sophie, Xing-xing & Wouter, bedankt voor de discussies rond ASL en de menig gedeelde scansessies. Wouter, dank voor je vertrouwen. Mijn ingewikkelde experimentele opstellingen mocht ik (op een veilige manier!) in de MRI blijven toepassen.

Beste Koekwouzen et al., Mark, Wouter, Renee & Aniek, bedankt voor jullie ondersteuning voor, tijdens en na het promotietraject. De discussies en PhD frustraties die we hebben gedeeld tijdens onze lange wandelingen en uitjes hebben een grote bijdrage geleverd aan de totstandkoming van dit proefschrift.

Lieve ouders en schoonouders, bedankt voor jullie ondersteuning in en interesse voor deze meer jaren onderneming. Vader en Moeder, bedankt voor de vrijheid die jullie mij gegeven hebben. Lieve Bex, bedankt dat je er altijd voor me was (ook al was ik niet altijd even gezellig in de nasleep van mijn promotie). Op nog vele jaren samen jong blijven!

Curriculum Vitae

Jasper Verbree was born in Zevenhuizen (zh) on January 9th, 1986. After graduating from the Oranje-Nassau College in 2004, he started studying Technical Medicine at the University of Twente. During his clinical internships he contributed to projects concerning, cochlear implants, radiotherapy, deep brain stimulation and transthoracic catheter navigation. In August 2012 he obtained his Masters' degree at the University of Twente with a thesis on non-invasive and quantitative measurements of cerebral oxygenation with MRI performed during an internship at the department of Radiology, Academic Medical Center, Amsterdam.

In September 2012, he started his PhD research at the C.J. Gorter Center for High-Field MRI, Leiden University Medical Center. His main research topics were identifying the relation between cardiac function and brain perfusion, integration of human physiological experiments in an MRI-environment and investigating the influence of cardiac pulsations on pseudo-continuous arterial spin labeling MRI. He worked in close multi-disciplinary collaboration to setup and perform experiments in both C.J. Gorter Center and the Laboratory for Clinical Cardiovascular Physiology at the Academic Medical Center, Amsterdam. In January 2017, he started his work as a software developer in Rotterdam.

